Title
Fundamental Study on the Effects of Irreversible Electroporation Pulses on Blood Vessels with Application to Medical Treatment

Author
Maor, Elad

Publication Date
2009

Peer reviewed|Thesis/dissertation

Fundamental Study on the Effects of Irreversible Electroporation Pulses on Blood Vessels with Application to Medical Treatment

By

Elad Maor

M.D. (Ben Gurion University of the Negev) 2007

A dissertation submitted in partial satisfaction of the

requirements for the degree of

Doctor of Philosophy

in

Biophysics

in the

Graduate Division

of the

University of California, Berkeley

Committee in charge:

Professor Boris Rubinsky, Chair

Professor Stanley A. Berger

Professor Harold Lecar

Professor Mohammad R.K. Mofrad

Fall 2009

Fundamental Study on the Effects of Irreversible Electroporation

Pulses on Blood Vessels with Application to Medical Treatment

By

Elad Maor

Abstract

Fundamental Study on the Effects of Irreversible Electroporation

Pulses on Blood Vessels with Application to Medical Treatment

by

Elad Maor

Doctor of Philosophy in Biophysics

University of California, Berkeley

Professor Boris Rubinsky, Chair

Background: Irreversible electroporation (IRE) is a biophysical phenomenon in which a series of electric field pulses selectively damages only the lipid bilayer of the cell membrane. This work is a fundamental study on the effect of IRE on blood vessels, evaluating the feasibility and efficiency of endovascular IRE to destroy vascular smooth muscle cells (VSMC) in the arterial wall.

Methods & Results: Time dependent finite-element simulations of the electric field and bio-heat transfer equations were used to analyze the electric field and the temporal behavior of the temperature due to electroporation pulses. The Henriques and Moritz thermal damage integral was used to demonstrate that an endovascular electrode geometry exists with which IRE pulses can be applied across the arterial wall with no thermal damage.

In-vitro experiments with VSMC compared different electroporation protocols in order to find the electric field threshold for efficient IRE. *In-vivo* experiments with rodents demonstrated for the first time that IRE can ablate the VSMC population of the arterial wall, and that the ablation persists at 28 days. By comparing eight different

electroporation protocols it was demonstrated that best ablation efficiency can be achieved with 90 square direct current pulses of 100μs at a frequency of 4 Hz delivering electric field of 1,750 V/cm across the vessel wall. In addition, a separate experiment demonstrated that IRE attenuated neointimal formation in rodent carotid arteries evaluated 28 days following angioplasty damage.

In-vivo experiments with New-Zealand white rabbits evaluated the use of endovascular IRE. Using custom made endovascular devices with four longitudinal electrodes on top of an inflatable balloon, IRE was successfully applied to the vessel walls of eight iliac arteries. Independent pathology analysis confirmed the efficient ablation of the VSMC population evaluated at 7 and 35. In-vivo experiment with the same animal model using angioplasty damaged iliac arteries, showed that endovascular IRE attenuated neointimal formation and luminal loss 35 days following angioplasty.

Conclusions: Non-thermal IRE is an efficient cell ablation method that can be used in an endovascular minimally-invasive approach. It holds the potential to treat multiple clinical problems, in particular the problem of coronary restenosis and cardiac arrhythmias.

Professor Boris Rubinsky, Chair

DEDICATION

In memory of my father, Yosi Moalem.

TABLE OF CONTENTS

ACKNOWLEDGEMENTS

I would like to thank Professor Boris Rubinsky, my primary mentor, whom I met for the first time in Israel during his sabbatical leave. Professor Rubinsky supervised my dissertation and guided me in my studies throughout the program. He provided me with support and encouragement, and offered me this once in a lifetime opportunity to conduct a fundamental interdisciplinary research. I would also like to thank Dr. Antoni Ivorra whose knowledge in electric engineering and bio-impedance was essential to so many aspects of my work. Dr. Ivorra's warm personality and professional aid have contributed significantly to the quality of this dissertation. Many thanks to all of my colleagues and friends at the bio-thermal lab: Dr. Jessica Preciado, Dr. Yair Granot, Greg Troszak, Charlotte Daniels, Mary Phillips and all other current and past members of the Rubinsky lab. I would like to thank everyone at the Biophysics graduate group: the group chair - Professor Isacoff, the class of 2007, and of course the one and only Kate Chase who kindly guided me from my first days in Berkeley to my dissertation submission.

I would like to thank the members of my qualifying exam and dissertation committees: Professor Harold Lecar, for broadening my knowledge of biological membranes biophysics, heading my qualifying exam committee and critically reading my dissertation. Professor Stanley Berger, for sharing with me his overwhelming knowledge of biological fluid mechanics. And last but not least Professor Mohammad Mofrad and Professor Susan Marqusee.

Finally, I would like to thank my wife, Ronny, for encouraging me to make this journey to Berkeley, for patiently reading my abstracts and papers, and for her support during the wonderful years we spent here with our kids.

I. CHAPTER ONE: BACKGROUND

1. Irreversible electroporation (IRE) phenomenon

Electroporation is a modality whereby microseconds electric pulses are applied across the cell membrane and increase its permeability. For a detailed scientific discussion of the phenomena of electroporation in general see, for example, the book chapter by Weaver and Chizmadzhev. [1] The essential features of electroporation include[2]:

(1) Application of short electrical pulses

(2) Charging of lipid bilayer membranes

(3) Rapid, localized structural rearrangements within the membrane

(4) Transitions to water-filled membrane structures ("pores")

(5) Increase in ionic and molecular transport

The radius of electroporation induced "pores" is on the scale of nanometers and they may reseal sometime after the end of the pulse, or cause an irreversible damage to the membrane. Temporary permeabilization is known as reversible electroporation and if the permeabilization leads to cell death it is known as irreversible electroporation (IRE).[3]

Based on computer models, the contemporary view is that hydrophilic "pores" are created in the membrane and that it is these "pores" who are responsible for the observed increase in membrane permeability (formerly known as "membrane electric breakdown") .[4,5] The pores radii expand as a function of the transmembrane potential and the length of the pulse. One commonly used equation to describe pore formation is:

$$\Delta W\,(r,U) = 2\pi\gamma r - \pi\Gamma r^2 - 0.5CU^2\pi r^2 \qquad (1)$$

where ΔW is the amount of work ,r is the pore radius, U is the potential difference across the membrane, γ is the lipid bilayer line tension of the inner surface of the pore, Γ is the lipid bilayer surface tension of the membrane, and C is the difference in specific capacitance due to the replacement of the membrane lipids by water.[1] Models of pore evolution focus on single cell electroporation, while the effects of electric field on cell membrane in tissue or suspension might be different.[6]

❖ *Irreversible electroporation*

A general observation over many of the electroporation experiments is that under certain conditions (e.g. high electric field or long pulse duration) cell viability decreases. Electroporation can cause cell death by direct or indirect mechanisms:

1. Direct - Very strong electric field can completely fragment the cell's membrane, inducing immediate cell necrosis.

2. Indirect - Electroporation can induce a relatively long and significant increase in molecular transport across the membrane, followed by complete recovery of the membrane. However, in some cases the degree of molecular exchange between the cells and their environment is too high for the cells to recover. In these cases cells succumb to the change in the intracellular environment.[1] It has also been suggested that electroporation might indirectly kill cells by charge-induced damage to the DNA. [7] In contrast to the direct effect, the indirect effect of IRE induces cell death by activating apoptotic pathways.[8]

A recent *in-vitro* work by Pinero *et al.* demonstrated that with electric pulse of 750 V/cm lasting 1,200 μs , 50% of the cells killed were likely to die through necrosis

(immediately after the discharge), while the rest of the cells underwent apoptosis.[9] In addition, Matsuki *et al.* demonstrated that an electric field as low as 75V/cm can induce apoptosis, if the pulse duration was long enough.[10] Although the exact mechanism of action of IRE remains relatively speculative, the experimental data is clear: electric field pulses increase molecular transport across biological membranes, and can induce cell death.

IRE can be induced by different combinations of parameters like electric field magnitude, pulse shape, length and frequency. The work that will be presented in the chapters below will focus only on those combinations of direct-current (DC) pulses that will not induce significant thermal damage (for more details see chapter II). More specifically, the work will focus only on 100μs square pulses, with frequency and electric field magnitude being the only parameters changed or compared.

❖ *Applications of reversible electroporation*

The reversible mode of electroporation has been used in basic research for more than 25 years to transfer DNA-molecules into cells *in-vitro*. Reversible electroporation can be used *in-vivo* for gene transfer or to facilitate local drug delivery.[11-13] Large number of clinical trials are currently underway , evaluating the use of reversible electroporation for naked plasmid DNA delivery ("nonviral" gene delivery). These trials are focusing on problems like malignant melanoma, head and neck cancer, cutaneous cancer, pancreatic cancer, breast cancer, as well as some infectious diseases (HIV and Hepatitis C). [14]

❖ *IRE vs. reversible electroporation*

The major advantage of IRE is simplicity. One of the major challenges with reversible electroporation is to temporarily open the cells membrane without inducing cell death. This challenge limits the range of possible electroporation parameters and requires tight control over the process. In contrast, IRE can be used in a much wider range of electroporation pulses with the only concern being the temperature in the treated volume (for more details see discussion in Chapter II). In addition, in order to destroy cells in-vivo, reversible electroporation requires the use of an adjuvant agent (chemotherapy). The injected agents raise the issue of drug tolerability, which complicates the immediate clinical application of these approaches.

❖ *Clinical applications of IRE*

The application of the irreversible electroporation mode for the treatment of solid tumors has become clinically relevant after it was demonstrated that electroporation pulses can be applied without causing thermal damage.[15] This has delineated irreversible electroporation as a non-thermal ablation technique, and separated it from radiofrequency or cryosurgery that are the common ablation approaches in the clinical practice.

The irreversible mode was recently used, for the first time in humans, for the *in-vivo* treatment of solid prostate tumors. Currently, clinical research is focusing on the use of IRE for the treatment of solid tumors and solid metastases in a minimally invasive approach.

This dissertation will focus on the effect of IRE on blood vessels, and it potential clinical application for the treatment of coronary restenosis.

2. The normal artery

Arteries carry blood from the heart to peripheral organs. Although viewed in the past as passive elastic tubes, arteries are a living organ that can adapt and change in response to different stimuli.[16] Composed mainly of two cell types and extra-cellular fibers, arteries can be described microscopically as tri-layered: the outermost layer is known as the ***tunica adventitia*** and is composed of loose connective tissue, including collagen fibers, some fibroblasts and macrophages, and small blood vessels and nerves. The middle layer is the ***tunica media***, which is made up mainly of smooth muscle cells with some elastic fibers and collagen fibrils. The elastic fibers between the *tunica media* and the out tunica adventitia are called the external elastic lamina. The innermost layer, which is in direct contact with the flow of blood is the ***tunica intima***. In the normal artery, this layer is made up of endothelial cells and basal membrane, that is also called internal elastic lamina. The *tunica intima* has an important role in the pathogenesis of atherosclerosis, post-angioplasty restenosis and other vascular pathologies.[17] An example of a normal iliac artery of New-Zealand white rabbit is shown in Figure I-1.

❖ *Cellular components*

Endothelial cells are the innermost component of the normal artery. They are in direct contact with the flowing blood, and play a major role in arterial adaptation to changes in blood flow and/or pressure. The surface of the endothelial cells is coated with molecules that prevent blood coagulation and help maintain the blood in its liquid state. The peripheral blood contains endothelial progenitor cells (EPCs) that can help regenerate areas of damaged endothelium.[18]

Vascular Smooth muscle cells (VSMC) are the cellular component of the *tunica media*. These cells can contract and relax in response to different stimuli (i.e. changes in blood pressure , decrease in end organ perfusion rate, injury of the arterial wall). VSMC have two distinct phenotypes: contractile and synthetic, and the phenotype can change in response to certain stimuli. Proliferation and activation of VSMC contributes to the formation of lesions in the arterial wall such as atherosclerotic plaque, restenosis following angioplasty and in-stent restenosis following stent implantation.

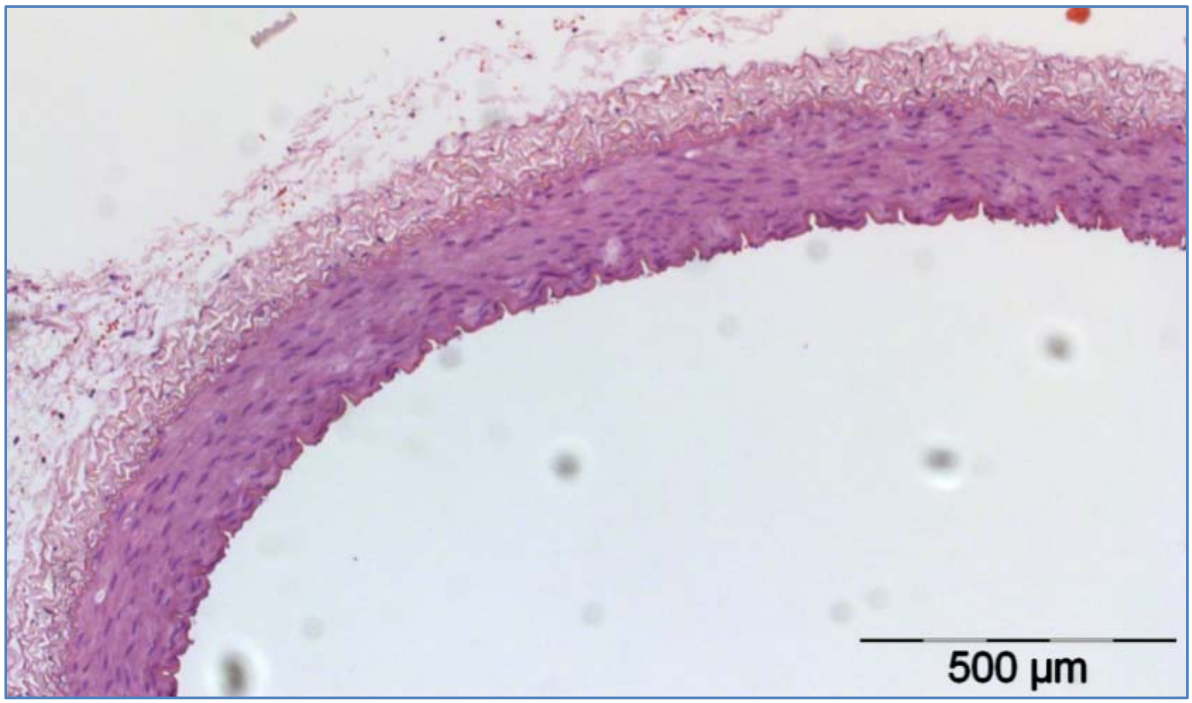

Figure I-1: Normal iliac artery of New-Zealand white rabbit demonstrating the tri-layered structure of the artery.

3. The problem of restenosis

The beating of the human heart is dependent on continuous blood flow through the coronary arteries. Myocardial infarction ("heart attack") is the result of abrupt interruption in blood supply to part of the beating heart, usually due to plaque-rupture in an atherosclerotic coronary artery. The gold-standard treatment for acute myocardial

infarction is reperfusion. Reperfusion can be achieved pharmacologically (intravenous thrombolytic therapy), mechanically (balloon angioplasty), or surgically (bypass surgery).

Coronary balloon angioplasty is one of the most important achievements of interventional cardiology in the last century. It is a minimally invasive procedure in which, under angiography guidance, a catheter is advanced to the occluded arterial segment and a balloon is inflated in order to allow reflow of blood to the heart muscle. The first human coronary balloon angioplasty was performed by Andreas Gruentzig in 1977.[19] Since then, balloon angioplasty has become the standard and most commonly preformed revascularization procedure in the world. Initially the revascularization procedure was referred to as percutaneous transluminal balloon angioplasty (PTCA), however , due to advances in endovascular device technology the revascularization procedure is referred to today as percutaneous coronary intervention (PCI), a broader term reflecting the various intervention procedures that can be performed in an endovascular approach. The most common intervention includes the implantation of a balloon-expandable, stainless-steel, slotted tube ("stent") at the site of a coronary stenosis.

The problem of post-angioplasty restenosis should be separated from the problem of in-stent restenosis. Post-angioplasty restenosis refers to the luminal loss following balloon angioplasty without stent implantation. However, most procedures today include stent implantation, and the major challenge is the problem of in-stent restenosis. These two problems are discussed separately.

❖ *Post-angioplasty restenosis*

During angioplasty, overdistension of the diseased vessel causes endothelial disruption, internal elastic lamina fracture, and medial dissection. Restenosis of treated arteries following balloon angioplasty is the principal cause of failure of revascularization in about 30-50% of the patients.[20] Although there is no clear definition, restenosis can be defined as >50% diameter stenosis at follow-up angiography. The prognosis of early coronary restenosis is generally benign. Although patients with untreated lesions may experience acute MI and death due to plaque rupture, restenosis generally presents as a gradual recurrence of anginal symptoms, permitting adequate time for evaluation and retreatment. [21]

Restenosis is the result of the trauma to the dilated artery and involves several factors, including thrombus formation, elastic recoil of the dilated artery, vascular remodeling, proliferation of VSMC and endothelial regeneration.

1. Thrombus formation

In pig coronary arteries, injury caused by distension with an oversized stent initially causes thrombus formation, followed within a few days by significant macrophage and lymphocyte infiltration and finally by smooth muscle cell migration and proliferation in the intima.[17] Leukocyte infiltration is also common in hypercholesterolemic rabbit arterial lesions but not in rat lesions. Anticoagulation and anti-platelets therapy during balloon angioplasty can minimize the contribution of thrombus formation to the problem of arterial restenosis.[22]

2. Elastic recoil

Elastic recoil is not an active process, and refers to the immediate loss in luminal diameter after dilatation with balloon angioplasty.[23] Ardissino et al. demonstrated that the elastic properties of the dilated vessel do not influence the active process of restenosis. However, they concluded that because elastic recoil negatively influences the initial results of angioplasty, further reductions in lumen diameter during follow-up can reach restenosis threshold.[24] The implantation of a stent following angioplasty almost completely eliminates the decrease in vessel dimensions caused by elastic recoil. [25] Thus, in the era of stent implantation the major challenges are other processes involved in restenosis.

3. Vascular remodeling

Vascular remodeling, sometimes called "chronic recoil", refers to the chronic constriction of the arterial lesion site in the weeks and months following balloon angioplasty. Lafont et al. demonstrated in a rabbit model of restenosis that late residual stenosis correlated with chronic constriction (evaluated histologically) but not with neointimal-medial growth or adventitial growth, and concluded that arterial remodeling rather than VSMC proliferation dominates the vascular response to angioplasty.[26] Kakuta et al., using a similar rabbit restenosis model also concluded that differences in compensatory enlargement, not neointimal formation, accounted for restenosis.[27] Studies in porcine and human models confirmed the important role of chronic adventitial processes and vascular remodeling in post-angioplasty restenosis.[28-30] There are investigators who believe that VSMC proliferation is not the major contributor to post-angioplasty luminal loss, and that vascular remodeling as well as other processes are more important in post-

angioplasty restenosis.[17] However, since vascular remodeling can be prevented with stent implantation, proliferation of VSMC is believed to be the major challenge of preventing in-stent restenosis in the stent era.

4. VSMC proliferation

Normal adult arteries have a very thin intima that develops spontaneously after birth. Atherosclerotic arteries have a thicker and more complex intimal layer. The term "neointima formation" refers to the formation of a large intimal layer in response to arterial injury. [17] The process is most likely a non specific arterial response to injury (similar to fibrosis formation in response to dermis injury in the skin). The neointima is composed of proliferating VSMC of monoclonal or oligoclonal origin.[17] In an excellent review focused on the arterial intima, Schwartz et al. describe VSMC proliferation as a four steps process[17]:

Step 1 - Medial smooth muscle cell proliferation within 24 hours following the injury. This step is believed to be the result of basic fibroblast growth factor (bFGF) release from dying VSMC.[31]

Step 2 - Smooth muscle cells migration across the internal elastic lamina as soon as 4 days after the injury in rat model and proliferation in the neointima.[32]

Step 3 - VSMC closest to the lumen may replicate for weeks and months. However, in spite of cell replication the proliferation rate decreases and is matched by cell loss. Thus, the damaged artery can exist in a stable state.[33]

Step 4- The neointima can be stimulated to show a further increase of replication by growth factors or other molecules.[34] This increased responsiveness was described by Schwartz et al. as the fourth step.

Endothelial regeneration

Endothelial integrity and regeneration are an important aspect of restenosis pathophysiology. Jamal et al. demonstrated that even severe medial injury does not lead to intimal proliferation in the absence of endothelial denudation,[35] Clowes et al. demonstrated that in areas without endothelial recovery VSMC actively proliferate even one year after angioplasty damage in rat model. They concluded that the regeneration of the endothelium inhibits proliferation of the underlying neointimal cells.[32,33] In fact, lack of endothelial regeneration was suggested as the reason for the failure of several anti-restenosis strategies.[36-38]

❖ *In-stent restenosis*

The processes involved in post-angioplasty restenosis include thrombus formation, elastic recoil, vascular remodeling, VSMC proliferation and endothelial recovery. As discussed above, elastic recoil and vascular remodeling contribute significantly to post-angioplasty restenosis. However, most angioplasty procedures today involve stent implantation. The stent, a balloon-expandable stainless-steel slotted tube, provides a firm scaffold. It achieves larger post-procedural lumen dimensions by withstanding acute elastic recoil. In addition, stents appear to reduce restenosis by resisting chronic arterial remodeling forces. However, despite the advantages of the stent, restenosis remains a significant problem, with in-stents restenosis rates of 10-20% in bare-metal stent lesions.[39]

The pathophysiology of in-stent restenosis involves the same processes that were described for post-angioplasty restenosis. The main difference of in-stent restenosis is the major contribution of neointima tissue proliferation to late luminal loss, with minor contribution of vascular remodeling. Hoffmann et al. evaluated 115 bare-metal stents lesions using intravascular ultrasound, and found that the minimum lumen diameter increased from 1.13±0.65 mm before intervention to 3.19±0.51 mm after intervention. At follow-up, the minimum lumen diameter decreased to 2.13±0.82 mm. In addition, their study showed that late lumen loss within stents correlated strongly with tissue growth (neointimal tissue accumulation) and only weakly with stent recoil. [40] As for chronic stent recoil - Painter et al. demonstrated using intravascular ultrasound that that late recoil of stents rarely occurs, and when it does occur, late stent recoil is minimal.[41] It seems that the stents efficiently resist the vascular remodeling forces of the treated artery.

Thus, in contrast to post-angioplasty restenosis, VSMC proliferation and neointima formation are the major challenge of in-stent restenosis therapeutic approaches. A discussion of the various restenosis therapeutic approaches follows.

4. Restenosis therapy approaches

Different methods to prevent or attenuate post-angioplasty restenosis have been suggested. The common target in all of these methods is the local vascular smooth muscle cells (VSMC) population at the site of the vessel wall injury. These methods include, among others: cryoplasty, brachytherapy, photodynamic therapy, drug-eluted stents and genetic manipulations using molecular vectors.

❖ *Cryoplasty*

This method is based on the fact that low temperatures induce cell death. Yiu et al.[42] have demonstrated that super cooling of smooth muscle cells to -10 ºC for 10, 60, or 120 seconds and then re-warming back to 37 ºC induces apoptosis without evidence of necrosis. This method has already been evaluated in humans for femoro-popliteal artery disease, using PolarCath balloon (Boston Scientific, Natick, MA). An initial report in 15 patients with stenosis of the superficial femoral artery demonstrated an 18-month patency rate of 83.3%.[43] A following prospective multicenter registry reported 9-months clinical patency rate of 82.2% for all lesions in 102 patients with claudication symptoms.[44,45] Tanguay et al.[46], using even lower temperatures have shown that cryoenergy can reduce arterial remodeling following carotid artery balloon angioplasty.

❖ *Brachytherapy*

Localized ionizing radiation (brachytherapy), with ß or γ sources, has shown some promise in randomized clinical trials to reduce the recurrence of in-stent restenosis.[47-49] Radiation therapy can be used as a preventive modality by preceding or following arterial wall injury, and treatment takes several minutes.[50] It has also shown benefit in a continuous mode with low-dose radioactive endovascular stents.[51] Radiation therapy, however, has been associated with logistical issues and clinical events such as late thrombosis and edge restenosis, due to incomplete vessel healing caused by delayed re-endothelialization.[37,38,36] The problem of late thrombosis can be solved by prolonged antiplatelet therapy. However, the main limitation is still the so-called 'edge effect' (high neointima formation at the border to the irradiated segment).[52]

❖ *Photodynamic therapy*

Photodynamic therapy has emerged as another treatment of vascular lesions associated with injury and atherosclerotic plaque.[53,54] Intravascular PhotoPoint PDT (Miravant Medical Technologies, Santa Barbara, California, USA) is a newly developed proprietary catheter-based system for photo-selective delivery of a non-ionizing, non-thermal energy source of visible light to activate a photosensitizer localized to the artery wall. The light generates reactive oxygen species, which inhibit smooth muscle cell proliferation. Waksman et al. demonstrated that intracoronary photodynamic therapy reduces intimal proliferation without suppressing re-endothelialization in a porcine model of restenosis.[53]

❖ *Drug-eluting stents*

Drug-eluting stents provide sustainable local delivery of an antiproliferative agent (Sirolimus or Paclitaxel) at the site of vessel wall injury. The sustainable release of anti-mitotic drugs prevents proliferation and migration of VSMC, dramatically reducing intimal hyperplasia and arterial restenosis. [55-58] A discussion focusing on drug-eluting stents and their clinical benefits is beyond the scope of this introduction.

Economic burden and safety issues are the main concern with drug-eluting stents.[59] Recent publications have raised concern regarding the safety of this method, mainly due to high rates of late in-stent restenosis.[60,61] However, large meta-analysis of 38 clinical trials concluded that the risks of mortality associated with drug-eluting and bare-metal stents are similar, and that Sirolimus-eluting stents seem to be clinically better than bare-metal and Paclitaxel-eluting stents.[62] In addition, drug-eluting stents are inferior

to an open heart coronary bypass surgery in the case of three-vessel disease or left-main disease mainly due to higher rates of revascularizations.[63]

❖ *Local molecular therapies*

The potential of DNA-based modalities to attenuate post-angioplasty restenosis is based on the ability to deliver small molecular vectors into vascular smooth cells cytoplasm in the local site of vessel wall injury.

One possible molecular therapy is to artificially increase the local expression of molecules that prevent restenosis or support arterial healing. Makinen et al.[64] demonstrated that delivery of vascular endothelial growth factor (VEGF) to human lower limb artery increased vascularity following angioplasty. VEGF is a molecule with strong angiogenic properties and plays an important role in vascular healing following stent implantation.[65] However, Hedman et al.[66] failed to show any reduction in restenosis following intracoronary VEGF transfer after balloon angioplasty. Another example is the study by Janssens et al. , in which human endothelial nitric oxide synthase gene transfer inhibited neointima formation.[67]

Another possible molecular therapy is silencing the expression of molecules that have an essential role in vascular smooth muscle cell proliferation. Aubart et al. designed siRNA molecules that specifically silence an important protein of VSMC proliferation. The siRNA molecules were introduced to VSMC using an adenoviral vector, and reduced neointimal formation in a carotid rodent model.[68] In a different experiment three different siRNA molecules were used to silence the expression of endothelial adhesion molecules expression, an important step in the process of graft restenosis. [69]

❖ *Endothelial progenitor cells based therapies*

Circulating endothelial progenitor cells (EPCs) play an important role in repair of injured vascular endothelium and neovascularization. Increase in the number of EPCs, induced by cell transfusion or enhanced mobilization, can enhance restoration and integrity of the endothelial lining and suppress neointimal formation.[18] By isolating EPCs from rabbit peripheral blood, He et al. demonstrated in a rabbit model of carotid artery denudation, that the administration of autologous EPCs accelerated endothelialization and significantly improved endothelium-dependent relaxation when assessed 4 weeks after denudation. The cells were incorporated to the vessel wall , contributed to the recovery of the endothelium ,and did not damage the contractile function of the smooth muscle cells.[70] In another study, Kong et al. injected granulocyte-colony stimulating factor (G-CSF) to recruit circulating EPCs following rat carotid artery balloon angioplasty. Neointima thickness was reduced by approximately 60% in the G-CSF–treated animals compared with control animals at 2 and 4 weeks after injury. The authors concluded that cytokine-induced EPCs mobilization might be a suitable therapeutic strategy for prevention of restenosis after revascularization procedures.[71]

❖ *Pharmacologic therapies*

In addition to local ablation of VSMC, clinical trials are also investigating the possibility of restenosis attenuation using systemic drugs. The renin-angiotensin system was of a special interest, but clinical trials with ACE inhibitors failed to inhibit restenosis in humans.[72,73] Another candidate was Octreotide, which is a somatostatin analogue with antiproliferative properties on smooth muscle cell growth in vitro. However, clinical trial with three weeks of Octreotide treatment failed to reduce restenosis rate after coronary

angioplasty in humans.[74] Heparin was also evaluated in clinical trials, but similar to other candidates, failed to attenuate restenosis.[75]

5. Challenges in designing an endovascular IRE device

In designing a prototype for endovascular IRE, many challenges needed to be addressed. This section will present the major challenges that were encountered during the design and testing of the first successful endovascular IRE device:

❖ *No thermal damage*

One of the most important aspects of IRE is its ability to damage only the cell's membrane. In order to achieve this goal it is important to prevent significant heating that will cause protein denaturation. Applying electric field to biological tissue is bound to create Joule heating effect, but with short pulses (microseconds) and low frequencies (1-10 Hz), the amount of heat created is low and can be balanced with physiological heat conduction and convection. The study of Davalos, Mir and Rubinsky [3], which showed that IRE can ablate substantial volumes of tissue without inducing a thermal effect and therefore serve as an independent and new tissue ablation modality, opened the way to the use of IRE in surgery. However, no simulation has yet addressed the problem of endovascular IRE application. When planning an endovascular IRE device, the challenge of avoiding thermal damage can be resolved by using the finite element method in order to find those IRE sequences that do no induce thermal damage. For more details, see the solution of the problem in chapter II.

❖ *Minimally invasive and small*

Angioplasty procedures are done in a minimally invasive manner, with the device inserted into the arterial vasculature through a small incision in the artery or vein's wall (the most common sites are the femoral artery followed by the radial artery). The introducers through which the device is inserted are usually 4F-7F (4/3 mm - 7/3mm) in diameter ,and the device must be small enough in order to pass through the introducer.

Treated arteries are usually 2 mm in diameter or more, and therefore the device needs to be small but also expandable. Therefore, all suggested prototypes include an inflatable balloon, with expandable electrodes attached to its outer surface.

❖ *High voltage and high current*

One of the fundamental properties of IRE is the application of high electric field, which translates to a combination of high potential difference together with closely located electrodes. For prototypes described in Chapter II, potential difference range was between 350 and 600 volts, with electric current in the range of 5 to 20 amperes. Thus, although the device needs to be small enough, it also has to stand high current density across the electrodes.

❖ *Small distance between electrodes*

One way to reduce potential difference, and thus current density through the electrodes, is to decrease the distance between device electrodes. However, the smaller the distance between the electrodes, the more complex and delicate is the device.

❖ *Maximize damage to VSMC*

The target of the endovascular IRE device is the VSMC population of the vessel wall. The vessel wall is tri-laminar, and the VSMC are located in its second layer. The effective thickness of the Tunica Intima and Tunica Media combined is approximately 200 μm in rabbit iliac arteries, and similar dimensions are found in major human coronary arteries.

Any electrode configuration has to have an electric field distribution that will induce IRE in the first 200 μm surrounding the electrodes. The challenge becomes even harder for diseased human coronary arteries where the thickness of the vessel wall is larger due to atherosclerotic plaque as well as, in some cases, acute thrombosis.

❖ *Allow re-endothelialization*

The endothelium is any important component of the vessel wall. One of the central functions of the vascular endothelium is to maintain blood fluidity. Under physiological conditions, this occurs through the production of factors that inhibit blood coagulation.[76] Following angioplasty damage, complete endothelial recovery can occur within 7 days. [77] However, some of the approaches for attenuating post-angioplasty restenosis continuously apply insult to the vascular endothelium and VSMC populations. This insult is hypothesized to have an important role in late thrombosis.[36,61]

Therefore, endovascular IRE device should be used in a single-use preventive mode, without continuous insult to the vessel wall. This approach will allow permanent ablation of the entire VSMC population, while the remaining vessel wall scaffold will serve as the

basis for endothelial repopulation by adjacent and/or circulating endothelial progenitor cells.[78,70]

II. CHAPTER TWO: THEORETICAL FEASIBILTY OF ENDOVASCULAR IRE

An electric field applied across biological tissue is bound to induce a Joule heating. This chapter examines how the Joule heating thermally affects the vessel wall, and whether it is feasible to apply multiple electroporation pulses without inducing significant thermal damage. The chapter begins with the mathematical equations and continues with comparing three possible endovascular electrodes designs. Next, it describes the time-dependent finite element solution of the problem. The last sections of the chapter describe the results of the finite-element solution to the complete problem, and discuss its meaning and significance.

1. Mathematical equations

The problem is modeled as two or three-dimensional, depending on the complexity of the device geometry. An endovascular IRE device is located in the center of the geometry, surrounded by infinitely large biological homogenous isotropic tissue (for more details see 2 below). Electrical, thermal and biological parameters that are used in this analysis are summarized in Table II-1.

Quantity	Symbol	Units	Value	Ref.
Tissue electrical conductivity	σ	[S]/[m]	0.6	[79]
Tissue thermal conductivity	K	[W]/[m] [K]	0.5	[15]
Tissue heat capacity	Cp	[J]/[Kg] [K]	3750	[15]
Tissue density	ρ	[Kg]/[m^3]	1000	[15]
Blood heat capacity	C_b	[J]/[Kg][K]	3640	[15]

Blood density	1080	[Kg]/[m^3]	1000	[80]
Blood perfusion rate	ω_b		0.0001	[81]
Electroporation pulse duration		[msec]	0.1	[82]
Molecular collision frequency	A	1/[sec]	$5.6x10^{63}$	[83]
Energy Barrier	E	[J]/[mole]	$4.3x10^5$	[83]
Electrode conductivity	σ_e	[S]/[m]	$4.032\ x10^6$	
Electrode thermal conductivity	K_e	[W]/[m] [K]	100	
Initial temperature	T_0	[K]	310.15	
Gas Constant	R	[J]/[mole] [K]	8.13	

Table II-1 - Biophysical constants used in the numerical simulation

The governing equations (electric field and bio-heat transfer) with a solution for a single electroporation pulse were described elsewhere with needles and with parallel plates geometries.[15,84] In brief, the Joule heating is evaluated by solving the Laplace equation for potential distribution:

$$\nabla(\sigma\nabla\varphi) = 0 \qquad (1)$$

$$p = \sigma|\nabla\varphi|^2 \qquad (2)$$

where φ is the electric potential (volts), σ is the electrical conductivity (S/m) and p is the heat generation rate per unit volume (W/m^3). The heating of the tissue resulting from electroporation can be calculated by adding the Joule heating source term to the Pennes bio-heat transfer equation:

$$\nabla(k\nabla T) + \omega_b c_b(T_a - T) + q + \sigma|\nabla\varphi|^2 = \delta\rho c_p \frac{\partial T}{\partial t} \qquad (3)$$

where k is the thermal conductivity of the tissue (W/m K), T is the absolute temperature, ω_b is the blood perfusion rate (s^{-1}), c_b is the heat capacity of the blood (J/Kg K), Ta is the

arterial temperature , q is the basal metabolic heat generation (W/m^3), ρ is the tissue density (Kg/m3) and c_p is the heat capacity of the tissue (J/Kg K).

Using the transient temperature solution of equation (3) , a kinetic model of thermal damage base on the Arrhenius formulation can be used.[85] The model calculates the Henriques and Moritz thermal damage integral:

$$\Omega(t) = \int A e^{-\frac{E}{RT}} dt \qquad (4)$$

where T is the transient temperature from equation (3) , Ω is a dimensionless indicator of damage, A is a measurement of molecular collision frequency (s^{-1}), E is an energy barrier that molecules surmount in order to denature (J/mole), R is the gas constant (J/mole-K) and t is the time (s). The values of A and E are unique and are based on experiments in different tissue evaluating different kinds of damage. Our analysis is based on values of A and E that are appropriate for thermal damage of human arterial tissue.[83] Ω can be calculated for specified location in the domain, Ω(x,y,z), for the maximal temperature in the domain, Ω_{max}, or for the average temperature of any dub-domain, $\Omega_{average}$.

Electroporation pulses are discrete square DC pulses of length t_1, with a pulse frequency rate of f. Thermal damage analysis takes into account both the resistive heating during the pulses, as well as the time interval with no resistive heating between the pulses. For multiple pulse electroporation protocols, the problem is solved separately for each time interval (either pulse or inter-pulse pause), with the transient solution at the end of the time-interval used as the initial condition for the next time-interval:

$$\Omega(t) = \sum_{i=0}^{N-1} \left(\int_{i\tau}^{i\tau+t_1} Ae^{-\frac{E}{RT}} dt + \int_{i\tau+t_1}^{i\tau+t_1+t_2} Ae^{-\frac{E}{RT}} dt \right) \quad (5)$$

where N is the total number of electroporation pulses, t_1 is the pulse duration interval, t_2 is the time interval between the end of the pulse and the beginning of the next pulse, and τ is the sum of t_1 and t_2. The frequency of the electroporation protocol is defined as:

$$f = \frac{1}{\tau} \quad (6)$$

Boundary conditions

The problem was modeled as a hollow tube (artery) inside a large homogenous tissue block, with the endovascular electrodes located on the inner surface of the hollow tube. For the electric potential equation, the electrodes were represented by a fixed voltage (Dirichlet) boundary condition, with one electrode having a positive potential and the other one set to zero:

$$\varphi_1 = V_0 \quad (7)$$

$$\varphi_2 = 0 \quad (8)$$

where Vo is the potential difference (volts) applied across the electrodes during the electroporation pulses. Zero electric flux (Neumann) boundary condition was applied at all the boundaries of the model not in contact with the electrodes:

$$\frac{\partial \varphi}{\partial n} = 0 \quad (9)$$

For the bio-heat equation, initial temperature in the entire domain was set to the physiologic temperature (273.15°K). The boundaries along the hollow tube were taken to

be adiabatic (Neumann) boundary conditions to predict the maximal temperature rise along the arterial wall:

$$\frac{\partial T}{\partial n} = 0 \qquad (10)$$

The outer surface of the large tissue block was defined as constant physiological temperature (Dirichlet) boundary condition:

$$T = 293.15°K \qquad (11)$$

The next two sections will show in details how the above equations are used in order to solve the problem for two different three dimensional geometries, using COMSOL Multiphysics (version 3.5a) and Matlab (version 2008b, for full script see Appendix I) . At the end of the solution, one has a quantitative estimate of the amount of thermal damage to the vessel wall. The estimate is based on the value of Ω. The physical meaning of the value of Ω will be discussed in the results section of this chapter (see section 4 below).

2. Device geometries

The solution of the heat transfer problem can give variable solutions, depending on the electrodes geometry. This section will describe three alternative electrode prototype designs that were considered during the research, and will emphasize the advantages and disadvantages of the different designs. All three designs have the following properties in common:

1. The artery is modeled as a 2.5 millimeter hollow tube of biological tissue. This is an average diameter of rabbit iliac artery, which is the animal model being used in this research work.
2. Electrodes in all three designs are expandable or flexible. This property is important for the use of these designs in an endovascular , minimally invasive approach.
3. All designs have at least two electrodes. Electric field is applied in the space between the electrodes.
4. Electrodes are in direct contact with the vessel wall and are insulated from the arterial lumen space.
5. Electrodes have an effective treatment length of 2 centimeters.

❖ *Prototype A - longitudinal silver-coated balloon*

The longitudinal design (Figure II-1 and Figure II-2) was one of the first prototypes considered. Its main advantage is the simplicity of its design. It is composed of two electrodes on the surface of inflatable balloon. The electrodes are made out of silver-coated ink, few hundred microns in thickness, and are highly conductive. Each of the electrodes has two isopotential longitudinal "legs". The end result of the geometry is four longitudinal electrodes , two of them with $\varphi=V_0$ and two with $\varphi=0$, with one "leg" every 90 degrees. The inner surface of the electrodes is in contact with an inflatable balloon that is serving as an electric insulator. The main problem with this geometry is a non-uniform electric field ,and therefore areas of relatively high temperature during the application of electroporation pulses (see results in section 4 below). Although most of its geometry is

longitudinal, all four "legs" have a round shape head in the area of treatment, and therefore this geometry is modeled as a three dimensional one.

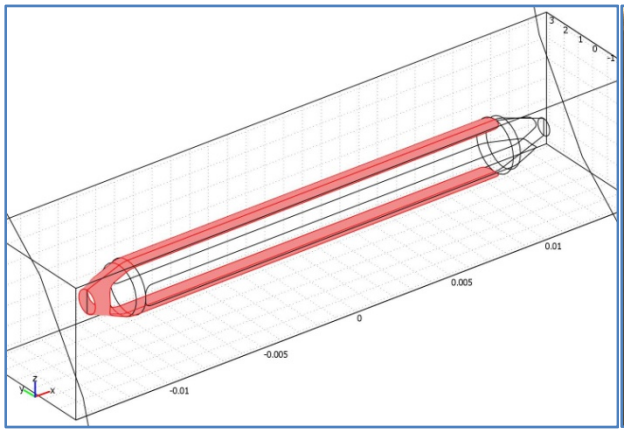

Figure II-1 - Geometry of prototype A showing the two ground electrodes in pink color. The two other electrodes are transparent in this drawing. Length of the device is 2cm.

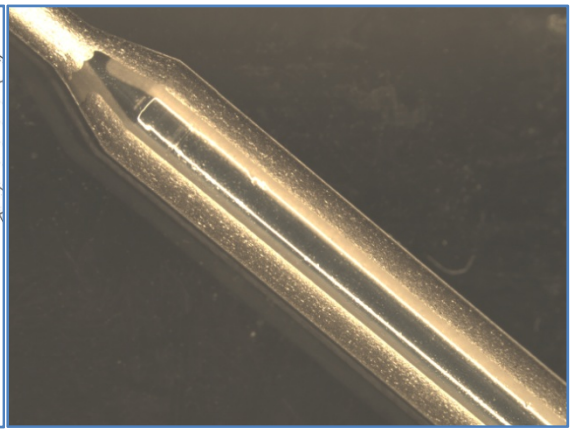

Figure II-2 - Real picture of prototype A showing an angioplasty balloon with sliver coated ink electrodes on its outer surface (Assembled by Jim Mitchell, Angiodynamics Inc., Queensbury , NY)

❖ *Prototype B - helical silver-coated balloon*

Prototype B is a helical design (Figure II-3 and Figure II-4) with some similarities to prototype A. It is also based on silver-coated ink electrodes on top of an inflatable balloon. This design, however, has two helical electrodes. Electrodes are 1 millimeter in width, and the distance between adjacent electrodes is also 1 millimeter. One electrode is with electric potential $\varphi=V_0$ and the other is with $\varphi=0$. The inner surface of the electrodes is in contact with an inflatable balloon that is serving as an electric insulator. The main advantage of this geometry is a highly uniform electric field across the vessel wall (see results in section 4 below). The main problem with this design was in the implementation - it failed in real life experiments due to problems discussed in chapter VI. Due to its complex geometry this problem is modeled as a three dimensional one.

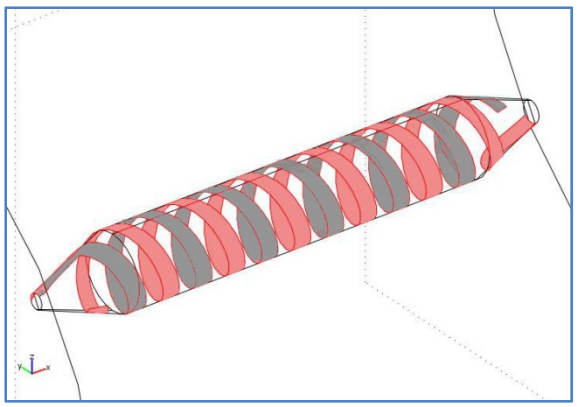

Figure II-3 - Geometry of prototype B - Geometry of prototype B showing the one helical electrode in pink and the other in gray. Length of the device in 2cm.

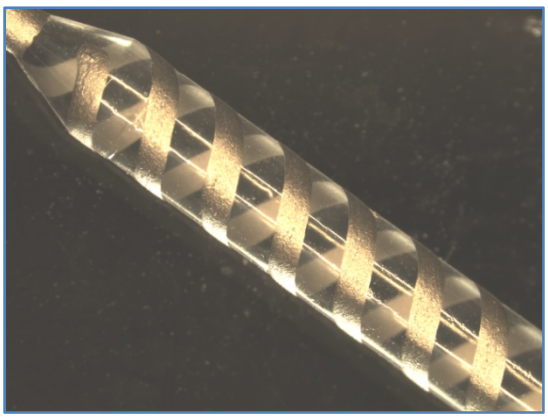

Figure II-4 - Real picture of prototype B showing an angioplasty balloon with sliver coated ink electrodes on its outer surface. (Assembled by Jim Mitchell, Angiodynamics Inc., Queensbury , NY)

❖ *Prototype C - flexible nitinol cage*

Prototype C (Figure II-5 and Figure II-6) is composed of four flexible Nitinol (Nickel titanium (NiTi)) electrodes. The electrodes can be retracted into a flexible tube. Once introduced into the arterial lumen, the electrodes can be easily expanded by pushing them forward out of the flexible tube. The analysis focuses only on the expanded geometry, in which all four electrodes have direct contact with the vessel wall. The geometry of this design is similar to prototype A: four electrodes, two with electric potential $\varphi=V_0$ and two is with $\varphi=0$, alternating every 90 degrees. An inflatable balloon is located in the inner space between the electrodes, and serves as an electric insulator. The electrodes are insulated at the edges, are exposed only in the central 2 centimeter area that is in direct contact with the vessel wall. Due to its simple geometry, this prototype can be modeled as a two dimensional problem, where the vessel wall and the electrodes are modeled as an infinitely long tubes.

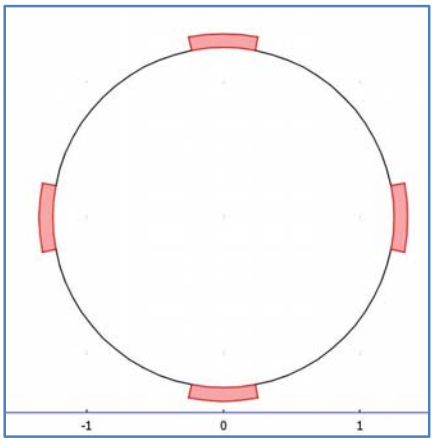

Figure II-5 - Two dimensional geometry of prototype C. This is the geometry that was used in the numerical analysis

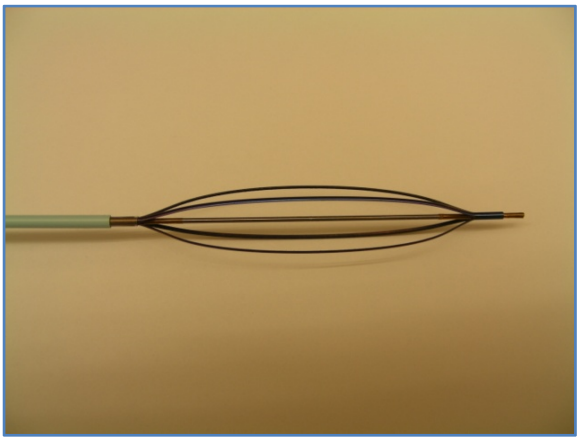

Figure II-6 - Real picture of prototype C in its inflated state. The four legs are 2 cm in length. (Assembled by Jim Mitchell, Angiodynamics Inc., Queensbury , NY)

3. Solving the finite-element problem

IRE is applied using short square pulses, with frequencies ranging between 1 and 10 Hz. Number of pulses can range from a single pulse to 100 pulses. Although pulse length can also vary, this analysis focuses only on 100 μsec pulses. Device geometry, pulses number, pulse frequency and potential difference between the electrodes (V_0) are varying parameters.

The complete Matlab script for solving the problem can be found in Appendix 1. The function calculated the maximal and the average values of Ω in the vessel wall based on the following parameters: the geometry (*fem*), the potential difference (*V0*), the frequency which is given as the time interval between consecutive pulses (*pauseLength*), and the total number of pulses applied (*pulseNumber*).

The script is based on a COMSOL object that includes the geometry, the finite element mesh, domain properties and boundary conditions. The COMSOL object is exported to Matlab, and the following steps are taken:

❖ *Electric Field Solver*

The first step of the numerical solution is solving the Laplace equation for potential distribution. The solution for this equation is static and not time-dependent. The electrodes are modeled as electric conductor (steel, $4x10^6$ [S/m]) , and the tissue is modeled as an isotropic biological tissue with constant and isotropic electric conductivity of 0.6 [S/m] (a more 'realistic' solution, with different conductivity in the longitudinal versus the radial axis[86], had a minor influence on the overall result). There are two important aspects to the solution:

1. The solution of the problem gives a resistive-heating value in units of [W/m^3] for each element in the biological tissue domain. These values are used in the time-dependent solver of the heat equation below.

2. The solution gives the values of the electric field magnitude in [V/m] in the tissue surrounding the electrodes. With higher potential difference, larger areas around the electrodes are exposed to IRE. For a details discussion of the results , see section 4 (Results, below).

❖ *Transient Heat Transfer Solver*

The numerical solution of the problem is based on multiple time-dependant finite-element solver iterations. The iterations alternate between a resistive-heating pulse interval and inter-pulse intervals. The temperature is increasing during the pulse due to resistive heating, and then decreases due to heat conduction within the biological tissue.

The solver uses the same geometry that was exported from COMSOL, with the resistive-heating values of the electric field solution already stored. It starts by solving a 100 µsec

interval with heat generated due to resistive heating. The solution is used as the initial condition for the inter-pulse interval, where no resistive-heating is generated.

The number of iterations and the length of the inter-pulse interval (i.e. the frequency) be changed using the Matlab script.

After the last iteration, an additional interval of 3 minutes is added to the solution. This interval includes no resistive heating, and it is added to the simulation in order to account for the entire thermal damage due to IRE treatment.

❖ *Thermal Damage Integral (Ω) calculation*

The temperature values at the end of each iteration and at every second in the 3 minutes following the last pulse are stored in memory. Two values are stored for each time point: the maximal temperature in the biological tissue domain, and the average temperature in the first 200 micrometers of the biological tissue domain. These first 200 micrometers ring corresponds to the vessel wall.

Using a numerical integration , the Arrhenius equation is integrated over time to yield the value of Ω. The solution gives two values:

1. Maximal Ω - corresponds with thermal damage in areas with highest temperature.
2. Average Ω - corresponds with average thermal damage within the vessel wall.

4. Results

The results are presented separately for the three prototype. Since the results of the numerical simulation of prototypes B and C were superior compared with prototype A

(with respect to electric field distribution) , more finite-element simulations are presented with these two prototypes.

For all three prototypes, four assumptions were included when solving the numerical problem:

1. **The minimal electric field for successful IRE ablation is 1,750 [V/cm]** - This assumption is based on the results of Chapter IV, where it was demonstrated that 90 electroporation pulses with electric field of 1,750 V/cm caused ablation of 94% of the VSMC population in the vessel wall.
2. **Ablated area should in include the first 250 μm around IRE balloon** - This assumption is based on anatomical properties medium-sized arteries (human carotid arteries, rabbit iliac arteries etc.), and includes only the *Tunica intima* and *Tunica media*.
3. **The potential difference between the electrodes is limited** - This assumption is based on ex-vivo measurements of the maximal potential difference possible before the conductor fails (experiments done in agar gel with electric resistivity similar to that of biological tissue). This is especially true for the first two prototypes, where the thickness of the silver-coated ink is around 100 μm, and both devices failed with potential difference of 400 V.
4. **Amount of heat generated by the electrodes in negligible** - Compared with the resistivity of the biological tissue around it, the resistivity of any electrical conductor is very small. Numerical solutions as well as analytic solution of much simplified versions of the problem show that the heat generated due to Joule

heating within the electrodes is negligible compared with that generated within the biological tissue.

There are many ways to present the data. Most of data presented will include either spatial electric field distribution (static solution) or the spatial temperature as a function of time (transient solution). Colored plots of 2 or 3 dimensional isosurfaces were created using the post-processing option of COMSOL Multiphysics version 3.4, while in other cases temperature values were exported to Microsoft Excel in order to present the multiple (parametric) solutions in a single X-Y plot.

❖ *Prototype A - longitudinal silver-coated balloon*

This four "legs" configuration was one of the earliest prototypes examined. A representative solution of the electric field problem (Equation 1) is shown in Figure II-7 for ΔV=350 V. The figure demonstrates the main disadvantage of this prototype: with potential difference of 350 volts the electric field values in the vessel wall range between 300 V/cm and 700 V/cm. There is relatively large electric field range with most electric field concentrated in volume around the edge of the "legs", while in the rest of the vessel wall volume electric field values are lower (too low for IRE effect).

Due to lack of electric field homogeneity compared with the two other prototypes, it was decided not to pursue additional numerical simulation of this model.

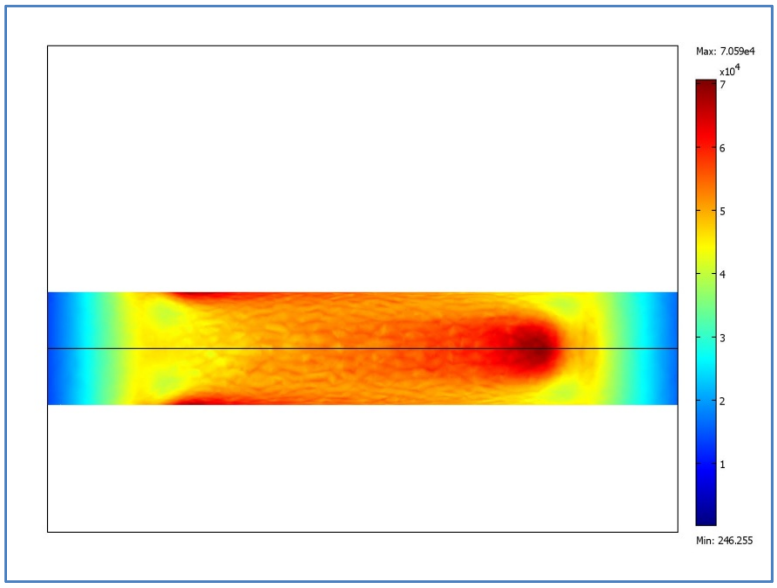

Figure II-7 - Electric field distribution (ΔV = 350 Volts) - This is a two dimensional projection of the 3D solution to the problem with potential difference of 350 Volts. The solution in shown as an isosurface within the larger biological domain, at a distance of 250 µm away from the electrodes. Color-Scale is in units of V/m.

❖ *Prototype B - helically silver-coated balloon*

The helical prototype was considered very promising and was even used in preliminary large animal experiments described in Chapter VI. A representative solution of the electric field problem (Equation 2) is shown in Figure II-8 for ΔV=350V. As can been seen in the figure, with potential difference of 350 volts, the electric field values in the vessel wall range between 1,500 and 3,500 V/cm.

The results of the electric field simulation were encouraging, with the electric field high enough in the entire volume of the vessel wall around the balloon. All further simulations were done with ΔV of 350 volts. The next step was solving the bio-heat equation problem ,and evaluating the degree of thermal damage due to the electric field. An example of the maximal temperature behavior as a function of time is shown in Figure II-9, for 90 pulses

at a frequency of 1 Hz. The result of this simulation is acceptable in terms of the degree of thermal damage with thermal damage integral (Ω) value of 2.43×10^{-6}, significantly lower than the threshold value of 1.

Similar transient solutions were computed for higher frequencies, in order to show what is the highest frequency with acceptable value of Ω. Results are summarized in Table II-2, showing that 0.81% of native collagen molecules will be thermally damaged due to 90 pulses at a frequency of 4 Hz.

Frequency (Hz)	Maximal temperature (°C)	Damage integral (Ω)	Damaged Molecules
0.25	41.53	1.53×10^{-7}	0.000015%
1	50.99	2.43×10^{-6}	0.000243%
2	59.64	5.68×10^{-5}	0.005682%
4	72.45	0.008124036	0.809113%

Table II-2 - Thermal damage calculation for four different frequencies showing the negligible percentage of molecules damaged in all four cases. All calculation used the maximal temperature in the volume of the vessel wall, and therefore the results are to be considered "worse case" estimate of the amount of damage.

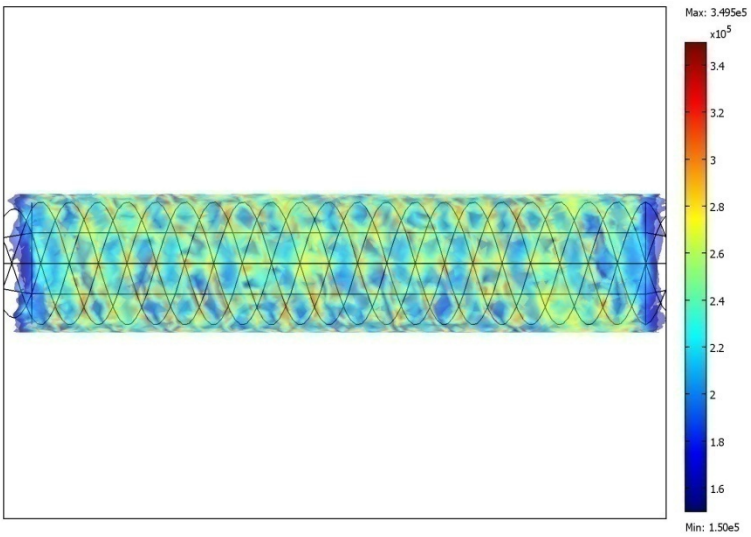

Figure II-8 - Electric field distribution (ΔV = 350 volts) - This is a two dimensional projection of the 3D solution to the problem with potential difference of 350 volts. The solution in shown as an isosurface within the larger biological domain, at a distance of 250 µm away from the electrodes. Color-Scale is in units of V/m.

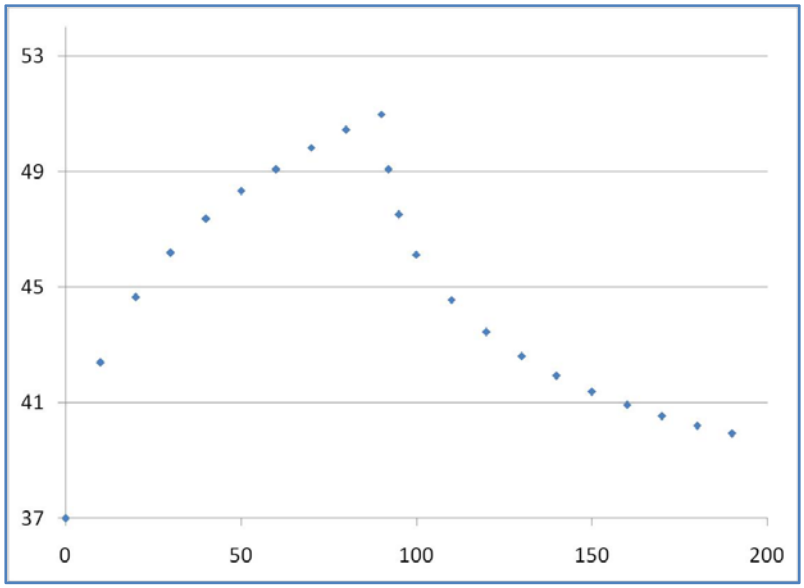

Figure II-9 - Maximal Temperature (°C) as a function of time (seconds) due to 90 electroporation pulses with ΔV=350 volts. The maximal temperature value is 51°C.

❖ *Prototype C - flexible nitinol cage*

Although prototype B was an acceptable model for endovascular IRE (from both the electric field perspective as well as from the thermal damage perspective), it failed in "real-life" experiments due to problems discussed in Chapter VI. Therefore, a third device geometry was developed and the results of its simulation are presented in this section. This device, called prototype C, was successfully used in large animal experiments.

Due to the simplicity of the device geometry, all calculations were done using a two dimensional geometry discussed above (Page 28). An example of electric field distribution due to ΔV=600 V is presented in Figure II-10, showing that all the vessel wall experience an electric field that is higher than 1,500 V/cm.

This simulation was done using ΔV=600 V, while previous two devices were simulated with ΔV=350 Volts. This is due to electric failure of the conductor in prototypes A and B as a result of its very thin thickness. The nitinol electrodes of prototype C are far more robust and did not fail even at potential differences higher than 600 Volts.

Since the potential difference was not a limiting factor for this prototype, transient solutions of the bio-heat equation were done with different values of ΔV. Maximal and average temperature in the vessel wall were calculated for each time point (see method above for details, or Appendix 1 at the end of this document) , and were compared between different possible IRE sequences. Figure II-11 is an example of the transient solution for the specific case of 90 electroporation pulses, with ΔV=600 Volts and at a frequency of 4 Hz.

For each transient solution, thermal damage integral (Ω) was calculated for both the maximal as well as for the average temperature in the domain. In accordance with our in-vivo experiments, we compared thermal damage due to 10, 50 and 90 electroporation pulses with increasing values of ΔV , up to values that were to induce significant damage. Results of the thermal damage integral (Ω) as well as the percentage of thermally damaged molecules for each IRE sequence are summarized in Table II-3. Temperature at the corners of the conductors were significantly higher, resulting a significant change between the thermal damage integral calculated with maximal temperatures vs. average temperatures, as can be seen in the table.

Sequence	ΔV	Max Ω	Average Ω	Damaged molecules (Max)	Damaged Molecules (Average)
90 pulses, 4Hz	400	9.62E-08	6.94E-08	0.000010%	0.000007%
90 pulses, 4Hz	500	9.58E-05	7.09E-06	0.009582%	0.000709%
90 pulses, 4Hz	600	1.20E-02	3.17E-04	1.187906%	0.031720%
90 pulses, 4Hz	**700**	**2.65E+00**	**2.47E-02**	**92.903098%**	**2.444067%**
50 pulses, 4Hz	400	2.19E-07	6.20E-08	0.000022%	0.000006%
50 pulses, 4Hz	500	4.81E-06	4.43E-07	0.000481%	0.000044%
50 pulses, 4Hz	600	2.28E-04	6.81E-06	0.022814%	0.000681%
50 pulses, 4Hz	700	1.87E-02	1.79E-04	1.856629%	0.017878%
50 pulses, 4Hz	**800**	**2.35E+00**	**7.11E-03**	**90.415357%**	**0.708221%**
10 pulses, 10Hz	400	2.38E-08	1.10E-08	0.000002%	0.000001%
10 pulses, 10Hz	500	1.71E-07	1.41E-08	0.000017%	0.000001%
10 pulses, 10Hz	600	3.39E-06	2.15E-08	0.000339%	0.000002%
10 pulses, 10Hz	700	1.12E-04	4.48E-08	0.011233%	0.000004%
10 pulses, 10Hz	800	5.35E-03	1.39E-07	0.533480%	0.000014%
10 pulses, 10Hz	900	3.42E-01	6.34E-07	28.987215%	0.000063%
10 pulses, 10Hz	**1000**	**2.76E+01**	**3.81E-06**	**100.000000%**	**0.000381%**

Table II-3 - Thermal damage calculation for different pulse sequences showing Ω and the percentage of damaged molecules. Calculation was performed for both the maximal as well as the average temperature in the domain.

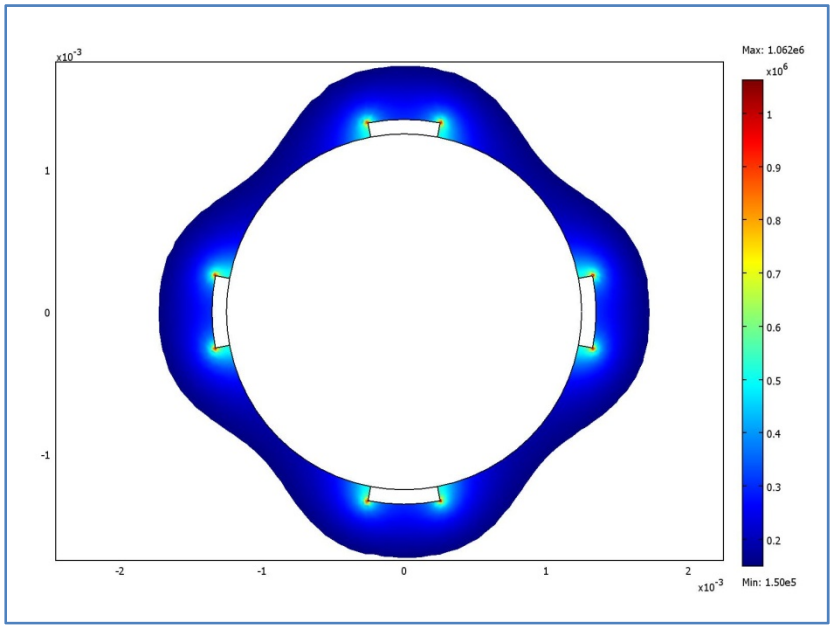

Figure II-10 - Electric field distribution (ΔV = 600 Volts) - This is the two dimensional solution of the problem presenting in color only electric field values above 1,500 V/cm. Color-Scale is in units of V/m. The figure shows that with this potential difference electric field is relatively uniform and high enough throughout the vessel wall. Note the high electric field as a result of the edge effect in the corner of the conductor.

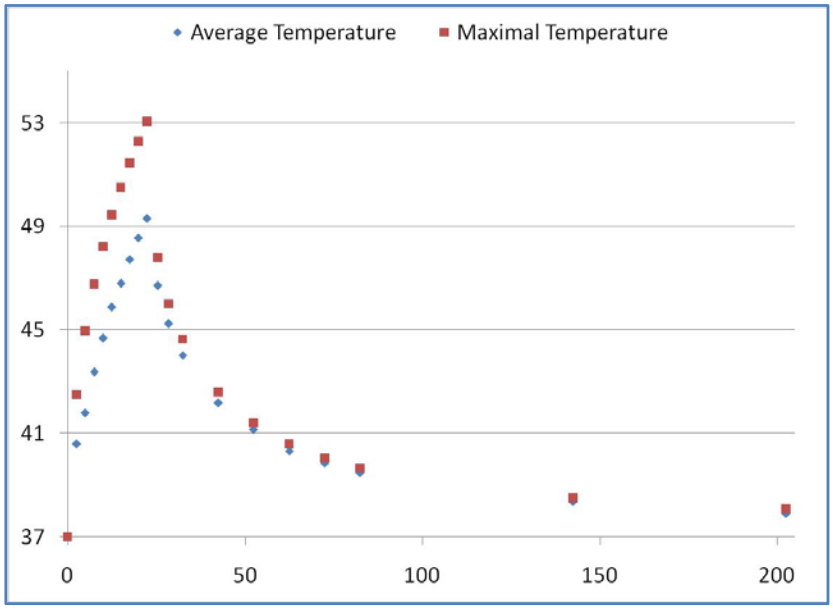

Figure II-11 - Maximal and average temperature (°C) as a function of time (seconds) due to 90 electroporation pulses with ΔV=600 volts, at a frequency of 4 Hz. The maximal temperature value is 53.1°C and 49.3°C, respectively.

5. Discussion

This chapter focused on solving the theoretical problem of endovascular IRE, and demonstrated the feasibility of non-thermal IRE.

The solution of prototype C demonstrated that 90 pulses at a frequency of 1Hz with ΔV=600 volts caused thermal damage to less than 2% of native collagen molecules in the vessel wall. These parameters, as demonstrated in Chapter IV, are high enough in order to induce IRE ablation. This result, presented here for the first time, is the theoretical background for successful large animal experiment presented in Chapter VI.

❖ *Physiologic realism and model assumptions*

When interpreting the results, one should remember that information regarding the parameters used in the simulation (biophysical constants, tissue properties, boundary limits of the heat equation etc.) was scarce, and that assumptions had to be made in order to solve the problem. In order for the solution to be applicable to *in-vivo* experiments, it was important to make "worse case" assumptions, i.e. assumptions that will always increase (and never decrease) the temperature in the vessel wall. With such assumptions, the results of the problem with respect to the maximal temperature and the thermally-safe IRE threshold can be used even with limited available data. Here are the assumptions made during the solution:

1. Tissue conductivity

Extended review of the literature failed to find data focusing on the tissue conductivity of the vessel wall. Moreover, the vessel wall is anisotropic and tissue conductivity changes

considerably during electroporation pulse application.[87] Therefore an assumption had to be made. Tissue conductivity was set to 0.6 S/m, a significantly low value, probably lower than the true conductivity of the vessel wall [79], which is made mainly of smooth muscle cells and elastic fibers. The lower the conductivity, the higher the resistive heating of the tissue. Therefore, the thermal damage values were increased using this assumption.

2. Heat Convection

The complexity of the heat transfer problem was simplified considerably. The problem was modeled as a single large isotropic cylindrical tissue domain, with constant temperature of 37°C at the outside boundary and thermal insulation at the inside boundary (balloon interface). No heat convection was included except for blood perfusion rate of 0.0001 sec^{-1} , which is a low value, probably lower than the true perfusion of the vessel wall.[81] This assumption ignores significant heat convection through the adjacent vein (for example the iliac vein), as well as blood convection through small blood vessels in the *tunica adventitia* (commonly known as *vasa vasorum*).

3. Maximal versus Average temperature

Maximal temperature of the vessel wall was used in calculating the thermal damage integral (Ω), ensuring that the amount of thermal damage is minimal even in the maximal areas of resistive heating (e.g. areas of maximal electric field, usually due to "edge effect" around corners of the conductor).

❖ *Interpreting the thermal damage integral (Ω) value*

The dimensionless indicator of thermal damage, Ω, is a function of two process parameters (molecular collision frequency and energy barrier) together with the transient analysis of temperature. In fact, Ω is the logarithm of the relative concentration of "reactants":

$$\Omega(\tau) = \ln \frac{C(0)}{C(\tau)} \tag{12}$$

where C(0) and C(τ) are the amount of native (undamaged) molecules in time zero and τ, respectively. Therefore at Ω=1, a standard point of comparison 63.2% of the molecules in the arterial wall have already been changed into damaged state. [85] Equation (9) can also be presented in a different way to describe the fraction of denaturated molecules:

$$F_d = 1 - \frac{c(\tau)}{c(0)} = 1 - e^{-\Omega} \tag{13}$$

This interpretation is based on two process parameters (molecular collision frequency and energy barrier) that are specific for the tissue discussed. The analysis in this chapter used values specific for human arterial wall tissue that were calculated based on thermal damage experiments done with human aorta.[88] The results of that experiments showed that the process parameters for aortic wall tissue are similar to those of collagen molecule (collagen is indeed a major extra cellular component of the vessel wall, and is responsible for the arterial tensile properties).

❖ *Optimal IRE protocol*

When designing an IRE protocol there are at least 6 parameters that can be changed: pulse length, potential difference, pulse frequency, number of pulses, pulse shape (e.g. unipolar square pulse) and electric field distribution (electrode configuration) .

All simulations assumed that pulses are unipolar, square and 100 μsec in length. However, different simulations were analyzed in order to explore the three remaining parameters.

From the electric field distribution perspective, prototypes B and C offered the most uniform electric field. A uniform electric field ensures that all the vessel wall will be exposed to an electric field that is high enough without areas with significant resistive heating. Due to implementations concerns with prototype B , it was decided to continue the work only with prototype C.

As for the combination of pulse number frequency and potential difference, three protocols were similarly safe:

A. 90 pulses at 4Hz with ΔV=600 volts , yielding maximal Ω of 0.012

B. 50 pulses at 4Hz with ΔV =700 volts, yielding maximal Ω of 0.0187

C. 10 pulses at 10Hz with ΔV =800 volts, yielding maximal Ω of 0.00535

Although all protocols are equally safe, protocol A uses the largest number of pulses. In-vivo experiments presented in Chapter IV demonstrated that increasing the number of pulses improve ablation efficiency even if the electric field is reduced. Therefore, as will be shown later, protocol A was chosen for large animal experiments.

III. CHAPTER THREE: IRE EFFECT ON SMOOTH MUSCLE CELLS *IN-VITRO*

1. Motivation and objectives

The most fundamental data needed for successful endovascular IRE experiments are the sensitivity of the vascular smooth muscle cell (VSMC) population to electroporation pulses. Cells can die due to different electroporation protocol parameters (i.e. electric field magnitude, pulse frequency, pulse shape, number of pulses and pulse length).

Considerable amount of data is available about the sensitivity of cancerous cells to electroporation pulses. [89-93] However, it is not clear whether IRE sensitivity of VSMC population is lower, comparable to, or higher than that of cancerous cells.

Addressing the problem of IRE threshold *in-vitro* requires a method for electroporating cultured cells with a controlled and predictable electric field magnitude.

The objective of this chapter was to develop a reliable and reproducible method for electroporation of cultured cells and to try using this method to answer the following questions:

1. How does IRE threshold of VSMC differs from the IRE threshold of cancerous cells in vitro ?
2. What is the correlation between electric field magnitude, number of electroporation pulses and the percentage of cell death ?

These questions can be answered with *in-vitro* or *in-vivo* experiments. This chapter focuses on *in-vitro* results, while the next chapter will discuss results of *in-vivo*

experiments. *In-vitro* experiments have two main advantages. First, the ability to grow cells on a two-dimensional surface, thus enabling application of controlled electric field distributions. Second, the simplicity of growing cells in culture allows multiple repetitions, increasing the number of observations and different pulse strength/number combinations investigated. In addition, *in-vitro* experiments help in creating a knowledge base that will reduce the number of animal experiments needed and thus will save animal lives.

2. Methods

❖ *Cell culturing*

VSMC from rodent aorta (ATCC # CRL-2018) were obtained from UCSF cell culture facility. Cells were cultured in DMEM (GIBCO #21063-029 , Invitrogen Corp.) supplemented with 10% fetal calf serum (GIBCO# 10091-148, Invitrogen Corp.), penicillin and streptomycin (Gibco # 15070-063, Invitrogen Corp), sodium hypoxantine thymidine (HT #11067-030 Gibco), and non essential amino acids (Gibco #11140-050, Invitrogen Corp.). Cells were re-plated in 6 wells clusters and allowed to propagate until 100% confluence was achieved.

Chinese Hamster Ovary cell line (CHO-S) was purchased from Invitrogen (Cat# 11619-012) and cells were grown in CD CHO medium in suspension (Invitrogen cat# 31033-020). Cells were centrifugated and re-suspended in DMEM with fetal calf serum. Cells were serum readapted for 4 passages (DMEM with 10%FCS as previously described). Cells were plated in 6 wells clusters and allowed to reach 100% confluence.

In the day of the experiment, cell cultures were washed with DPBS (Invitrogen #14190-144) and 2 ml of fresh growth medium was added to each well.

❖ *Controlled single layer electroporation system*

System Concept

The basic concept of this system is building an electroporation apparatus and a method of electroporation in which the system is made of three layers: top layer of cell-culture media with relatively high electric conductivity (comparable to physiologic saline), middle layer of adherent cultured cells (heterogeneous, anisotropic conductivity) , and third lower layer of insulating plastic surface to which the cells adhere (Figure III-1).

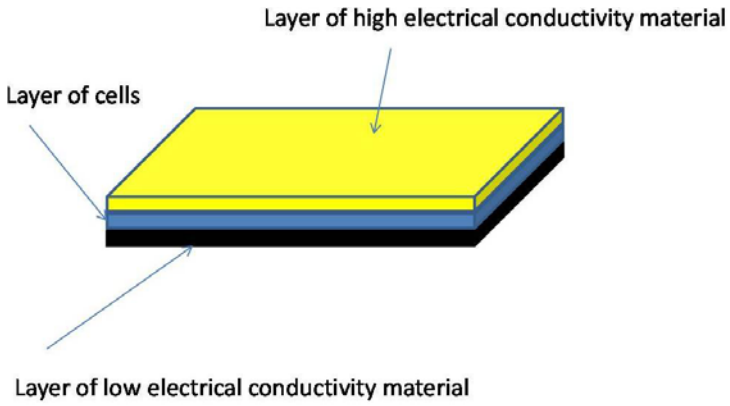

Figure III-1 - The basic concept of the system is shown here. The layer of the cells in grown on a plastic well (non conductive), and with highly conductive medium on top (resistivity similar to that of normal saline). This allows the high conductive layer to determine the electric field distribution even in the non-homogeneous layer of adherent cells.

The layer of cells has non-homogeneous electrical properties which depend on the size, morphology and density of the cells. The challenge of the design is to apply a well controlled 2-D or 1-D electrical field on the layer of the cultured cells, despite the heterogeneity conductivity of this layer. It is evident that if voltages would be applied through the single layer of cells the cells would experience variable electrical fields because of the heterogeneous nature of the layer of cells.

This problem is resolved by applying the same potential difference across the cultured cells (middle layer) and the highly conductive culture media covering them (upper layer). Due to the high conductivity of the upper layer, and the small thickness of the cultured cell layer, the 2-D or 1-D electrical field which develops in the upper layer is almost identical to the electric field of the lower layer (Finite element simulation of the problem is shown in III-2).

The main outcome of this design is similar electric field behavior on both upper layer that is largely dependent on the properties of the upper, isotropic layer. The electric field across the upper layer can be simulated using simple two or one dimensional finite element simulation (Finite element simulation of 2 needle electrodes example is shown Figure III-3).

The two dimensional implementation involves two needle electrodes that are perpendicular to the three layered system. The needles are immersed within the culture media (upper layer) , pushed across the cultured cell layer, and pressed against the insulating plastic surface. The distribution of the electric field of two needles immersed in homogenous saline in shown in Figure III-2.

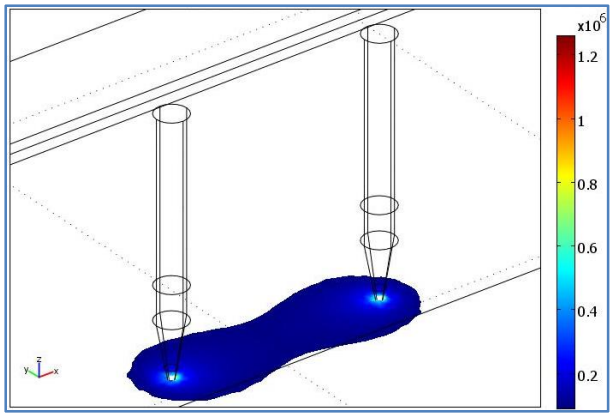

III-2 - Three dimensional simulation showing cross section of the two needles and the electric field around them across the lower layer , non-homogenous cultured cell surface. The plot is showing only electric field larger than 900[V/cm], due to potential difference of 800[V].

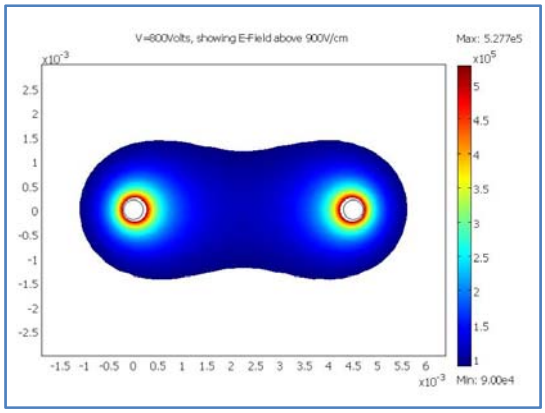

III-3 - Two dimensional simulation of two round electrodes with potential difference of 800[V]. The plot is showing only electric field larger than 900[V/cm].

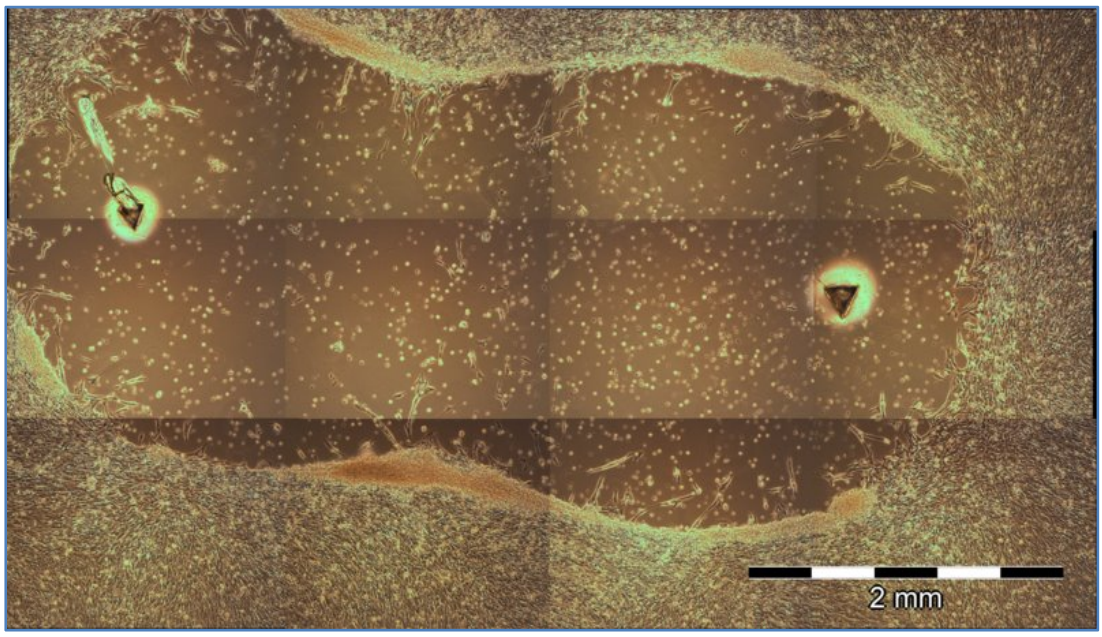

III-4 - Two dimensional ablation of adherent VSMC. Area of dead cells surrounds both needles and correlated very well with figure III-2 and figure III-3

Analytic solution of the two needle configuration

By applying IRE pulses to cultures cells, cells in areas of high electric field will die and disappear from the culture (see Result subsection below). In order to correlate the area of

dead cells with the electric field threshold, there is a need to solve the problem analytically. An analytic solution enables correlating the area of dead cells with threshold electric field value.

The geometrical model (Figure III-5) for this case consists of a thin layer of resistive material (thickness = t and resistivity = ρ) and two highly conductive cylinders (+ and -) of radius a with centers separated at a distance s. The voltage difference between both cylinders is kept at ΔV. This causes current injected into the system through cylinder (I+) towards cylinder (I-).

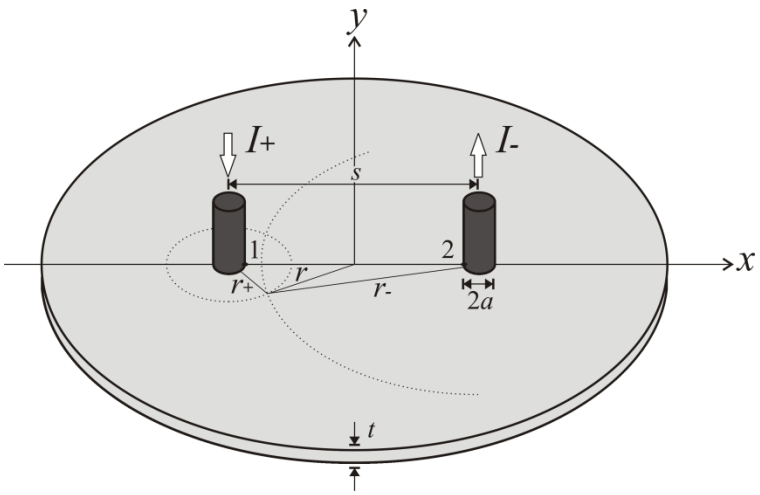

III-5 Illustration of the parameters used in the analytic solution (Illustration made by Dr. Antoni Ivorra)

The electric field at each point (r) is obtained by means of the superposition principle: the contribution from both current sources (I+ and I-) is calculated independently and then added.

$$E(r) = E(r)_{I+} + E(r)_{I-} \qquad (2)$$

We employ the Ohm's law to calculate both contributions:

$$\mathrm{E(r)_{I+} = \rho \mathbf{J}(r)_{I+} = \rho\left(\frac{I}{2\pi t r_{+}}\hat{r}_{+}\right)} \quad (3)$$

$$\mathrm{E(r)_{I-} = \rho \mathbf{J}(r)_{I-} = \rho\left(\frac{-I}{2\pi t r_{-}}\hat{r}_{-}\right)} \quad (4)$$

where **J** denotes the current density, uniformly distributed around each current source. In the particular case of the point x along the axis between both needles, the electric field magnitude is:

$$\mathrm{|E(x)| = \frac{k}{2}\left(\frac{1}{x + {}^{s}/_{2}} - \frac{1}{x - {}^{s}/_{2}}\right)} \quad (5)$$

where

$$\mathrm{k = \frac{\rho I}{\pi t}} \quad (6)$$

And now we need to calculate *I* in order to obtain *k*. We calculate the voltage difference ΔV due to the injected current. The superposition principle is employed again to obtain the voltages at the needle surfaces (points 1 and 2).

$$V_1 = V_{1,(I+)} + V_{1,(I-)};\ V_2 = V_{2,(I+)} + V_{2,(I-)};\ \Delta V = V_1 - V_2 \quad (7)$$

If the voltage at ∞ is defined as 0[V], then the voltage at any point is:

$$V(r) = -\int_{\infty}^{r} E(r)dr \quad (8)$$

using Ohm's law we get:

$$V_{1,(I+)} = \int_{\infty}^{a} \frac{\rho I}{2\pi r t}\,dr = -\frac{\rho I}{2\pi t}(\ln a - \ln \infty) \quad (9)$$

$$V_{1,(I-)} = -\int_{\infty}^{s-a} \frac{\rho(-I)}{2\pi r t}\,dr = \frac{\rho I}{2\pi t}(\ln(s-a) - \ln \infty) \quad (10)$$

$$V_1 = V_{1,(I+)} + V_{1,(I-)} = \frac{\rho I}{2\pi t}(\ln(s-a) - \ln a) \quad (11)$$

and in an equivalent way for V_2:

$$V_2 = V_{2,(I+)} + V_{2,(I-)} = -\frac{\rho I}{2\pi t}(ln(s-a) - ln\, a) \quad (12)$$

hence,

$$\Delta V = V_1 - V_2 = \frac{\rho I}{\pi t}\left(\ln\left(\frac{s-a}{a}\right)\right) \quad (13)$$

So finally we get the expression for k:

$$k = \frac{\Delta V}{\ln\left(\frac{s-a}{a}\right)} \quad (14)$$

Using equations (14) and (5) we can get the value of the electric field in any point on two dimensional surface of the cultured cells. ***By measuring the radius of the dead cells area around one of the two needles (x) the magnitude of the electric field threshold for cell death (IRE threshold) can be calculated.***

❖ *Experiment details*

For two dimensional experiments, two stainless steel cylindrical electrodes were used. Electrodes had needle shape sharp edges, and were 4.5 mm apart. For one dimensional experiments , two parallel razor blades were connected with a distance of 1.5 mm apart. Electrodes were used to electroporate the adherent cells without changing their growth medium. Electrodes were lightly pressed against the plastic surface to achieve good contact and a visible marking for inverted microscope analysis.

A sequence of 10 direct current pulses , 100 μs each, at a frequency of 1 pulses per second, was applied between the electrodes using a high voltage pulse generator intended for electroporation procedures (ECM 830, Harvard Apparatus, Holliston, MA). For the two dimensional experiments potential differences of 0, 200, 400, 600, 800, 1,000 and 2,000 Volts were compared. Experiments were also repeated applying constant potential difference of 500 Volts, with increased number of electroporation pulses (10, 15, 20, 25, 30 and 35 pulses). VSMC and CHO-S cells experiments evaluated reversible electroporation using Propidium Iodide (PI) as a marker of reversible electroporation. VSMC experiment were also repeated without PI, in order to evaluate IRE threshold.

Cell cultures without PI - Areas of dead cells were measured 20 hours following electroporation application. Radius of dead cells area was measured, and together with the analytic solution the electric field magnitude that corresponded with IRE threshold was calculated.

Cell cultures with PI - PI molecules do not penetrate cell's membrane, but when cells are exposed to electroporation pulses PI molecules penetrate into the cell interior. Once inside the cells, PI creates a complex with nucleic acids (DNA and/or RNA) , and becomes fluorescent. Fluorescent areas surrounding the electroporation electrodes were measured and the radius was used together with the analytic solution in order to calculate the electric field magnitude that corresponded with reversible electroporation threshold.

3. Results

❖ *VSMC experiments with PI*

Table III-1 summarizes experiments done with VSMC and PI without changing pulse numbers. The table includes experiments with different potential difference (ΔV) , and for each ΔV the analytic solution was used in order to calculate the electric field threshold for reversible electroporation. All experiments were done using 10 pulses of 100 µsec. Total number of independent observations is 36 (see example in Figure III-6), and the average threshold for reversible electroporation is 1,141±126 V/cm. This threshold decreases with increasing the number of pulses, as described in the next paragraph.

ΔV	K	x (µm)	Calculated E-Field (V/cm)
850	266	2388	1,046
850	266	2474	1,043
850	266	2756	1,049
850	266	2090	1,077
800	250	1772	1,081
800	250	2146	1,006
800	250	2224	997
800	250	1583	1,146
750	234	1711	1,031
750	234	1521	1,098
750	234	1784	1,011
750	234	1603	1,067
700	219	1376	1,089
700	219	1130	1,244
700	219	1410	1,073
700	219	1368	1,093
650	203	1147	1,143
650	203	1030	1,236
650	203	1178	1,122
650	203	1200	1,107
600	188	1054	1,122
600	188	1022	1,148
600	188	829	1,351
600	188	791	1,403
550	172	874	1,187
550	172	973	1,092
550	172	874	1,187
550	172	669	1,479
500	156	1163	871
500	156	684	1,320
500	156	685	1,318

500	156	883	1,070
500	156	823	1,132
500	156	689	1,312

500	156	866	1,087
500	156	747	1,226

Table III-1 - Thirty six independent observations of reversible electroporation areas of VSMC in the presence of PI

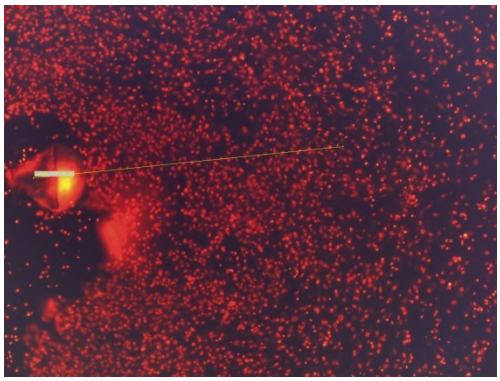

Figure III-6 - VSMC culture few minutes following electroporation in the presence of Propidium Iodide. On the left side you can see the area of the needle, surrounded by a small area of already detached dead cells. The intensity of the red color is decreasing with increasing distance from the needle electrode.

Table III-2 summarizes experiments done with VSMC and PI while changing pulse numbers. For each pulse combination there are four independent observations. All experiments were done with ΔV=500 V and pulses length of 100 µsec. The right most column shows the average value for each pulse sequence with its standard deviation.

# Pulses	ΔV	K	x (µm)	Calculated E-Field (V/cm)	Average E-Field (average +SD, in [V/cm])
15	500	156	1,151	877	1,090±161
15	500	156	842	1,112	
15	500	156	718	1,267	
15	500	156	851	1,102	
20	500	156	1,021	957	1,007±78
20	500	156	867	1,086	
20	500	156	1,073	922	
20	500	156	891	1,063	

25	500	156	1,531	729	790±100
25	500	156	1,094	910	
25	500	156	1,243	831	
25	500	156	1,701	689	
30	500	156	1,274	818	815±21
30	500	156	1,305	805	
30	500	156	1,219	843	
30	500	156	1,332	794	
35	500	156	1,377	778	748±42
35	500	156	1,369	780	
35	500	156	1,487	742	
35	500	156	1,694	691	

Table III-2 - 20 independent observations of reversible electroporation threshold due to varying number of electroporation pulses. All observation were done with VSMC in the presence of PI

❖ *VSMC IRE threshold*

Table III-3 summarizes 19 independent experiments done with VSMC without PI. The table includes experiments with different potential difference (ΔV) , and for each ΔV the analytic solution was used in order to calculate the electric field threshold for irreversible electroporation. All experiments were done using 10 pulses of 100 µsec. Total number of independent observations is 19, and the average threshold for reversible electroporation is 1,414±124 V/cm. This value is 23% higher compared with the electric field threshold for reversible electroporation.

ΔV	K	x (µm)	Calculated E-Field (V/cm)
800	250	1,067	1,482
800	250	1,419	1,220
800	250	1,316	1,280
800	250	1,047	1,502
750	234	994	1,464
750	234	1,051	1,405
750	234	1,217	1,265
750	234	1,211	1,269
700	218	828	1,577

700	218	1,000	1,361
700	218	985	1,376
700	218	956	1,408
650	203	936	1,329
650	203	970	1,293

600	187	721	1,515
600	187	798	1,393
550	171	686	1,448
550	171	584	1,662
500	156	545	1,605

Table III-3 - Nineteen independent observations of irreversible electroporation areas of VSMC with varying ΔV

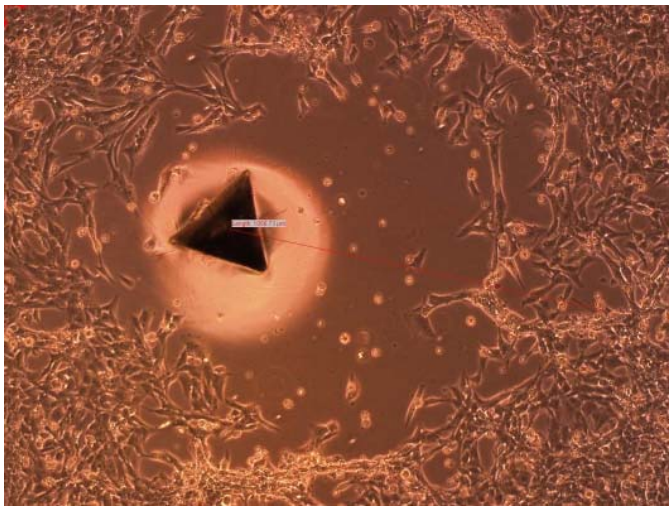

Figure III-7 - VSMC culture few hours following electroporation. The large triangle is the marking of the needle electrode, and the area without cells corresponds with dead cells due to IRE. The other needle cannot be seen in this magnification.

Table III-2 summarizes experiments done with VSMC without PI while changing pulse numbers. All experiments were done with ΔV=500[V] and pulses length of 100 [μsec]. The right most column shows the average value for each pulse sequence with its standard deviation.

# Pulses	ΔV	K	x (μm)	Calculated E-Field (V/cm)	Average E-Field (average +SD, in [V/cm])
15	500	157	615	1,445.12	1350±134
15	500	157	726	1,255.23	
20	500	157	914	1,041.83	1065±33
20	500	157	865	1,088.10	

25	500	157	1175	864.30	846±26
25	500	157	1253	826.93	
30	500	157	1340	791.13	808±23
30	500	157	1259	824.27	
35	500	157	1186	858.69	818±58
35	500	157	1380	776.46	

Table III-4 - Ten independent observations of IRE threshold due to varying number of electroporation pulses. All observation were done with VSMC cells without PI

❖ *CHO-S Cells Experiments with PI*

Table III-5 summarizes experiments done with CHO-S cells and PI without changing pulse numbers. The table includes experiments with different potential difference (ΔV) , and for each ΔV the analytic solution was used in order to calculate the electric field threshold for reversible electroporation. All experiments were done using 10 pulses of 100[μsec]. Total number of independent observations is 20 (see example in Figure III-6), and the average threshold for reversible electroporation is 1,417±218[V/cm]. This threshold decreases with increasing the number of pulses, as described in the next paragraph.

ΔV	K	x (μm)	Calculated E-Field (V/cm)
700	201	782	1,526
700	201	779	1,531
700	201	1,011	1,248
700	201	959	1,299
650	187	808	1,380
650	187	787	1,410
650	187	799	1,393
650	187	811	1,376
600	173	499	1,921
600	173	549	1,766
600	173	699	1,435
600	173	628	1,572
550	158	670	1,363
550	158	583	1,536
550	158	592	1,516

550	158	573	1,559
500	144	737	1,145
500	144	635	1,297
500	144	832	1,037
500	144	843	1,026

Table III-5 - Sixteen independent observations of reversible electroporation areas of CHO-S in the presence of PI

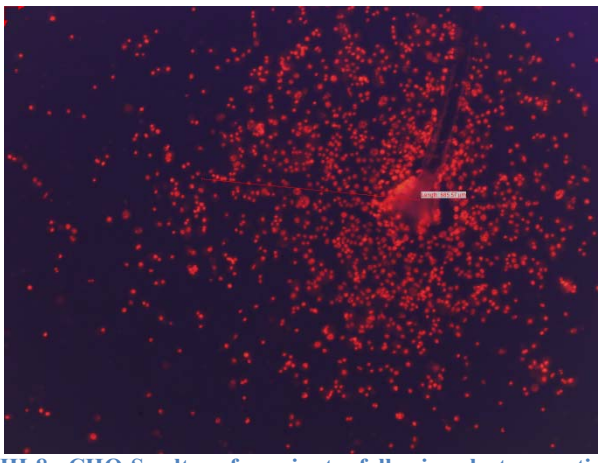

III-8 - CHO-S culture few minutes following electroporation in the presence of Propidium Iodide.

Table III-6 - summarizes experiments done with CHO-S and PI while changing pulse numbers. For each pulse combination there are four independent observations. All experiments were done with ΔV=500[V] and pulses length of 100 [μsec]. The right most column shows the average value for each pulse sequence with its standard deviation. Results for 20 and 25 pulses were not significantly different , and the threshold values for these eight observations do not show the expected decrease in threshold. However, compared with other groups (10,15 and 30 pulses) , the results are consistent and show a decrease in electric field threshold with increasing number of pulses.

# Pulses	ΔV	K	x (μm)	Calculated E-Field (V/cm)	Average E-Field (average +SD, in [V/cm])
10	500	144	737	1,145	1,126±126
10	500	144	635	1,297	
10	500	144	832	1,037	
10	500	144	843	1,026	
15	500	144	824	1,045	1,058±58

15	500	144	884	988	
15	500	144	889	984	
15	500	144	686	1,215	
20	500	144	1,526	678	
20	500	144	1,147	814	804±94
20	500	144	1,137	819	
20	500	144	991	905	
25	500	144	1,003	897	
25	500	144	994	903	849±65
25	500	144	1,109	833	
25	500	144	1,260	763	
30	500	144	1,356	728	
30	500	144	1,206	786	
30	500	144	1,340	733	
30	500	144	1,417	708	743±25
30	500	144	1,270	759	
30	500	144	1,255	765	
30	500	144	1,333	736	
30	500	144	1,344	732	

III-6 - Twenty four independent observations of reversible electroporation threshold due to varying number of electroporation pulses. All observation were done with CHO-S cells in the presence of PI

4. Discussion

Novelty and advantages of suggested method

Electroporation is most commonly used for the introduction of DNA-molecules into cells which grow in suspension.[11] Cells are placed in a cuvette, with the cell suspension between two flat aluminum electrodes. Currently, the method is limited by the need to have the cells in suspension.

In the average lab, electroporation does not work for cells growing on adherent surfaces, and therefore necessitate suspending the cells prior to transfection. The process of detaching cells from their surface is commonly done with a mixture of trypsin enzyme (serine-protease) and EDTA (ethylenediaminetetraacetic acid). This process induces metabolic alterations and partial viability loss [94], changes cell morphology and destroys any organized cellular structures. Therefore, there is a need for a reliable and reproducible method for efficient transfection of cultured cells *in-vitro*. Such a method will enable to transfect cells in their adherent state and study the influence of various genetic manipulation on the cellular interactions *in-vitro*.

The challenge of applying controlled electric field across adherent cultured cells *in-vitro* is the subject of active research, with different approaches published. [95] One of the early methods described included growing the cells on glass coverslips and then positioning them between two electrodes and exposing them to voltage pulses with low ionic isotonic medium.[96-98] These methods were reported to have high transfection efficiency, but also suffered from relatively high mortality rate (around 50%). Subsequently, a similar approach was described in which the electrodes were placed above the adherent cell layer, with no direct contact between the electrodes and the cells.[99]

More advanced methods utilized special growing surfaces. One approach used porous membrane as a growing surface, where cells and porous membrane were placed between two electroporation electrodes.[100] Another approach had cells grown on surface with pairs of interdigitated titanium and gold electrodes.[101] A third approach used an

electrode assembly where the cells grow and are electroporated on optically transparent, electrically conductive indium-tin oxide (ITO).[95]

A major problem in all of the above methods is the anisotropic electric properties of the layer of cultured cells. Permeabilization is not only a function of electric field intensity and cell size but also of cell shape and orientation.[98] Therefore, there is a need to apply changing electric field across the two dimensional cells layer in a controlled method that will enable us to understand what is the electroporation threshold for reversible and irreversible electroporation.

The method described in this chapter has two major advantages. First, it can be done in the average lab using standard growth medium and plastic culturing plates., and works with any cell line that grows as an adherent monolayer. Second, it delivers a controlled electric field across the two dimensional layer of cultured cells. By correlating results of cell transfection or cell death with finite element simulation of the electric field, the optimal electroporation parameters can be found for future experiments with the same cell line under the same conditions.

Implication for endovascular IRE

The threshold for IRE ablation of VSMC *in-vitro* is 1,414±124 [V/cm], while reversible electroporation threshold for VSMC is 1,141±126 [V/cm]. These threshold values, reported here for the first time, are based on multiple independent observations. Compared with reversible electroporation, IRE requires a 24% increase in electric field magnitude. The relative narrow window for reversible electroporation might explain low

survival rates of cells exposed to uniform electric field in different electroporation applications.

These values hold only for the case of VSMC grown as a monolayer *in-vitro*. Data concerning the threshold of VSMC *in-vivo* is described in chapters IV and V. However, important statements can be made based on the results described here:

1. **Electroporation threshold (reversible and irreversible) decreases with increasing the number of pulses**. VSMC IRE threshold dropped by 42% when the number of pulses increased from 10 to 35 (from 1,414±124 to 818±58 [V/cm]). VSMC reversible electroporation threshold dropped by 34% when the number of pulses increased from 10 to 35 (from 1,141±126 to 748±42[V/cm]). Similar phenomena was observed in cancerous cells, with reversible threshold for CHO-S dropping by 48% when the number of pulses increased from 10 to 30 (from 1,417±218 to 743±25 [V/cm]). For any future design of electroporation device, this correlation can be used as coarse guide. Since most devices are limited by the electric field delivered across large areas, this phenomena can be used in order to better understand what is the tradeoff between decreasing the electric field and increasing the number of pulses.
2. ***In-vitro*, VSMC are more sensitive to electroporation compared with cancerous CHO-S cells.** Reversible electroporation threshold for CHO-S cells was 1,417±218 [V/cm], compared with 1,141±126 for VSMC. The change in electroporation threshold can be attributed in part to the different morphology of these two cell population. Cell shape and orientation are important factors in determining electroporation threshold.[98] Since VSMC are elongated while

CHO-S are round, VSMC have a larger membrane surface area which is exposed to the electric field. This might explain the higher susceptibility of VSMC to electroporation pulses.

IV. CHAPTER FOUR: IRE EFFECT ON BLOOD VESSELS *IN-VIVO*

1. Motivation and objectives

Previous chapter demonstrated that VSMC can be destroyed *in-vitro* with electroporation, and that a sequence of ten 100 μs pulses inducing electric field of 1,400 V/cm or above is high enough for IRE ablation.

However, results of cell culture cannot be applied for *in-vivo* vessel wall ablation. Electroporation threshold is dependent on cell morphology, orientation of the electric field and extra cellular components.[2,4] VSMC in cell culture differ from VSMC in arterial wall. Cultured cells have different shape, and the extra cellular space in the culture is missing the collagen and elastin fibers that are a major component of the vessel wall. In addition, blood vessels are composed of three different layers that are exposed to electric field, while the VSMC population of interest is located only in the middle layer, the *Tunica Media*.

Therefore, in-vivo experiments are necessary in order to understand what the IRE threshold is for VSMC in their physiological environment. In addition, *in-vivo* experiments are important with respect to other effects that electric pulses might have on the cellular and extra-cellular environment of blood vessels' wall.

This chapter describes *in-vivo* experiment with rodent carotid arteries. The motivation in these experiment was to understand what is the effect of IRE on blood vessels *in-vivo*, and to find those IRE parameters that can be used in larger animals to induce VSMC ablation.

Two different experiments are presented here:

Experiment A - In this experiment rodent carotid arteries were exposed to IRE, and were evaluated after 28 days. The objective of this study was to study the long term effect of IRE on blood vessels *in-vivo*. Specifically, it was designed to investigate IRE efficiency in ablating VSMC population and its effect on vessel wall integrity, blood thrombus formation and extra-cellular matrix components of the vessel wall.

Experiment B- In this experiment rodent carotid arteries were also exposed to IRE with the same electrode assembly. However, the objective of this experiment was to compare different electroporation sequence protocols. Animals is this experiment were euthanized after one week, and the number of VSMC was compared between different groups.

2. Methods

❖ *Animal model and electrode assembly for both experiments*

Sprague-Dawley rats weighting 150-350 grams were used in both experiments. All animals received humane care from a properly trained professional in compliance with both the Principals of Laboratory Animal Care and the Guide for the Care and Use of Laboratory Animals, published by the National Institute of Health (NIH publication No. 85-23, revised 1985).

Each animal was anaesthetized throughout the procedure with a combination of Ketamin and Xylazine. The left common carotid artery was exposed, and a custom made electrode clamp (Figure IV-1) with two parallel disk electrodes (diameter = 5 mm) was applied on the left common carotid artery, very close to its bifurcation to the internal and external carotid arteries. The distance between electrodes was approximately was measured with a digital caliper, and was usually around 0.3 mm. Current and voltage were recorded by

means of special oscilloscope probes (current probe was AP015 and high voltage probe was ADP305, both from LeCroy Corp.). From these two signals conductance was obtained during the pulses. The procedure was applied in three successive locations along the common carotid artery. At the end of the procedure the skin incision was sutured and animals were kept alive for a follow-up period of 28 days until they were euthanatized.

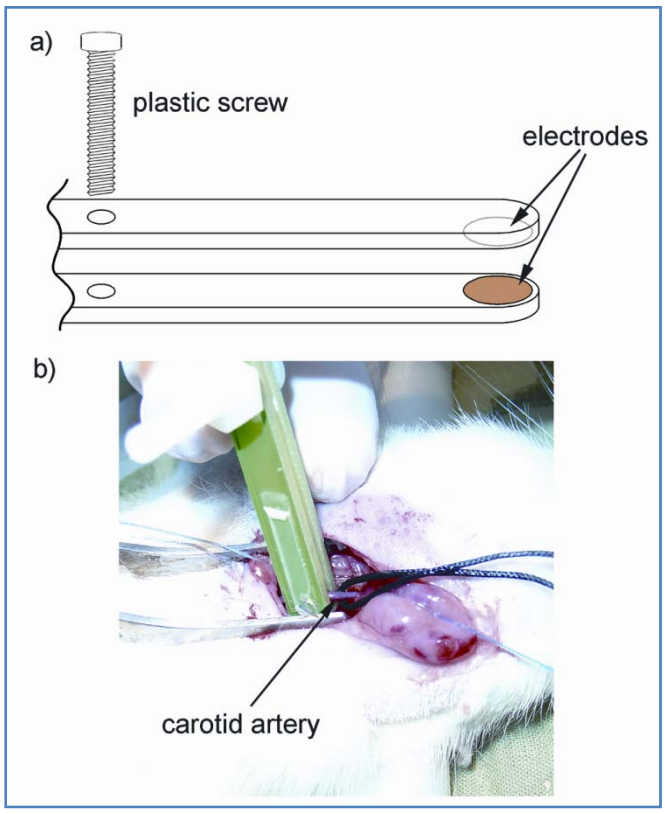

Figure IV-1 - Custom made electrode clamp employed to induce irreversible electroporation of the carotid artery. a) The clamp consists of two printed circuit boards (1.5 mm thickness) with disk electrodes (diameter = 5 mm) made of cupper (70 µm thickness) plated with gold (manufacturing process by Sierra Proto Express, Sunnyvale, CA, USA). b) Clamping of the carotid artery, the distance between electrodes was approximately 0.3 mm.

❖ *Experiment A protocol*

Six rats were used in this study. A sequence of 10 direct current pulses of 115 Volts (i.e. electrical field of approximately 3800 V/cm), 100 µs each, at a frequency of 10 pulses per second, was applied between the electrodes using a high voltage pulse generator intended

for electroporation procedures (ECM 830, Harvard Apparatus, Holliston, MA). The magnitude of the electrical field and the mode of application where chosen to simulate the upper and most extreme limit of IRE electrical parameters anticipated in a tissue ablation procedure that will not induce a thermal effect. The electrodes were also connected to an oscilloscope which measured the voltage and the current through the electrodes so that the conductance of the tissue during the electroporation could be obtained. In each animal the procedure was applied in three successive locations along the common carotid artery to produce a treated length of about 2 cm. At the end of the procedure the skin incision was sutured and the animals were kept alive under continuous veterinary supervision for follow-up until they were euthanatized. To determine the long term effects of IRE on a large blood vessel we have used four rats that were kept alive for 28 days. To sample the behavior throughout this period one of the six rats was euthanized after 24 hours, and another after 7 days.

❖ *Experiment B protocol*

Thirty three animals were used in this study. Animals were divided to 8 different groups (Table IV-1): for the first group the electroporation sequence was similar to that used in experiment A. Three groups used 10 pulses with decreasing electric field magnitude (1750, 875 and 437.5 V/cm). Four additional groups used higher number of pulses (45 and 90) for the two intermediate electric field values (1750 and 875).

All groups had their left common carotid artery treated in the same manner as in experiment A, with their right common carotid artery used as a control. At the end of the procedure the skin incision was sutured and animals were kept alive for a follow-up period of 7 days.

Group	Electric Field [V/cm]	# Pulses	Frequency [Hz]	# Animals
1	3500	10	10	5
2	1750	10	10	4
3	1750	45	4	4
4	1750	90	4	4
5	875	10	10	4
6	875	45	4	4
7	875	90	4	4
8	437.5	10	10	4

Table IV-1: The table shows the eight different electroporation parameters used in this study. Groups differ in the magnitude of the electric field applied, the number of the pulses and their frequency. All pulses were square pulses, 100μs in length. Frequency of 10 Hz was used for 10-pulses protocols, and was reduced to 4 Hz for 45 or 90 pulses protocols to prevent significant heating.

❖ *Histology analysis for both experiments*

Animals were euthanized with an overdose of Pentobarbital. The arterial tree was perfused with 10% buffered formalin for 40 minutes, and the treated left and untreated right (control) carotid arteries were exposed near the bifurcation of the internal and external carotid arteries. One slice of 1 cm of each artery was used for histological analysis in Experiment A. For experiment B each slice was cut to three and thus three consecutive slides of the treated areas were evaluated. Each slice was fixated with 10% buffered formalin, embedded in paraffin, and sectioned with a microtome (5-μm-thick). Serial sections were stained with hematoxylin and eosin. For experiment A only, Cell apoptosis was assessed by caspase-3 immunostaining. Consecutive fields of each artery were photographed at X200 magnification, and the number of nuclei in the internal media was counted. The circumference of every artery, as well as its internal lumen was

measured. The density of VSMC nuclei per millimeter was calculated (number/circumference).

In addition, selected sections were also stained with elastic Van Gieson (EVG) and Masson trichrome in order to evaluate extra-cellular elastic and collagen fibers, respectively. Immunostaining with CD31 and CD34 antibodies (Pathology Services Inc., Berkeley, CA) was used to evaluate endothelial layer.

3. Results

All the animals, 39 in total, survived the both experiments. During follow-up period, there were no signs of cerebrovascular events (paraplegia, paraparesis, etc.), no massive bleeding from treated arteries , and no case of mortality.

❖ *Experiment A*

The electrical conductance during the application of two series of pulses is shown, superimposed, in Figure IV-2. Each trace shows the conductivity only during the application of the pulse and not between pulses. In each of the ten segments it is possible to see two pulses (each from a different experiment at another location or animal) that are superimposed – to illustrate the general nature of the observed phenomenon. It is important to note the increase in conductance throughout the electroporation pulse. The overall increase of conductance during the application of each electroporation pulse is consistent with the mechanism of action of electroporation which causes permeabilization to occur on the cell membrane and thereby increases the conductivity of the tissue.

The sampling, 24 hours after IRE, shows that there was no significant difference between the control artery and the IRE artery. In both arteries the overall morphology was unharmed. Number of cells in the tunica media was similar (Table IV-2).

The sampling 7 days after IRE shows that the number of VSMC in the tunica media of the IRE artery was lower compared with their number in the tunica media of the control artery (86 nuclei per millimeter vs. 360 nuclei per millimeter, Table 1). Within a week, as much as 75% of VSMC in the IRE-treated artery disappeared from the tunica media, without any evidence of thrombosis, aneurysm formation or rupture of the artery (Figure IV-3). The elastic fibers' morphology was not different between the two groups. On H&E staining, some clusters of VSMC could still be identified in the most internal layer of the tunica media. These cells were apoptotic, as evident by caspase-3 immunostaining of the same slides (Figure IV-4).

The primary goal of this study was the long term effect of the IRE treatment. At 28 days, the number of VSMC cells in the tunica media was very low compared with their number in the control artery (Table IV-2, Figure IV-5). There was no evidence of thrombus formation and no change in the diameter of the artery compared with control arteries. The endothelial cells and the internal lamina morphology were well recovered, even in areas with substantial decrease in VSMC population (Figure IV-6). Compared with control artery, the endothelial layer of the IRE treated arteries was thinner and more condensed (Figure IV-6). Elastic fibers location and morphology was not different between the IRE artery and the control artery. In one artery, it was impossible to locate even one VSMC nuclei in the entire slide (Figure IV-5 b).

		Left Common Carotid				Right Common Carotid			
Animal #	Follow- up	Nuclei #	Circumference (mm)	Lumen (mm^2)	Nuclei per mm	Nuclei #	Circumference (mm)	Lumen (mm^2)	Nuclei per mm
1	24 Hours	300	2.53	0.418	119	240	2.35	0.250	102
2	7 Days	86	2.69	0.361	32	360	2.49	0.363	145
3	28 Days	0	2.76	0.337	0	440	2.43	0.376	181
4	28 Days	25	2.79	0.505	9	460	3.07	0.473	150
5	28 Days	170	2.65	0.300	64	250	2.15	0.254	116
6	28 Days	45	2.61	0.200	17	Missing Slide			

Table IV-2 - Morphometric analysis and nuclei count of all slides in experiment A

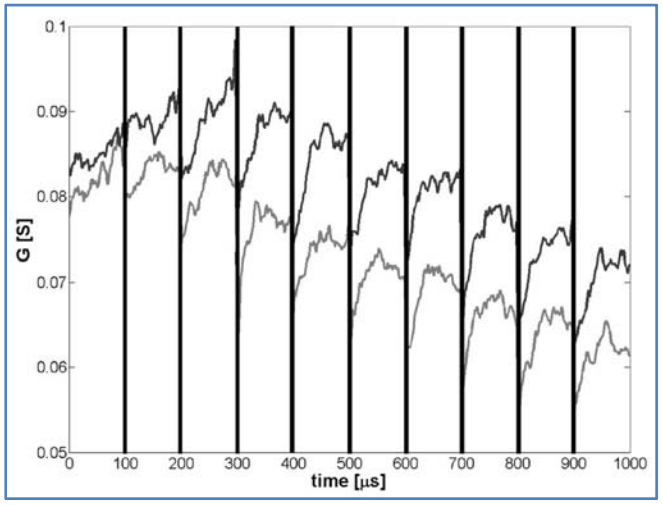

Figure IV-2 - Conductance of the arterial wall during repetitive direct current pulses. The figure shows conductance (expressed in Siemens) only during the application of pulses. It gives a superposition two different treatments at different locations. The fluctuating appearance of the signal is due to environment noise. The overall change in the conductance during each electroporation pulse is due to the permeabilization of the cell membrane due to electroporation.

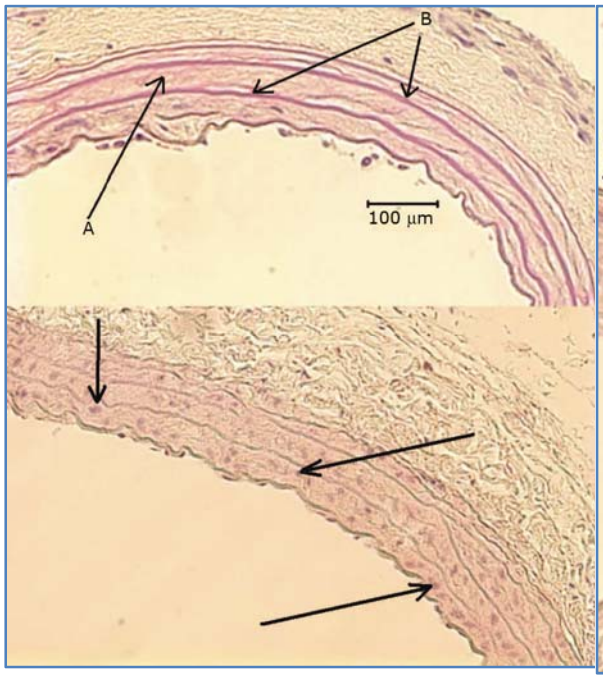

Figure IV-3 - IRE effect after 7 days (H&E X200 magnification). Top picture: Left common carotid artery 7 days after IRE (animal #2). In this picture it is possible to see the scarcity of vascular smooth muscle cells nuclei at the tunica media (arrow A). The elastic fibers morphology is maintained (arrow B). Bottom picture: Right common carotid artery of the same animal (animal #2). In this picture it is possible to see the normal density of vascular smooth muscle cells in the tunica media (cells marked with arrows).

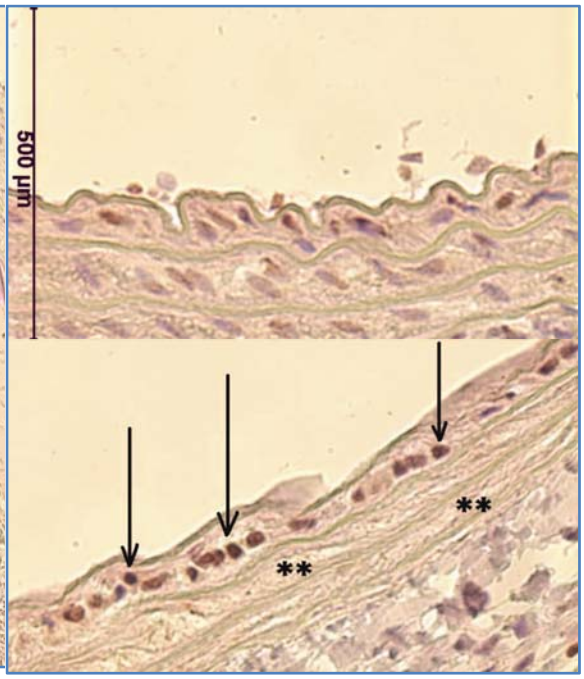

Figure IV-4 - Caspase-3 stain of tunica media (X400 magnification). Top picture shows normal right common carotid artery stained with Caspase-3. Bottom picture shows the left common carotid artery 7 days after IRE: It shows complete disappearance of VSMC from the external layers of the tunica media (marked with **). Most nuclei of the VSMC in the internal layer of the tunica media are apoptotic – condensed and stain positive for Caspase-3 (marked with arrows).

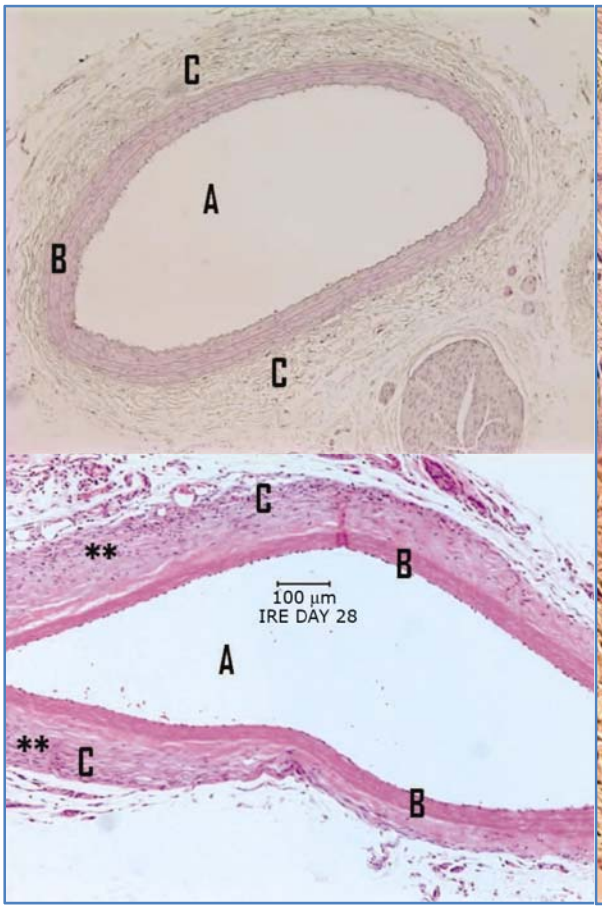

Figure IV-5 - IRE effect after 28 days (H&E X100 magnification). Top picture shows a normal right common carotid artery. Bottom picture shows a left common carotid artery 28 days after irreversible electroporation. There are almost no vascular smooth muscle cells in the tunica media, compared with control artery. The thickness of the tunica media is reduced. There is no neointimal formation. There is marked fibrosis and hypercellularity in the adventitia layer of the IRE artery, compared with the control. (A – intra-arterial lumen, B – tunica media, c – tunica adventitia, ** - area of fibrosis and hypercellularity)

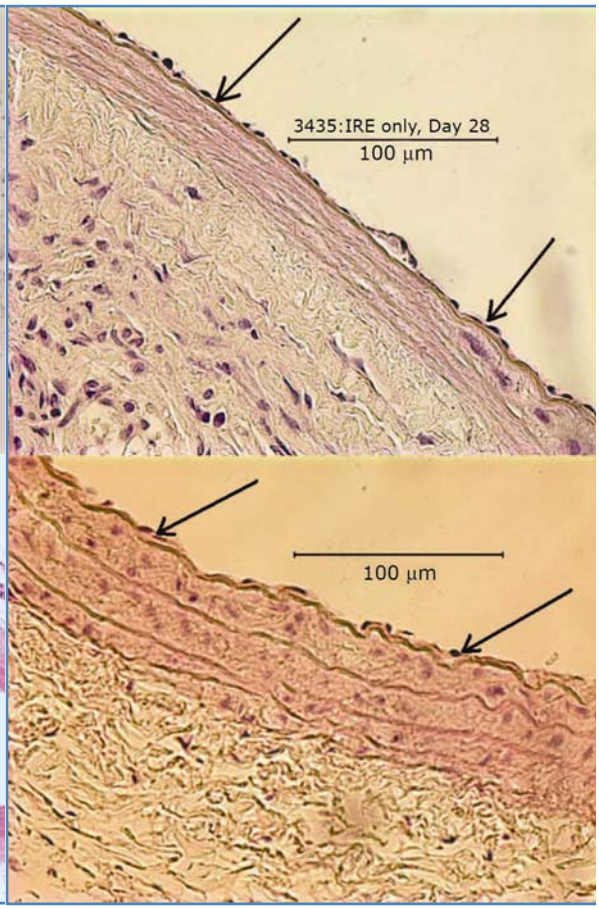

Figure IV-6 - Endothelial cells of IRE treated arteries (H&E X400 magnification). Top picture shows arterial wall 28 days after IRE. The picture shows a morphologically intact endothelial layer, similar to the endothelial layer of the control artery (bottom picture).

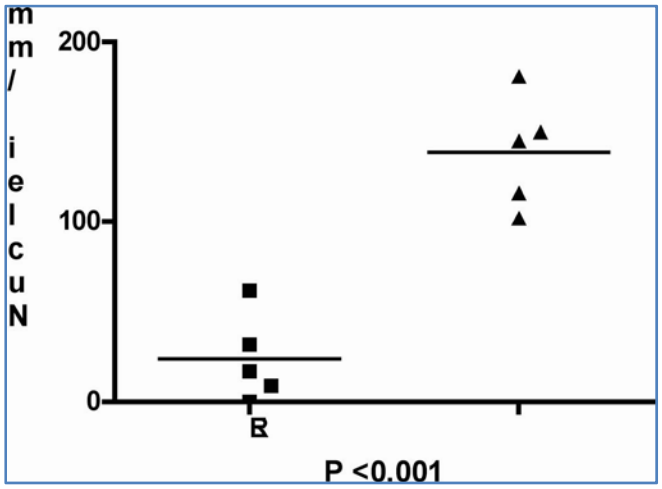

Figure IV-7 - Average nuclei number per millimeter in IRE arteries vs. control arteries (P<0.001)

❖ *Experiment B*

Results of all eight groups are summarized in Table IV-3 and Table IV-4. Best IRE ablation results were achieved with Groups 1 and 4 (Figure IV-8). Group 1 had 89% reduction in the number of VSMC compared with control (24±34 vs. 208±40, P<0.001) and group 4 had 94% reduction in the number of VSMC compared with control (13±21 vs. 213±33, P<0.001). Example of complete ablation of the entire arterial wall in shown in Figure IV-9.

While ten pulses of 3,500 V/cm were efficient, ten pulses of lower electric fields had a minor ablation effect (1750 V/cm, group 2: 167±66 vs. 214±38, P=0.05) or no effect at reducing VSMC population (groups 5 & 8, 875 and 437.5 V/cm respectively). Increasing the number of pulses with electric field of 1,750 V/cm improved the ablation efficiency (VSMC population reduction of 22%, 86% and 94% with 10, 45 and 90 pulses respectively). Similar trend of increasing efficiency was also apparent with electric field

of 875 V/cm (63% and 79% with 45 and 90 pulses, respectively), but efficiency values were not high enough even with 90 pulses (49±40 vs. 236±31, P<0.001).

Sub-analysis of ablation efficiency at the three separate layers of the Tunica Media shows that best results were achieved in the outer layers of the Tunica Media, and most VSMC that survived IRE were located in the inner most layer (Figure IV-10). For example, in the case of group 4, no VSMC nuclei could be located in the outer layer in all sections evaluated. All 6% surviving VSMC in this group were located in the inner layer of the Tunica Media (Figure IV-11).

Electric conductance changed during application of IRE (Figure IV-12). The conductance measured during the last pulse was lower compared with conductance measured during the first pulse in all groups except groups 5 and 8 (two groups with no significant IRE ablation effect). For the most effective protocols, conductance was reduced by 31±6% and 34±11% for groups 1 and 4 respectively.

IRE effect on other arterial wall components

Successful IRE ablation of VSMC induced a reduction in media thickness: 25% reduction in Group 1 (45±10 vs. 59±8) and 27% reduction in Group 4 (37±4 vs. 51±6) .No Change in media thickness was induced in the two non-successful IRE groups (61±9 vs. 58±7 in Group 5, 61±9 vs. 60±6 in Group 8).

Endothelial cells of treated arteries were similar in number and morphology to those of non treated control arteries, but were negative to both CD31 and CD34 antibodies (data shown only for CD34 staining, see bottom row in Figure IV-13). EVG stain demonstrated intact elastic fibers and preserved vessel wall, similar to that of control arteries (middle

row, Figure IV-13). Masson Trichrome stain demonstrated minor fibrosis in perivascular areas, with collagen being the dominant component of the Tunica Media following the complete loss of VSMC population (top row, Figure IV-13).

	3500X10 (Group 1)			1750X10 (Group 2)			875X10 (Group 5)			437.5X10 (Group 8)		
	Control	IRE	%	Control	IRE	%	Control	IRE	%	Control	IRE	%
Cell Number	208±40	24±34	11	214±38	167±66	78	196±30	208±58	106	213±38	209±25	98
Concentration	1±0.2	0.2±0.2	16	1±0.2	0.9±0.2	88	1±0.2	0.8±0.3	83	1.3±0.2	1.3±0.2	101
Area	2.2±0.4	1.8±0.3	81	2.1±0.2	1.8±0.3	86	2±0.4	2.8±0.4	136	1.7±0.4	1.6±0.3	98
Thickness	59±8	45±10	75	57±3	54±5	94	58±7	61±9	105	60±6	61±9	102

Table IV-3 - Effect of 10 NITRE pulses - The table shows data of the four different 10-pulses protocols. All data are shown as average with standard deviation , and include the percentage of IRE values compared with control. Cell number is the average number of VSMC nuclei identified in the Tunica Media. Concentration is the ratio between the number of cells and the area of the Tunica Media (10-3 mm2). Area is the total area of the Tunica Media (10-1 mm2), and the thickness is the thickness of the Tunica Media based on five different measurements in each section in micrometers.

	1750X45 (Group 3)			1750X90 (Group 4)			875X45 (Group 6)			875X90 (Group 7)		
	Control	IRE	%	Control	IRE	%	Control	IRE	%	Control	IRE	%
Cell Number	204±20	30±33	14	213±33	13±21	6	230±53	85±66	37	236±61	49±40	21
Concentration	1.5±0.1	0.3±0.3	18	1.5±0.2	0.1±0.2	7	1.6±0.2	0.6±0.4	27	1.6±0.2	0.4±0.3	39
Area	1.3±0.1	0.97±0.2	73	1.5±0.3	1.3±0.2	77	1.4±0.2	1.3±0.2	70	1.5±0.2	1.1±0.2	88
Thickness	52±3	35±6	67	51±6	37±4	73	52±4	47±8	70	50±4	35±6	90

Table IV-4 - Effect of 45 or 90 IRE pulses - The Table shows data if the four different protocols with more than 10 pulses. All data are shown in the same manner as in Table IV-3.

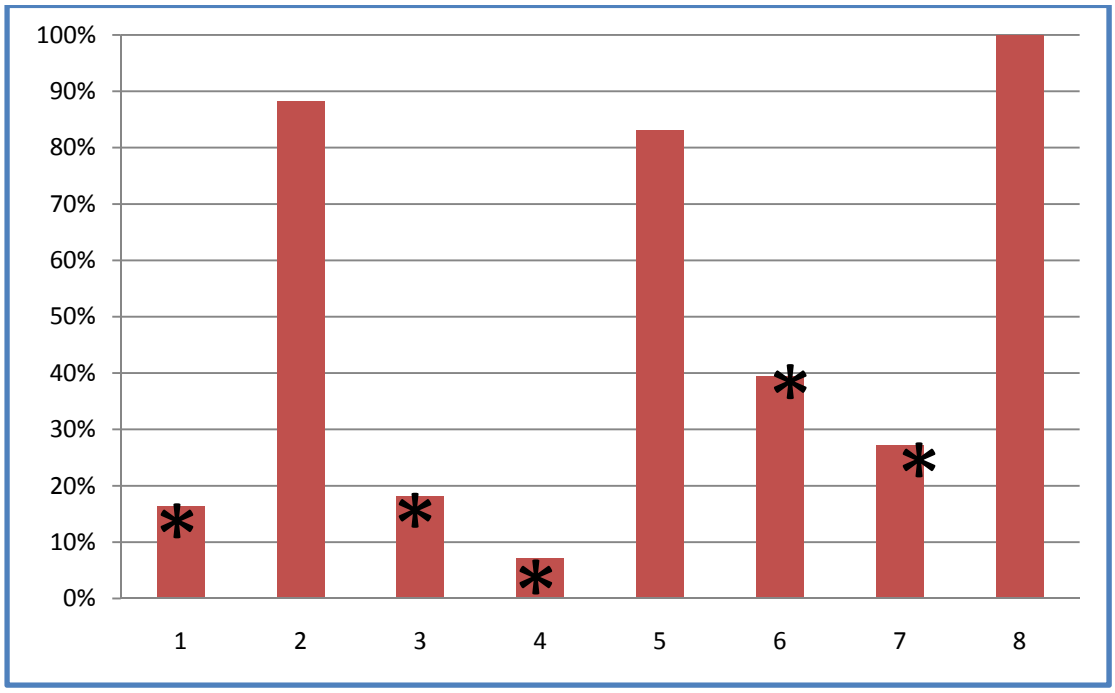

Figure IV-8 - Ablation effect due to different IRE protocols. The reduction in groups 1,3,4,6,7 was statistically significant (P<0.001). Ablation effect is shown as the percentage of VSMC cells in the treated artery compared with the right carotid artery of the same animal.

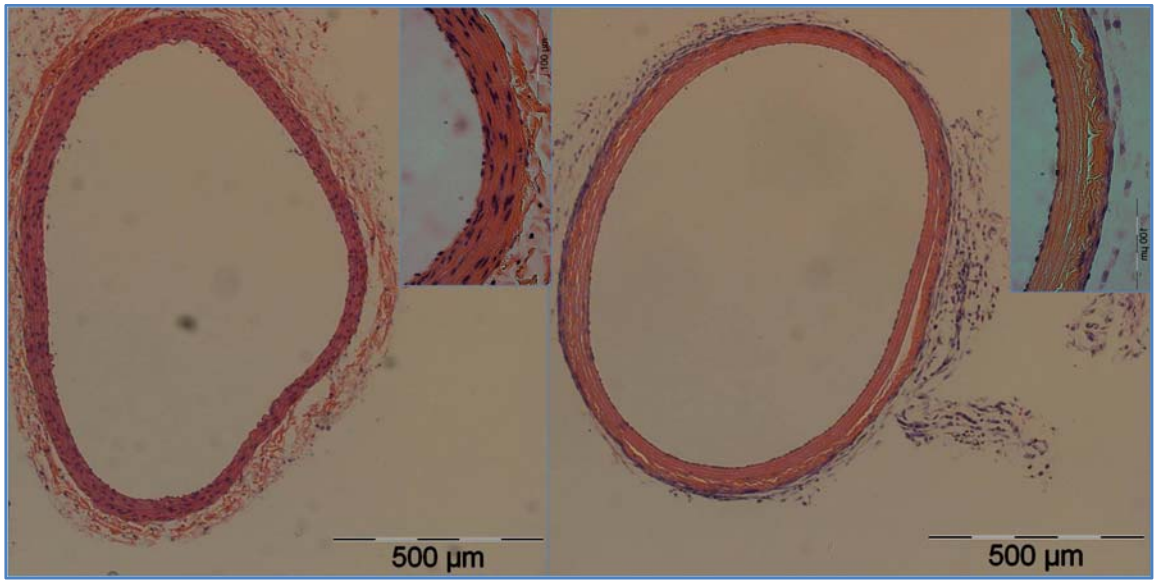

Figure IV-9 - Complete ablation of VSMC population one week following IRE (right picture) compared with right carotid artery of the same animal that was used as a control (left picture). Note the complete absence of VSMC cells compared with notable repopulation of the endothelial layer with endothelial cells.

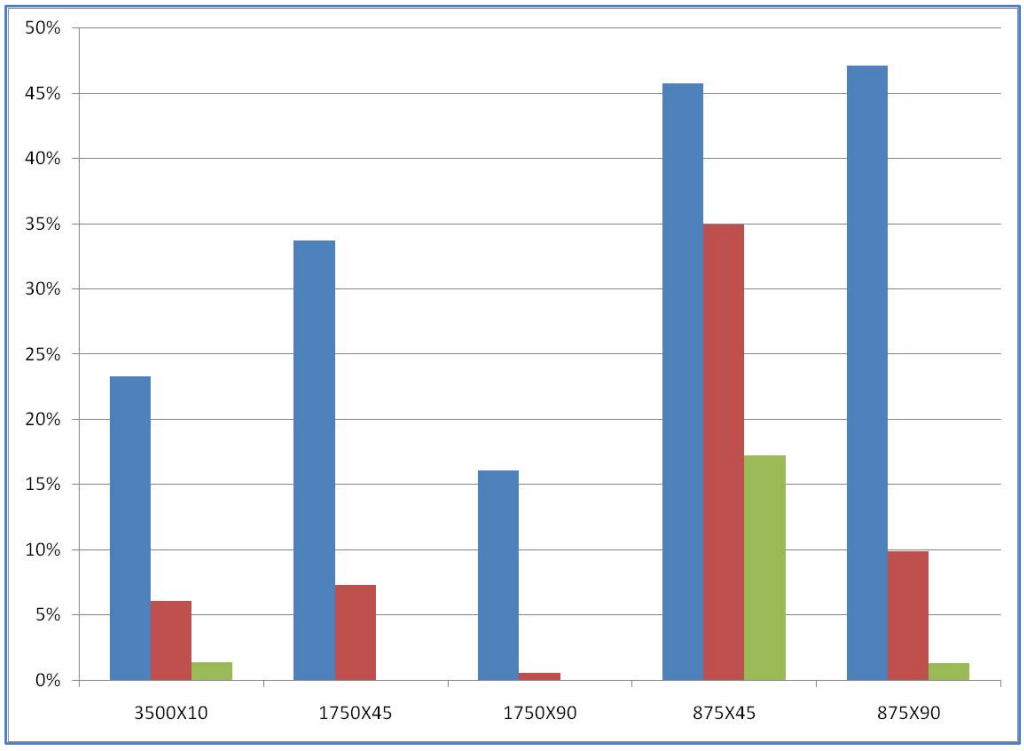

Figure IV-10 - Ablation effect on the sub-layer of the Tunica Media. Inner most, middle and outer sub-layer are in blue, red and green, respectively. Ablation effect is shown as the percentage of VSMC cells in the sub-layer compared with the same sub-layer in the right carotid artery of the same animal. Note the relative sparing of the inner most VSMC cells in all five groups, compared with the complete ablation of VSMC in the outer layers with 1750 V/cm (second and third groups in the figure).

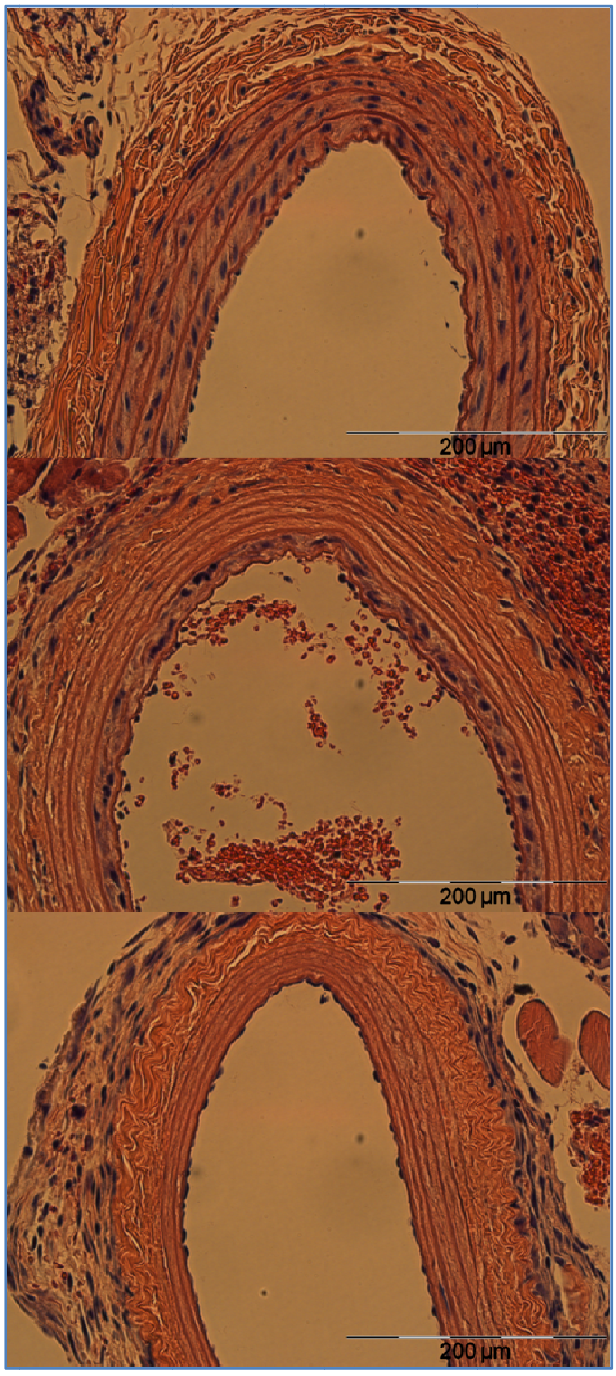

Figure IV-11 - Ablation effect on the sub-layer of the Tunica Media. Inner most, middle and outer sub-layer are in blue, red and green, respectively. Ablation effect is shown as the percentage of VSMC cells in the sub-layer compared with the same sub-layer in the right carotid artery of the same animal. Note the relative sparing of the inner most VSMC cells in all five groups, compared with the complete ablation of VSMC in the outer layers with 1750 V/cm (second and third groups in the figure).

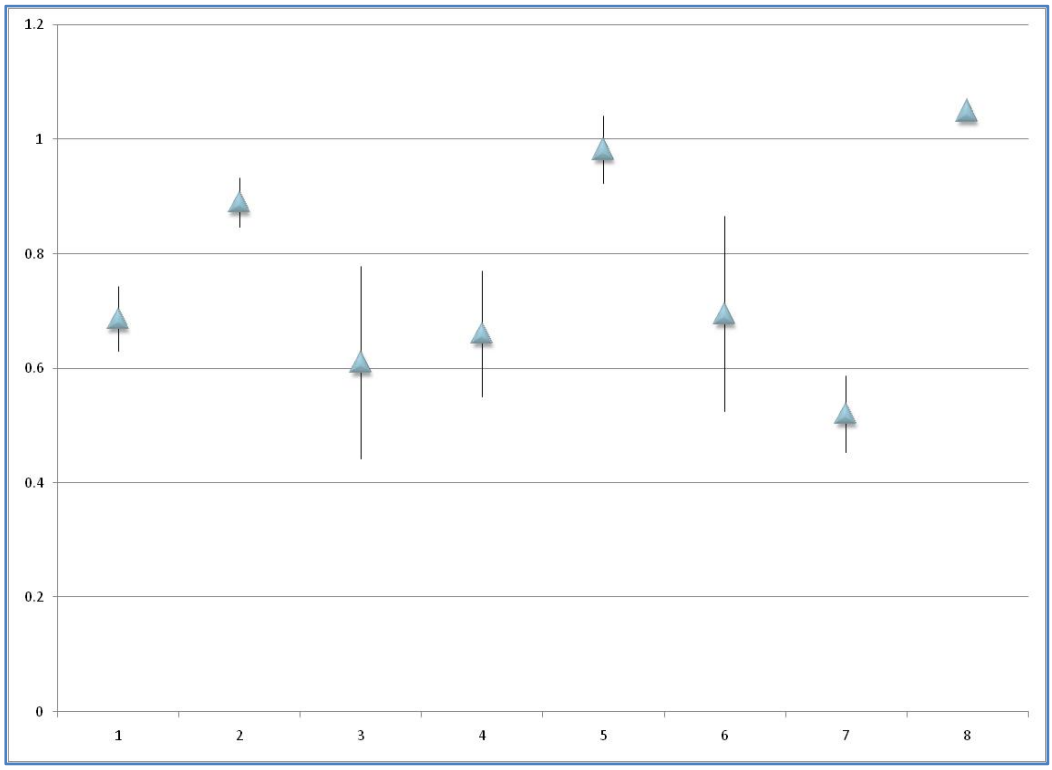

Figure IV-12 - Conductance change during IRE application. The change is shown as the ratio between the conductance value measured at the last electroporation pulse and the value at the first pulse. Groups 5 and 8 show no significant change in conductance, which correlated well with the histology result showing no significant ablation in these two groups.

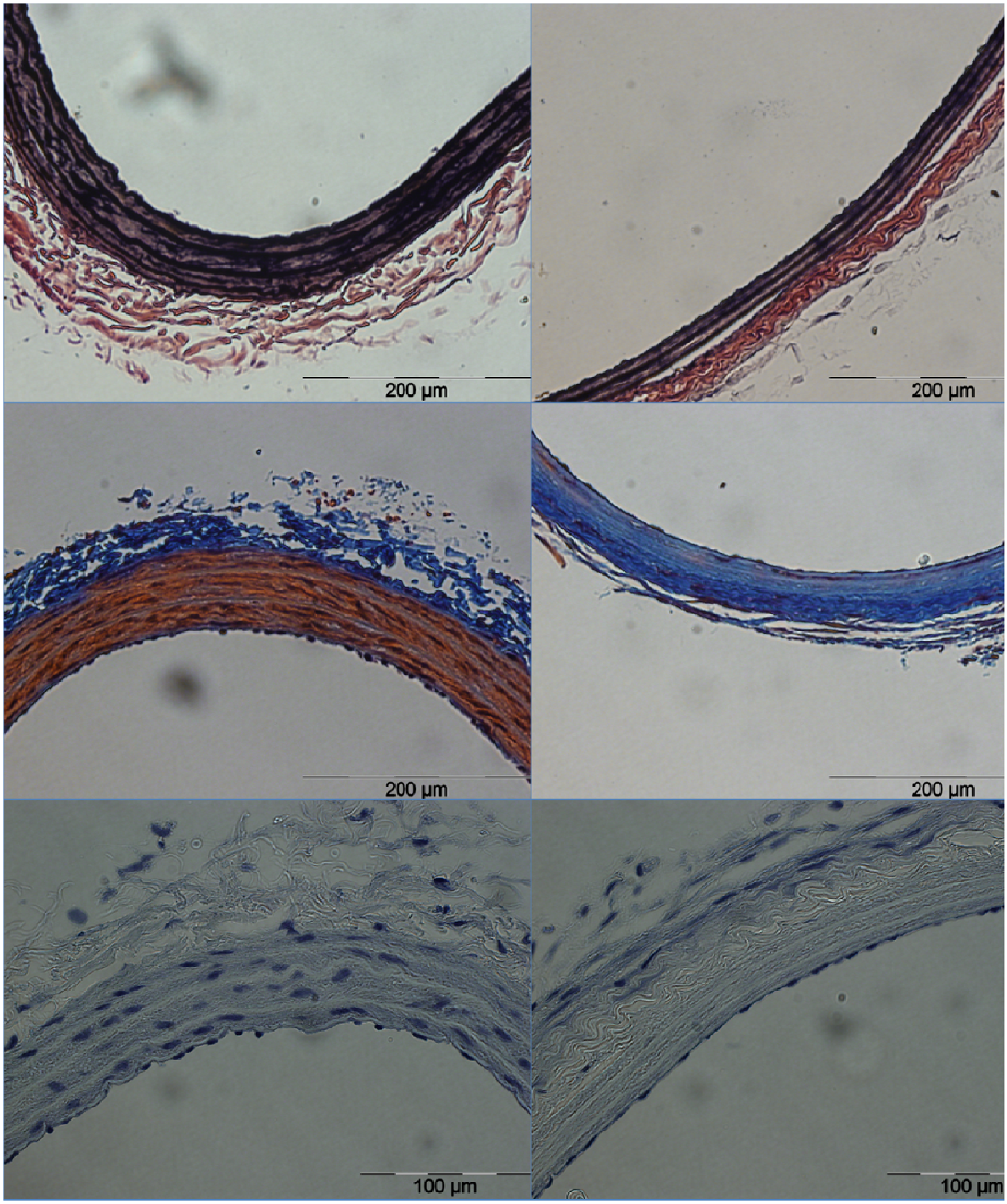

Figure IV-13 - Advanced histology staining. Left column shows control arteries and right column shows IRE-treated arteries. Top row - EVG stain showing undamaged elastic fibers in IRE-treated arteries (elastic Van Gieson, X40). Middle row - Masson Trichrome stain showing mild fibrosis in the perivascular area with dominance of collagen fibers in the Tunica Media of the IRE-treated Arteries (Masson Trichrome, X40) . Lower row - Negative staining of both arteries with CD34 antibodies at higher magnification (X60). Note the similar morphology and distribution of the endothelial cells.

4. Discussion

The results in this chapter include two separate experiments. However, due to common method and motivation , results are discussed here together. These results served as a guideline for IRE of larger vessels in larger animals, done in an minimally-invasive endovascular approach (for more details see chapter VI).

Experiment A was planned as a pilot study to examine the long term effects of IRE on a major blood vessel. The main finding is that IRE is indeed capable of ablating vessel wall VSMC and that all animals survived the application of IRE without any side effects. Considering that a major artery was treated, that IRE pulses where applied directly to the artery, and that electrical field magnitude was very high (on the scale of typical IRE pulses) this finding is indicative of the safety of treatment with respect to the application of IRE pulses near large blood vessels.

The findings of experiment A were reinforced by the results of experiment B. Furthermore, the main finding of experiment B was the high ablation efficiency of IRE sequence that includes 90 pulses of 1,750 V/cm at a frequency of 4 Hz compared with 7 other IRE sequences that were evaluated.

Four main observations are addressed below. First, the effect of different IRE sequences on vessel wall ablation efficiency . Second, in the effect of IRE on the extra cellular matrix. Third, electric behavior of the vessel wall during IRE pulses. And fourth, the temporal aspect of both experiments.

❖ *Optimizing IRE sequences*

Experiment B was designed in order to compare eight different IRE sequences, based on the preliminary results of experiment A that showed relatively high efficiency with 10

pulses of approximately 3,800 V/cm. Therefore, experiment B started with comparing decreasing electric field magnitudes in 10-pulses sequence (3,500, 1,750, 875, 437,5 V/cm). It continued with increasing the number of pulses to 45 and 90 in the two intermediate electric field values.

For groups 1 and 4 (see Table IV-1), where best ablation efficiency was observed, around 10% of VSMC population survived the ablation. Further analysis of the results demonstrated 100% efficiency in the outer layers of the Tunica Media, with all surviving cells located in the inner most layers of the arterial wall (Figures 3-4). The most probable explanation for this phenomena is the nature of the electric field. We assumed uniform electric field between the two electrodes, but since the arterial tissue is non-homogeneous with respect to its electric properties, the actual electric field in the inner most area of the artery was lower than expected. Better design with a more uniform electric field, might enable NTIRE to achieve higher ablation efficiencies compared with those reported in this study.

Our results show that reduction of electric field magnitude can be compensated by increasing the number of NTIRE pulses. These observation are in agreement with the results reported in Chapter III, where in-vitro IRE of VSMC demonstrated similar trend. Ten pulses of 3500 V/cm achieved similar effect to 90 pulses of 1750 V/cm. However, decreasing the electric field even more to 875 V/cm caused a decrease in NTIRE efficiency even with the use of 90 pulses. This important observation will be important in future NTIRE device designs. Intervention time can be reduced by increasing the potential difference between the different electrodes.

❖ *IRE effect on extra-cellular matrix*

The long term results of experiment A show that the effect of IRE on VSMC ablation was evident and persisted at 28 days. On the other hand, after 28 days, the extra cellular matrix component of the arterial wall were maintained, there was no evidence of necrosis, aneurysm formation, rupture or thrombosis. This again is consistent with the mechanism of action of irreversible electroporation. The mechanism of action of irreversible electroporation is to damage only the cell membrane and no other types of molecules in the tissue. Obviously the large blood vessel showed only ablation of cells and an intact cellular matrix. This is evidence of the safety of the procedure in relation to thermal treatment. It also explains why tissue treated by irreversible electroporation has a pronounced immunological response and rapid healing without scars.[91] The patency of the larger blood vessels provides exquisite access to immune cells as well as of nutrients to the treated tissue. The presence of the extracellular matrix provides a good scaffold for the formation of new and healthy tissue, as seen in the liver.[91]

The internal lamina and endothelial layer of IRE treated arteries had a much thinner and condensed appearance after 28 days, compared with control arteries. This observation might indicate that a different mechanism of recovery is involved in the reconstruction of the endothelial layer. A Plausible explanation might be a rapid regeneration of the endothelial layer from circulating endothelial progenitor cells in the circulation.

❖ *Electric behavior of the vessel wall during IRE pulses*

A common observation in previous electroporation studies, either reversible or irreversible, is that electrical conductance measured at the pulses increases during the sequence of pulse.[102] The only exception to this seems to be skeletal muscle under

IRE.[87] In that particular case, conductance measured at the pulses remains quite constant during the whole sequence and it can be explained as a saturation effect of the electroporation phenomenon. However, the fact that conductance decreases during the sequence is quite surprising as it contradicts what would be expected in a simple electroporation model: electroporation increases cell membrane permeability to ions and therefore its conductance also should increases. There is no definitive explanation for the conductance decrease observed here. A plausible hypothesis might be that IRE pulses cause contraction of the arteries by stimulating the vascular smooth muscle cells and that such contraction results in an increase of the electrical impedance of the arteries.[103-105] Another explanation could be based on the fact that electroporation disturbs the osmotic balance of the cells and causes cell swelling which in turn can result in a decrease of the conductance.[87] Nevertheless, such swelling cannot be manifested as fast as would be required here in order to explain the conductance decrease during the sequence, particularly in groups 1 and 2 (sequence duration = 1 second) of experiment B.

❖ *Temporal aspects*

The sampling at 24 hours and seven days following the application of the IRE pulses in experiment A, while not the primary goal of this long term effect study, provide interesting observations. This is why, while not part of a systematic study, the results are presented here. The observation that the effects of irreversible electroporation cannot be detected 24 hours after the application of the pulses is interesting. It is consistent with the mechanism of action of electroporation, i.e. the formation of nano-scale defects on the cell membrane, as well as with in-vitro results presented in Chapter III that showed that the disappearance of VSMC is not immediate. It also suggests that study of irreversible

electroporation requires long term experiments to observe an effect. The normal morphological appearance of the cells after 24 hours suggests that nano-scale defects on the cell membrane might not be the only mechanism involved in cell death. The high electrical field used might have damaged other crucial parts of the cell (including the chromosomes, cell proteins etc.), and this damage might have triggered apoptotic processes within the affected cells that were not evident with the standard H&E method.

The seven day sample is also very interesting. It appears that within seven days the number of VSMC nuclei drops and that the number of VSMC nuclei in the arterial wall following IRE ablation was significantly lower compared with control arteries. However, it appears that at seven days some cells where still visible and only apoptotic tests show that the cells are not alive. The process of cell death due to IRE is intriguing and obviously requires detailed research.

Experiment A evaluated four animals after 28 days. The results show that not only was the ablation efficient, but also demonstrate the limited regeneration capacity of the VSMC population of the vessel wall. For further discussion on the long term effect on IRE in large animal vessels, please see chapter VI.

With the three different time point observations available from experiment A, experiment B was designed to examine different IRE protocols. All 33 animals in experiment B were followed-up for 7 days period. It seems that destroyed cell disappear by day 7, as evident from the results of group 4 (see Table IV-4) where 94% of the cells disappeared after one week.

The results of experiments A and B guided the design of first endovascular IRE experiments in larger animals. This is why larger animals were euthanized after 7 days and 35 days. The first follow-up period was used to evaluate ablation efficiency , and the second one was used to study the long term effect of IRE on larger blood vessels. For more details see chapter VI.

V. CHAPTER FIVE: ATTENUATION OF NEOINTIMAL FORMATION

1. Motivation and objectives

Results of Chapters III and IV demonstrated the ability of electroporation pulses to destroy VSMC *in-vitro* and *in-vivo*, respectively. As discussed in the previous chapter, the ablation of VSMC in the treated vessel wall has a long term effect and cells did not appear in the treated area even after 28 days in rodent models.

The motivation for the experiment described in this chapter is base on the combination of high ablation efficiency and long term effect on the vessel wall. With these two properties demonstrated, IRE can now be evaluated as a treatment strategy for fighting post-angioplasty restenosis.

Two main processes are thought to contribute to post-angioplasty restenosis: vessel wall remodeling and VSMC proliferation.[106,107] The first process can be successfully prevented by the use of a stent. The stent prevents the loss of vessel lumen by preventing the inward remodeling of the arterial wall.

The process of VSMC proliferation cannot be stopped by deploying a stent. Methods for the prevention of VSMC proliferation were discussed in Chapter I. IRE, with its high efficiency and long term effect, might prove to be a new and promising tool in the armamentarium of the cardiologist fighting post-angioplasty restenosis.

The objective of the current experiment was to demonstrated the feasibility of IRE in preventing VSMC proliferation in a rodent model. The rodent model uses a intravascular balloon catheter in order to damage the vessel wall, and is considered one of the most preliminary animal models of post-angioplasty restenosis.

2. Methods

❖ *In-vivo experiment*

Eight Sprague-Dawley rats weighting 300-350 grams were used in this pilot study. All animals received humane care from a properly trained professional in compliance with both the Principals of Laboratory Animal Care and the Guide for the Care and Use of Laboratory Animals, published by the National Institute of Health (NIH publication No. 85-23, revised 1985).

Each animal was anaesthetized throughout the procedure. The left common carotid artery was exposed, and intimal denudation was performed as previously described in chapter IV.[108] Briefly, the left external carotid artery was incised, and a 2F Fogarty arterial embolectomy catheter (Edwards Lifesciences) was advanced through the incision to the left common carotid artery. The balloon was inflated and drawn back three consecutive times. At the end of the procedure the balloon was deflated, extracted and the left external carotid artery was ligated.

Four rats were used as control, and their skin incision was sutured immediately at the end of the procedure. In the remaining four rats, a custom made electrode clamp with two parallel disk electrodes (diameter = 5 mm) was applied on the left common carotid artery, very close to its bifurcation to the internal and external carotid arteries, at the exact site of intimal damage (see Figure IV-1 for further details). The measured distance between electrodes was approximately 0.3 mm. A sequence of 10 direct current pulses of 115 Volts (i.e. electrical field of approximately 3800 V/cm), 100 µs each, at a frequency of 10 pulses per second, was applied between the electrodes using a high voltage pulse

generator intended for electroporation procedures (ECM 830, Harvard Apparatus, Holliston, MA). Current and voltage were recorded by means of special oscilloscope probes (current probe was AP015 and high voltage probe was ADP305, both from LeCroy Corp.). From these two signals conductance was obtained during the pulses. The procedure was applied in three successive locations along the common carotid artery. At the end of the procedure the skin incision was sutured and animals were kept alive for a follow-up period of 28 days until they were euthanatized.

❖ *Histology*

Animals were euthanized with an overdose of Phenobarbital. The arterial tree was perfused with 10% buffered formalin for 40 minutes, and the left and right carotid arteries were exposed near the bifurcation of the internal and external carotid arteries. One slice of 1 cm from each artery, at the core of the treated area, was used for histological analysis. Each slice was fixed with 10% buffered formalin, embedded in paraffin, and sectioned with a microtome (5-µm-thick). One section was stained with hematoxylin and eosin. The endothelial layer was assessed by lectin immunostaining. Each slide was photographed at X200 magnification, and the following areas were measured: tunica media area, neointimal area and lumen area. The unequal variance t-test method was used to evaluate the statistical difference between the measured areas of the two different groups.

3. Results

All animals survived the procedures. Conductance of the arterial wall decreased during successive direct current pulses (Figure V-1). During the follow-up period there were no signs of cerebrovascular events (paraplegia, paraparesis, etc.) and there was no mortality.

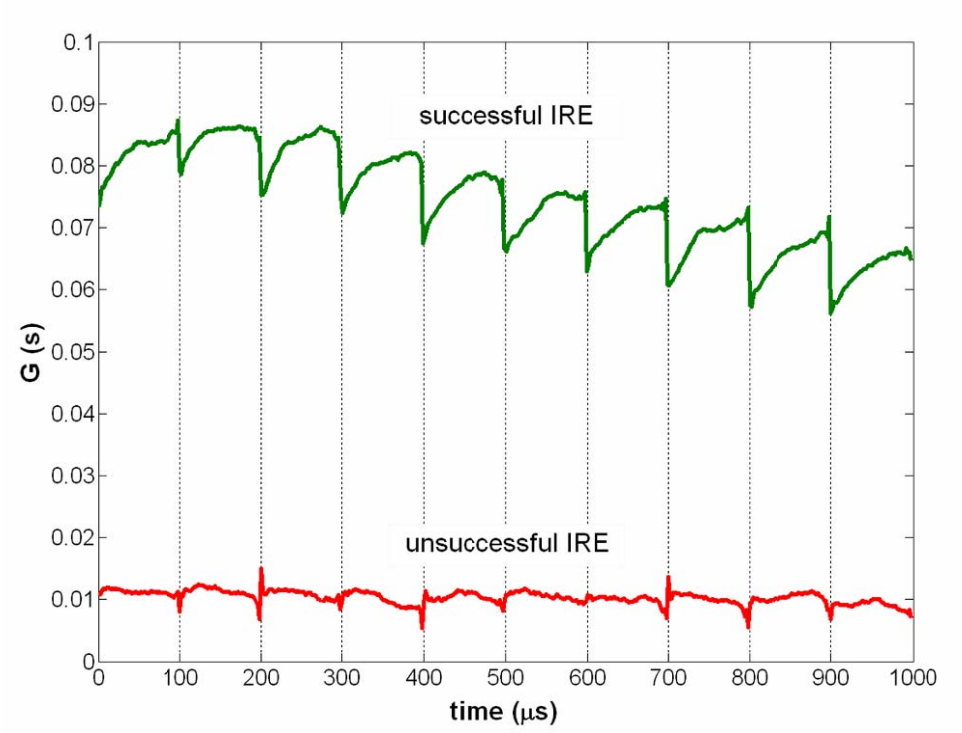

Figure V-1 - Examples of conductance or the arterial wall during repetitive direct current pulses. Conductance is measured only during the 100 μs pulses and here it is displayed without the 100 ms intervals between pulses. Two cases are shown: a trial in which successful irreversible electroporation was achieved and a case in which the voltage pulses apparently were not able to cause electroporation.

Conductance was measured during IRE pulses and was used to monitor the successful use of the electroporation device. Successful IRE was assigned to those cases in which significant conductance increase was observed during applied pulses, as depicted in the case shown in Figure V-1. IRE was successful in 3 of the 4 animals. There were no changes in conductance during the pulses applied to the fourth animal and this was considered to indicate unsuccessful IRE (see also Figure V-1). A constant observation in all successful IRE cases was that, despite increased conductance during each pulse, the overall conductance for the whole sequence decreased.

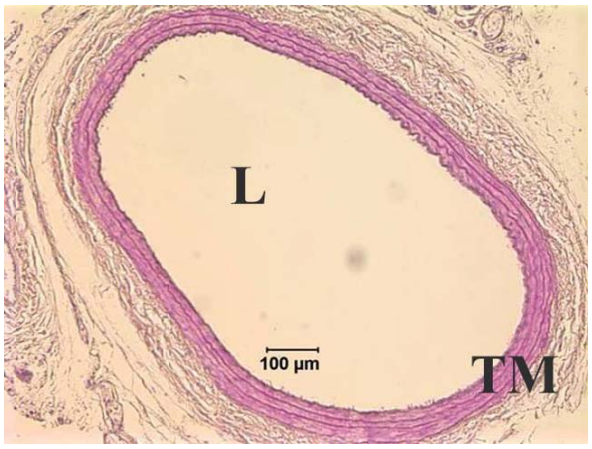

Figure V-2 - Right common carotid artery. This slide is an example of the appearance of a normal right carotid artery. (L- Intra-arterial lumen; TM – Tunica media)

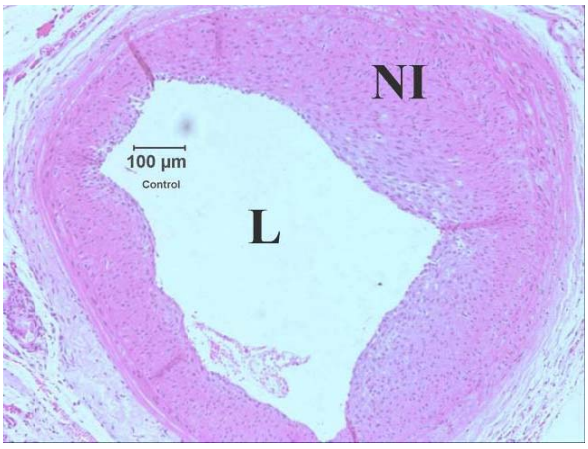

Figure V-3 - Left common carotid artery 28 days after intimal damage, showing high neointima to media ratio. (L- Intra-arterial lumen; NI – Neointimal Formation)

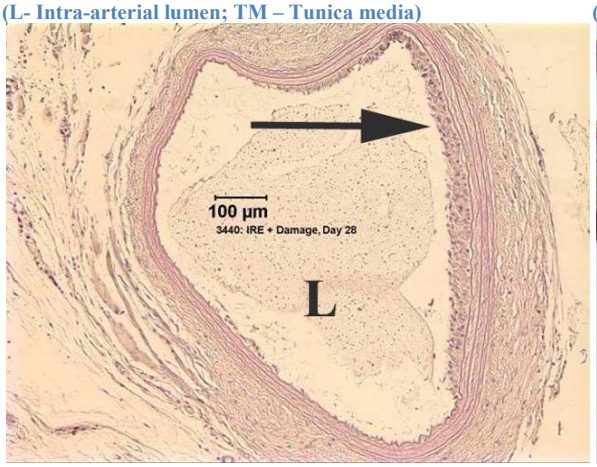

Figure V-4 - Left common carotid artery 28 days after intimal damage in an IRE treated rat, showing the scarcity of neointimal formation compared with figure 3b (L- Intra-arterial lumen; Arrow – minimal neointimal formation)

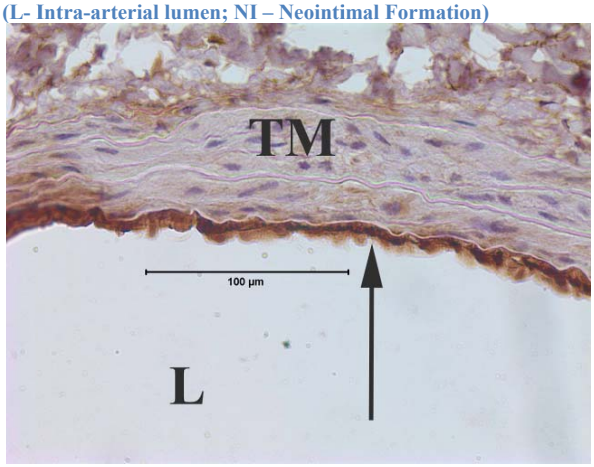

Figure V-5 - Figure 4a: Right common carotid artery. This slide is an example of the appearance of a normal control endothelial layer (L – Intra-arterial lumen; TM- Tunica media; Arrow – Endothelial layer)

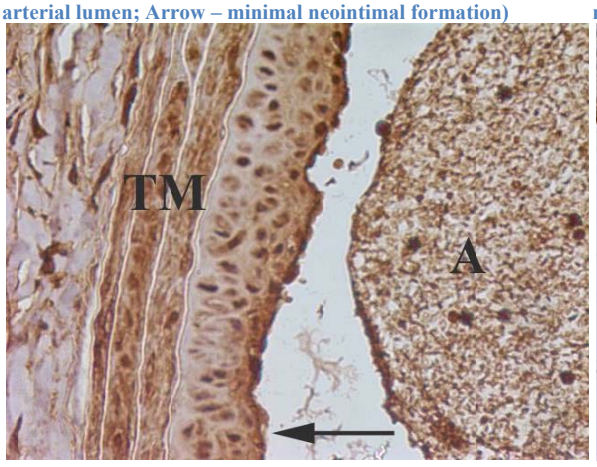

Figure V-6 - Left common carotid artery, 28 days after intimal damage and IRE. This slide shows the overall preserved appearance of the endothelial layer. (A – Intra-arterial lumen artifact; TM- Tunica media; Arrow – Endothelial layer)

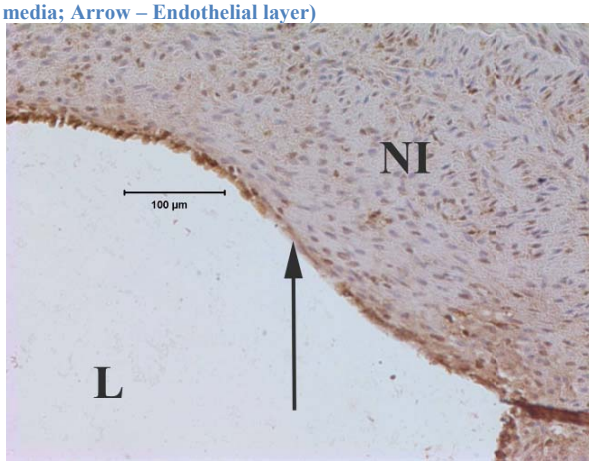

Figure V-7 - Left common carotid artery, 28 days after intimal damage. This slide shows the damaged and irregular endothelial layer in the control group. (L- Intra-arterial lumen; NI – Neointimal Formation; Arrow – irregular endothelial layer)

Animal #	Intervention	Tunica media area (mm2)	Neointima area (mm2)	Lumen area (mm2)	Neointima/Media ratio	Neointima/Media average ratio*
1	Intimal damage & successful IRE	0.17	0.18	0.27	1.07	
2	Intimal damage & successful IRE	0.08	0.03	0.32	0.38	0.57±0.4
3	Intimal damage & successful IRE	0.16	0.04	0.31	0.28	
4	Intimal damage & failed IRE **	0.08	0.21	0.05	2.69	
5	Intimal damage alone	0.17	0.17	0.30	0.99	
6	Intimal damage alone	0.11	0.11	0.30	1.01	1.67±1.0
7	Intimal damage alone	0.11	0.17	0.35	1.49	
8	Intimal damage alone	0.12	0.38	0.25	3.19	

Table V-1- Morphometric analysis of experiment slides; * P = 0.06; ** Unsuccessful IRE (See text)

After 28 days, histological analysis was used to compare the IRE-treated and the control group (Figure V-2, Figure V-3 and Figure V-4). Measurements of neointimal area, tunica media area and arterial lumen area are summarized in Table 1. Compared with control (including the one unsuccessful IRE animal), successful IRE induced a significant reduction in the neointima to media ratio (0.57±0.4 vs. 1.88±1.0, P = 0.02). In addition, compared with control (excluding the unsuccessful IRE animal), successful IRE induced a reduction in neointimal to media ratio that was less significant (0.57±0.4 vs. 1.67±1.0, P = 0.06).

Endothelial layer seems to have well recovered in the IRE-treated animals compared with control group animals. Endothelial integrity was similar in the IRE-treated group to its appearance in the unharmed right common carotid artery (Figure V-5, Figure V-6 and Figure V-7).

4. Discussion

This experiment is probably the first to show the ability of IRE to reduce restenosis.[109] There was a tendency toward a lower neointimal formation following successful IRE, compared with control animals. Based on histological analysis, the extra cellular matrix component of the arterial wall was maintained; there was no evidence of necrosis, aneurysm formation, or thrombosis, and there was remarkable recovery of the endothelial layer.

This experiment shows that compared with non-IRE treated controls, there was significant decrease in neointimal formation 28 days after intimal damage in IRE-treated arteries. In chapter IV it was shown that in the same model, IRE induced significant

reduction in the VSMC population without apparent damage to elastic fibers.[82] Clarke et al. investigated the role of VSMC per se in vascular disease. [110] Using transgenic mice expressing human diphtheria toxin receptor on all VSMCs, they showed that apoptosis of 50-70% of the VSMC population in normal arteries induced no endothelial loss, inflammation, reactive proliferation, thrombosis, remodeling or plaque formation. We believe that by selectively destroying the VSMC population without affecting the extracellular matrix, the specific non-thermal IRE ablation method developed here severely reduces the potential ability of neointimal formation, without significant damage to arterial function and overall structure.

IRE, and electroporation in general, produces nano-scale defects in the cell membrane and thereby facilitates unimpeded ion transport across the membrane.[111] Therefore, successful IRE results in immediate changes in the passive electrical properties of the tissue that can be measured and employed as a feedback mechanism for real time control of the technique. In fact, within the context of reversible electroporation, such strategy has been described previously for individual cells , cell cultures and tissues.[112-115]

A common, and expected, observation in previous studies in which in vivo conductance has been measured during the application of a sequence of high voltage pulses, either for reversible or for irreversible electroporation, is that electrical conductance increases during the sequence and not only within the pulses. The only exception seems to be the skeletal muscle under IRE. In that particular case, conductance measured at the pulses is quite constant during the whole sequence. However, the cases reported here are probably the first ones in which conductance decreases during the sequence of pulses. There is no definitive explanation for such phenomenon. A plausible hypothesis is that IRE pulses

cause contraction of the arteries [103] and that such contraction results in an increase of the impedance of the arteries, particularly of the smooth muscle tissue.[104,105]

It is not clear why IRE was not applied properly in one of the animals. Electrodes were probably not applied properly to the artery, and the resulting electrical contact was not good enough over the artery. Direct short-circuiting of the electrodes or through plasma or saline solution does not seem plausible because it would have caused larger conductivity than the measured conductivity during the pulses (Figure V-1).

Successful IRE depends on parameters such as electric field magnitude, pulse length and frequency. The reason for choosing the particular electrical parameters used in this study are consistent with the mode of application of IRE that was described in previous chapters. These are electrical parameters that were assessed to be high enough to ensure irreversible electroporation [116-118,89,91] but which do not cause damaging levels of Joule heating. We used a sequence of 10 direct current pulses of 115 Volts (i.e. electrical field of approximately 3800 V/cm), 100μs each, at a frequency of 10 pulses per second. These parameters where partially based on previous experiments that showed successful tumor cell ablation with IRE.[89,93,91] The electrical field used was higher than any previous report but low enough not to produce thermal damage within the constraints of the treated tissue dimensions. Further research will enable to better understand the electrical field magnitude needed for successful IRE of the arterial wall in humans and larger animals. There is also a need to better understand the relation between conductance measurements during the procedure and IRE efficiency.

Rodent carotid artery model was used in this experiment. This model is an acceptable animal model of restenosis [119,108] although the arteries were atherosclerotically changed. Further research will need to address the efficacy of IRE in atherosclerotically changed arteries.

The electrodes were clamping the artery on its outer surface, but this does not imply that this method will be used as an invasive procedure. In chapter VI prototype C is shown to ablate VSMC using an endovascular approach. Previous reports have already demonstrated the ability to design and use intra-vascular devices in order to induce reversible electroporation of the arterial wall.[116]

This experiment is preliminary and its statistical power is limited. Nevertheless, it propose and demonstrate for the first time the *in-vivo*, long-term results of non-thermal, non-pharmacological strategy to attenuate neointimal formation following angioplasty. It holds the potential to assist in the treatment of restenosis following coronary angioplasty and deliver the treatment with real time control over the application.

For a discussion of the advantages of IRE in the treatment of restenosis and atherosclerosis see Chapter 0.

VI. CHAPTER SIX: ENDOVASCULAR IRE IN LARGE ANIMALS

1. Motivation and objectives

The feasibility of endovascular IRE was discussed in Chapter II, and with the use of finite-element simulation it was demonstrated that both prototypes B and C can be used to apply a relatively uniform electric field across vessel walls. Moreover, it was demonstrated that both prototypes can apply electric field that is high enough to induce IRE without causing thermal damage to the vessel wall.

The results presented in Chapter IV demonstrated again the ability of electric field sequences to efficiently destroy VSMC, and established the correlation between electric field threshold and the number of pulses applied.

The theoretical and computational work of Chapter II , together with the *in-vitro* results of Chapter III, were followed by extensive *in-vivo* experiments presented in Chapter IV. It was shown there that IRE ablation of VSMC has a long term effect, and that a sequence of 90 pulses applying electric field of 1,750 V/cm or above were high enough to destroy practically the entire VSMC population of the arterial wall.

However, from the clinical perspective IRE will preferably be used in minimally-invasive endovascular approach. This necessitate an animal model that is large enough in order to work with endovascular devices comparable to those used in human peripheral and/or coronary arteries.

The results of chapter IV cannot be applied directly to an endovascular IRE device. The main difference between the model used in chapter IV (two parallel gold electrodes

clamping an exposed segment of the carotid artery, see Figure IV-1 page 66) and prototypes B and C is the orientation of the electric field.

In chapter IV, the electric field was perpendicular to the orientation of the smooth muscle cells. In contrast, for both endovascular device prototypes the electric field orientation is not perpendicular but rather circular in its orientation. Therefore, experimental data and proof is important in order to validate the results presented above and apply them to human endovascular IRE experiments.

The objectives of the experimental work with large animals presented below were:

1. To Evaluate the *in-vivo* feasibility of endovascular IRE prototypes B and C.

2. To evaluate the short and long term effect of non thermal IRE in large animal model.

Two reasons made New-Zealand white rabbits the optimal animal model for this series of experiments. First, New-Zealand white rabbits are one of the most investigated species with respect to atherosclerosis/restenosis induction and progression.[108,119] Second, the dimensions of its iliac arteries are similar to human coronary arteries. This animal model usually includes any combination of three type of injuries to induce atherosclerotic-like lesions [120,27]:

1. Systemic biochemical injury with high cholesterol diet.[121]
2. Local mechanical injury , usually with air dissection [122]
3. Balloon catheter injury, also called the Baumgartner technique.[123]

However, since the objective of the experiment described below was to test the device IRE ablation efficiency, and in order to minimize biological variability and any possible

biases, experiments were done with intact and uninjured iliac arteries. With respect to this experiment objectives (evaluating the ablation efficiency of VSMC) there was no need for an atherosclerotic lesion.

2. Methods

❖ *Device assembly*

The endovascular device used in this study was described in previous chapters. The catheter shaft consisted of a 0.5 mm diameter nickel titanium (NiTi) tube electrically insulated with a layer of polyimide and polyethylene terephthalate. Rectangular nickel titanium wire with cross sectional dimensions of 0.5 mm x 0.1 mm and an active length of 20 mm was used as the electrodes, with a bipolar design of 4 separate electrodes. The electrodes were orientated parallel to the axis of the balloon and evenly spaced in a radial pattern around the circumference of the balloon. The electrodes were positioned over a standard polyethylene terephthalate non-compliant balloon with an expanded diameter of 3 mm and a length of 20 mm.

❖ *In-vivo Procedure*

Eleven New Zealand white rabbits weighing 3.6-4.6 Kg were used in this study, which was approved by the Institutional Animal Care and Use Committee of ISIS services facility, Berkeley. Ketamin (35mg/kg body weight) and Xylazine (5 mg/kg body weight) were used for anesthesia induction, followed by endotracheal intubation and isoflurane for anesthesia maintenance. Animals were monitored continuously (oxygen saturation, ECG monitor, blood pressure, respiratory rate, CO_2 production and core body

temperature). Under sterile technique, the area over the right iliac artery was exposed. Arteriotomy was performed, and a 4F introducer was placed in the right femoral artery.

Endovascular IRE device of prototype B was inserted in a retrograde manner in two animals, and endovascular IRE device of prototype C was inserted in the same manner in 9 animals. Using angiography guidance, the catheter was advanced to the aortic bifurcation, and inflated along the first two centimeters of the right iliac artery. IRE protocol in all animals included 90 pulses of 100 μsec at 4 Hz frequency. Potential difference was 350 Volts for prototype B and 600 Volts for prototype C. Pulses were applied using a high voltage pulse generator intended for electroporation procedures (ECM 830, Harvard Apparatus, Holliston, MA). Current and voltage were recorded by means of special oscilloscope probes (current probe was AP015 and high voltage probe was ADP305, both from LeCroy Corp.). From these two signals conductance was obtained during the pulses.

E.C.G was recorded and printed before, during and immediately after the procedure. After removal of the balloon device, control angiography was performed to confirm patency of the vessel and to rule out any local bleeding of the treated artery. At the end of the procedure, the iliac artery was ligated, and the surgical wound was closed. Animals recovered and kept in the animal facility for a follow up.

Follow up time of 7 days was used for prototype B animals as well as for five of the prototype C animals. Follow up period of 35 days was used for four prototype C animals. The end of the follow up period, animals were anesthetized as described above and then

euthanized with an overdose of Phenobarbital. For each animal, both iliac arteries (3cm segments starting from the aortic bifurcation) were harvested and sent to histology.

❖ *Histology*

Formalin-fixed, intact segments of the left and right iliac arteries from eleven rabbits were submitted to independent pathology lab (Charles River Laboratories Pathology Associates). Treated segments of those arteries were delineated by sutures in their proximal edge. Six consecutive sections were prepared from each of the right iliac arteries, and three consecutive sections were prepared from each of the left iliac arteries. The tissues were processed through and embedded in paraffin. From each paraffin block, three 5μ sections were prepared and stain with hematoxylin & eosin (H&E), Masson's trichrome (MT), and Verhoeff's elastin (VE) stains. The sections were evaluated microscopically by an independent pathology expert (Charles River Laboratories Pathology Associates), who was blinded with respect to the slide's numbers. Photomicrographs of significant changes were prepared and are included in Appendix 2. Selected sections (one control, one 7-day artery and two 35-days arteries) were processed and evaluated using immunohistochemisty. Evaluation included Smooth muscle actin (SMA), proliferating cell nuclear antigen (PCNA), von willebrand factor (vWF) and S-100.

3. Results

For each artery segment, two parameters were evaluated: mural damage (i.e. VSMC ablation) and inflammation. The distribution (portion of the section circumference affected) and severity of the changes were scored.

1. Distribution score for both parameters were based on the following: 0 = No change; 1 = Less than 10%; 2 = 10%-24%; 3 = 25-75%; 4 = more than 75%.
2. Mural damage scores were based on the following changes: 0 = No Change; 1 = internal elastic lamina (IEL) fragmented or missing; 2 = less than 50% of VSMC affected; 3 = 50-75% of VSMC affected; 4 = >75% VSMC affected.
3. Inflammation scores were based on the following: 0 = no inflammation; 1= minimal; 2 = mild; 3 = moderate; 4 = marked (severe).

❖ *Results with Prototype B*

Device failure

Experiment included only two animals and was stopped due to device failure. High electric current measurements on the oscilloscope, implying a "short circuit", were the reason for stopping the experiments. On gross inspection of the devices immediately after the experiment there were clear areas were the silver-coated ink failed (

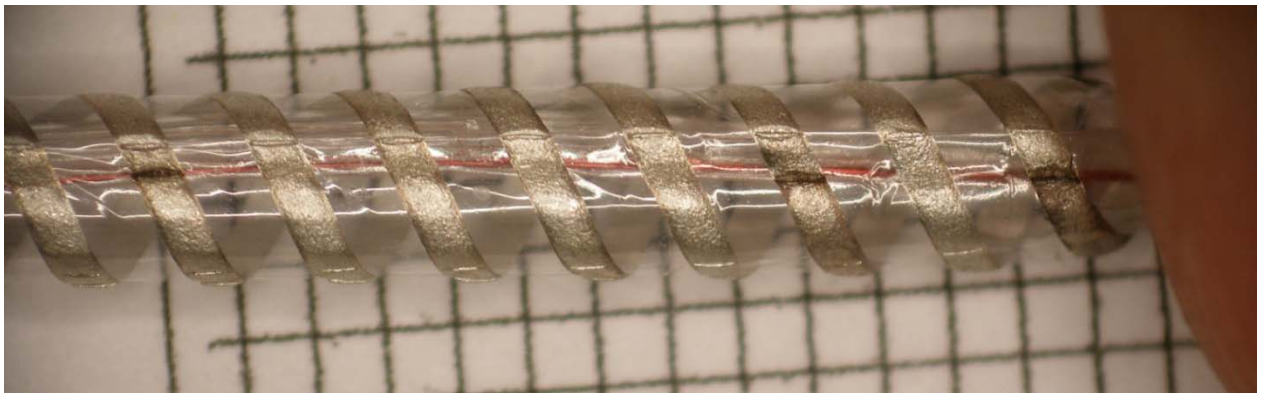

Figure VI-1) . These areas included both discontinuation of the conductor lining as well as changes most compatible will local sparks, along the lines of the balloon folding.

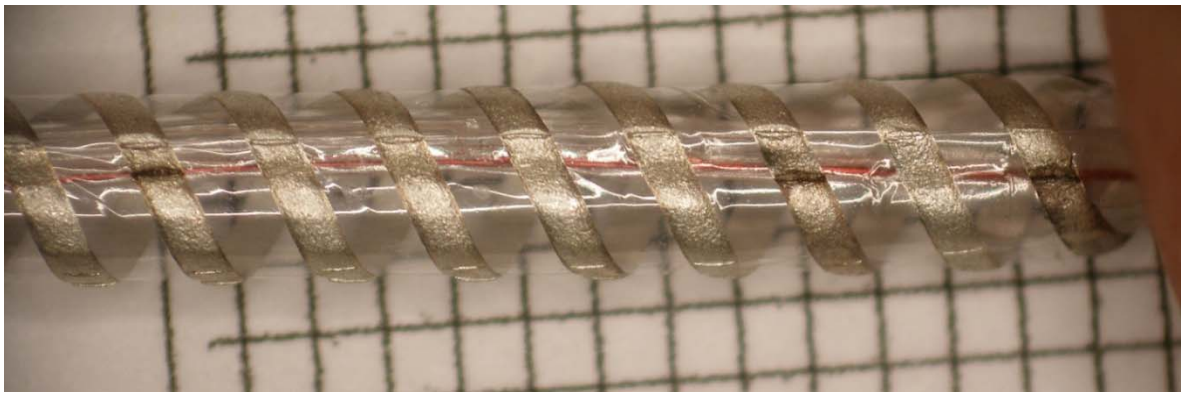

Figure VI-1 - Prototype B following *in-vivo* endovascular use. Note three areas of failure, corresponding with the line of the balloon folding.

Histology

The two animals survived, without infection or evidence of limb ischemia. On gross pathology both IRE-treated arteries were not different from control arteries, and there was no evidence of bleeding or thrombosis.

Severe mural damage was present in nearly all sections of both right (IRE-treated) iliac segments, while sections of left iliac segments were unremarkable. In the IRE-treated segments, VSMC population was partially to completely missing and was, in part, effected by fibrous connective tissue. Histology scores of mural damage (i.e. VSMC ablation) and local inflammation are summarized in Table VI-1.

Animal # / Section #	Wall ablation		Inflammation		Comments
	Dist.	Sev.	Dist.	Sev.	
L303- L / 1-6	0	0	0	0	Unremarkable .
L303 - R / 1	2	3	0	0	Partial ablation.
L303 - R / 2	3	4	1	1	Partial ablation.
L303 - R / 3	4	4	2	3	Most of VSMC have been destroyed.
L303 - R / 4	4	4	3	2	A portion of the section is artificially missing. Most of the endothelium and all of the VSMC have been destroyed.
L303 - R / 5	4	4	2	2	Nearly all VSMC have been destroyed. Small fibrinous mural thrombus.
L306 - L / 1-6	0	0	0	0	Unremarkable.
L306 - R / 1	2	3	2	2	Partial ablation.
L306 - R / 2	2	4	2	2	Same as L306 - R / 1
L306 - R / 3	4	4	2	2	Same as L306 - R / 1

L306 - R / 4	3	4	2	2	Same as L306 - R / 1
L306 - R / 5	2	4	2	1	Same as L306 - R / 1
L306 - R / 6	3	4	2	2	Same as L306 - R / 1

Table VI-1 - Independent pathology report of two animals treated with prototype B. Both animals were euthanized after one week.

❖ *Results with Prototype C*

Experiment included nine animals. With the exception of animals #L2319 and #L4124, experiments were unremarkable, with no problem with deploying the device, no bleedings, no E.C.G changes, and similar oscilloscope measurements with all animals. Five animals were euthanized after 7 days, including animals #L2319 and #L4124. Four animals were euthanized after 35 days.

Electrical conductance measurements

Electrical conductance was measured during each electroporation pulse, by recording the voltage and the current during the application of the electric field. Electrical conductance was recorded in ten out of the eleven electroporation sequences applied to eleven iliac arteries. Three of the recordings could not be used due to device failure (2 with prototype B and one with prototype C). The remaining 7 observations demonstrated a slight increase in electrical conductance between the last and first electroporation pulse. All conductance measurements are summarized graphically in Figure VI-2.

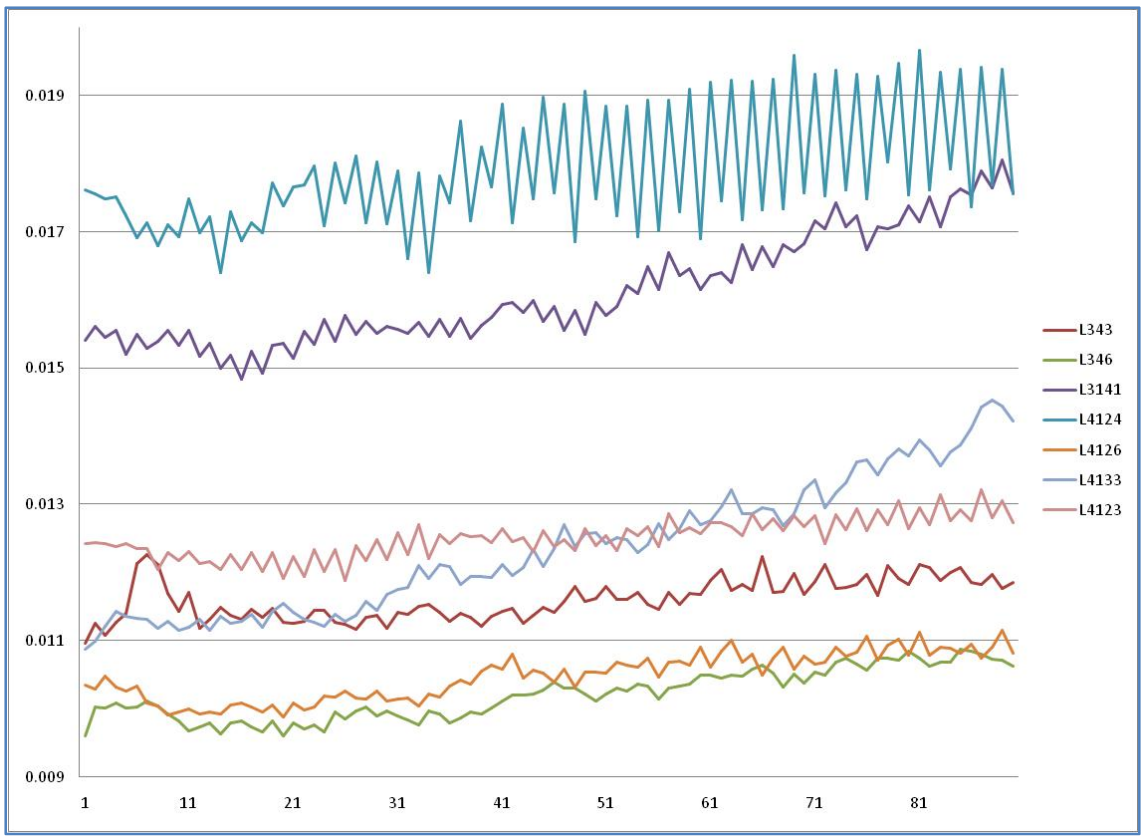

Figure VI-2 - Electrical conductance (I/V) in Siemens during electroporation pulses with prototype C. Note the slight increase in conductance between the last and first electroporation pulses.

Animal # L2319

Due to insufficient amount of pancuronium, only partial relaxation of striated muscles was achieved in this animal. During electroporation pulses application, muscle contraction caused significant movements of the entire animal. Electric current measurement during pulse application showed sudden increase in current after 20 pulses, consistent with 'short circuit' and device failure. Gross inspection of the device immediately after the experiment showed damaged electrodes, most probably due to contact between the electrodes during the animal movements. Therefore, it was decided not to include this animal in the final report.

Animal # L4124

Oscilloscope measurements during IRE-treatment showed that, in some of the pulses (around 20 out of 90) the electric current suddenly increased (maximum value not recorded due to saturation of the scope) towards the end of the pulse. On gross inspection, the endovascular device looked normal with no markings on the electrodes. The animal had some areas of partial ablation in the treated artery (see Table VI-2), but overall IRE-treatment was successful. A plausible explanation for the current measurements of this animal might be a discharge (i.e. a spark) that occurred during the treatment, manifested as "short circuit" on the oscilloscope. However, since most pulses were delivered normally, and since the endovascular electrodes were not damaged during the procedure, it was decided to include this animal in the final report.

Histology at 7 days

All animals survived, without infection or evidence of limb ischemia. On gross pathology IRE-treated arteries were not different from control arteries, and there was no evidence of bleeding or thrombosis. Histology scores of mural damage (i.e. VSMC ablation) and local inflammation are summarized in Table VI-2.

All right (IRE-treated) iliac arteries segments displayed severe, transmural ablation of VSMC in at least five of the six segments. In nearly all sections the damage was circumferential. The damage to the Tunica Media was characterized by complete loss of VSMC. Most inflammatory reaction was perivascular (chronic).

Mural inflammation (mononuclear cell infiltration) was noted only in animal #2391, probably due to thermal damage to the vessel wall.

Left iliac artery segments were unremarkable.

Animal # / Section #	Wall ablation		Inflammation		Comments [Figure Number(s)]
	Dist.	Sev.	Dist.	Sev.	
L2391- L / 1-3	0	0	0	0	Unremarkable [1,2,3]
L2391-R / 1	2	2	0	0	There was slight damage to the inner third of the media [4].
L2391-R / 2	2	4	0	0	The inner third of the media was mildly affected. In one focus the mild medial damage was transmural [5].
L2391-R / 3	4	4	4	2	Transmural damage; mild, chronic, perivascular inflammation and mild, multifocal, mural hemorrhage[6,7].
L2391-R / 4	4	4	3	2	Transmural damage; mild, chronic, perivascular inflammation [8,9]
L2391-R / 5	4	4	4	3	Transmural damage; Moderate, chronic, perivascular inflammation [10,11];
L2391-R / 6	4	4	2	2	Transmural damage; mild, chronic, perivascular inflammation [12,13]
L4123 - L / 1-3	0	0	0	0	[14,15,16]
L4123 - R / 1	1	4	2	1	Focal mild transmural damage [17, 18(normal), 19(damaged)]
L4123 - R / 2	4	4	3	2	Transmural damage; mild, chronic, perivascular inflammation [20,21].
L4123 - R / 3	4	4	4	2	Same as L4123 - R / 2 [22,23].
L4123 - R / 4	4	4	2	3	A small branch artery was also severely damaged [24,25].
L4123 - R / 5	4	4	3	2	Transmural damage; mild, chronic, perivascular and intramural inflammation [26,27].
L4123 - R / 6	4	4	3	2	Same as L4123 - R / 5 [28,29].
L4124 - L / 1	0	0	0	0	Unremarkable [30].
L4124 - R / 1	2	4	0	0	Inner third of media mildly affected. In one focus the mild medial damage was transmural and accompanied by focal neointimal proliferation [31,32].
L4124 - R / 2	4	4	4	3	Transmural damage; a portion of a branch artery was also severely damaged [33,34].
L4124 - R / 3	4	4	4	3	Same as L4124 - R / 2 [35,36,37]
L4124 - R /4	4	4	3	4	Transmural damage; marked fibrosis and chronic inflammation in the perivascular fat [38,39].
L4124 - R / 5	4	4	3	4	Same as L4124 - R /4 [40,41].
L4124 - R / 6	4	4	3	4	Same as L4124 - R /4 [42,43].
L4131 - L / 1-3	0	0	0	0	Unremarkable [44-46].
L4131 - R / 1	4	4	4	1	Transmural damage [47,48].
L4131 - R / 2	4	4	3	2	Transmural damage; a portion of a branch artery was also severely damaged [49,50].
L4131 - R / 3	4	4	2	1	Transmural damage [51,52].
L4131 - R / 4	4	4	2	1	Same as L4131 - R / 2 [53,54].
L4131 - R / 5	4	4	2	1	Transmural damage [55,56].
L4131 - R / 6	4	4	2	1	Transmural damage [57,58].
L4133 - L / 1-3	0	0	0	0	Unremarkable [59-61].
L4133 - R / 1	1	1	0	0	Focal damage in the mid-intima [62,63];
L4133 - R / 2	4	4	4	2	Transmural damage; chronic mural and perivascular inflammation [64,65];
L4133 - R / 3	4	4	3	1	Transmural Damage [66,67].
L4133 - R / 3	4	4	3	1	Transmural Damage [68,69].
L4133 - R / 3	4	4	3	1	Transmural Damage [70,71].
L4133 - R / 3	4	4	3	1	Transmural Damage [72,73].

Table VI-2 - IRE at 7 days - Independent pathology report of five animals treated with prototype C. Animals were euthanized after one week.

Histology at 35 days

All four animals survived, without infection or evidence of limb ischemia. On gross pathology IRE-treated arteries were not different from control arteries, and there was no evidence of bleeding or thrombosis. Histology scores of mural damage (i.e. VSMC ablation) and local inflammation are summarized in Table VI-3.

All right (IRE-treated) iliac arteries segments displayed severe, transmural ablation of VSMC in at least five of the six segments. In nearly all sections the damage was circumferential. The damage to the Tunica Media was characterized by complete loss of VSMC. In most cases, elastic lamina remained intact. Occasional mural inflammation was noted. This included mononuclear cells (primarily) as well as polymorphonuclear cells (neutrophils). Most of the chronic inflammatory reaction was perivascular, but some of the artery segments had inflammatory cells through the wall.

Some of the treated-arteries demonstrated asymmetrical, fibrous non-cellular neointima covering the intimal surface. In few segments small focus of metaplastic cartilage was noted.

Left iliac arteries (non-treated) were unremarkable.

Animal # / Section #	Wall ablation		Inflammation		Comments [Figure Number(s)]
	Dist.	Sev.	Dist.	Sev.	
L304-L/1-3	0	0	0	0	Unremarkable. [74,75,76]
L304-R/1	3	4	3	1	Most of the original media was effaced [77]. Thick fibrous neointima (partially "artifactually" separated) covered much of the intimal surface [78].
L304-R/2	4	4	3	1	Same as section R1[79]. The artery wall contained a large focus of metaplastic cartilage [80].
L304-R/3	4	4	4	2	Universal, transmural damage [81]. Mixed inflammatory cells infiltrated the artery wall [82].
L304-R/4	4	4	4	2	Same as R/3 [83,84].
L304-R/5	4	4	4	2	Same as R/3 [85,86]. A fibrinous mural thrombus partially covered the intimal surface.

L304-R/6	3	4	0	0	Most of the original media was effaced [87]. Mature neointima (fibrous tissue and smooth muscle cells) covered the intimal surface [88].
L343-L/1-3	0	0	0	0	Unremarkable. [89,90,91]
L343-R/1	3	1	0	0	Partial, minimal, medial fibrosis [92].
L343-R/2	4	4	3	1	Most of the original media was effaced [93]. Mature fibrous neointima covered the intimal surface [94].
L343-R/3	4	4	3	1	Universal, transmural damage [95]. Mixed inflammatory cells infiltrated the arterial wall [96].
L343-R/4	4	4	3	1	Same as section R/2 [97]. The artery wall contained large focus of metaplastic cartilage [98].
L343-R/5	4	4	3	1	Same as R/3 [99]. Thin fibrous neointima covered the intimal surface [100]. The artery wall contained a small focus of metaplastic cartilage.
L343-R/6	4	4	3	1	Same as R3 [101,102].
L346-L/1-3	0	0	0	0	Unremarkable [103,104,105].
L346-R/1	2	2	0	0	A small segment of media was fibrotic [106].
L346-R/2	4	4	0	0	Most of the original media was fibrotic [107,108].
L346-R/3	4	4	0	0	The entire media was fibrotic. Asymmetrical, fibrous neointima covered the intimal surface [109]. The artery wall contained a small focus of metaplastic cartilage [110].
L346-R/4	4	4	2	1	Universal, transmural damage [111,112].
L346-R/5	4	4	0	0	Universal, transmural damage [113]. Fibrous neointima ("artifactually" separated from the intima) covered a portion of the intimal surface [114].
L346-R/6	3	4	0	0	Approximately 70% of the media had been replaced by fibrous tissue [115]. Irregular, asymmetrical fibrous neointima covered about half of the intimal surface [116].
L4126-L/1-3	0	0	0	0	Unremarkable [117,118,119].
L4126-R/1	0	0	0	0	Unremarkable [120].
L4126-R/2	4	4	3	1	The entire media was fibrotic. Thin, asymmetrical, fibrous neointima covered the intimal surface [121,122].
L4126-R/3	4	4	3	1	Same as R/2 [123]. The damage extended a short distance into the ostium of a small branch artery [124].
L4126-R/4	-	-	-	-	Section was lost during preparation.
L4126-R/5	4	4	0	0	The entire media was fibrotic. Thin, asymmetrical, fibrous neointima covered the intimal surface [125]. The artery wall contained a large focus of metaplastic cartilage [126].
L4126-R/6	4	4	0	0	The media was partially fibrotic [127]. Thin, asymmetrical fibrous neointima covered the intimal surface [128].

Table VI-3 - IRE at 35 days - Independent pathology report of four animals treated with prototype C. Animals were euthanized after five weeks.

Immunohistology

Advanced histology results are summarized in Figure VI-3. Smooth muscle actin (SMA) stain was homogeneously positive in the Tunica Media of the control arteries, but was absent from all IRE-treated segments evaluated at 7 and 35 days. Local areas of positive SMA were noticed in the small neointima covering the intimal surface of arteries evaluated at 35 days. Proliferating cell nuclear antigen (PCNA) stain was negative in the control arteries as well as in the 7-days segments. Positive PCNA stains were noted in the perivascular areas of the arteries evaluated at 35 days, as well as some mild positive stain within the Tunica Media itself. Von willebrand factor (VWF) lightly stained the endothelial layer of control arteries. After one week, strong VWF staining of the cells lining the inner layer of the treated arteries was noted, although it was not continuous on all segments evaluated. After five weeks, the inner layer of the treated arteries showed homogeneous circumferential and strong VWF staining. Foci of cartilaginous metaplasia contained cells that stained positively for the S-100 antigen.

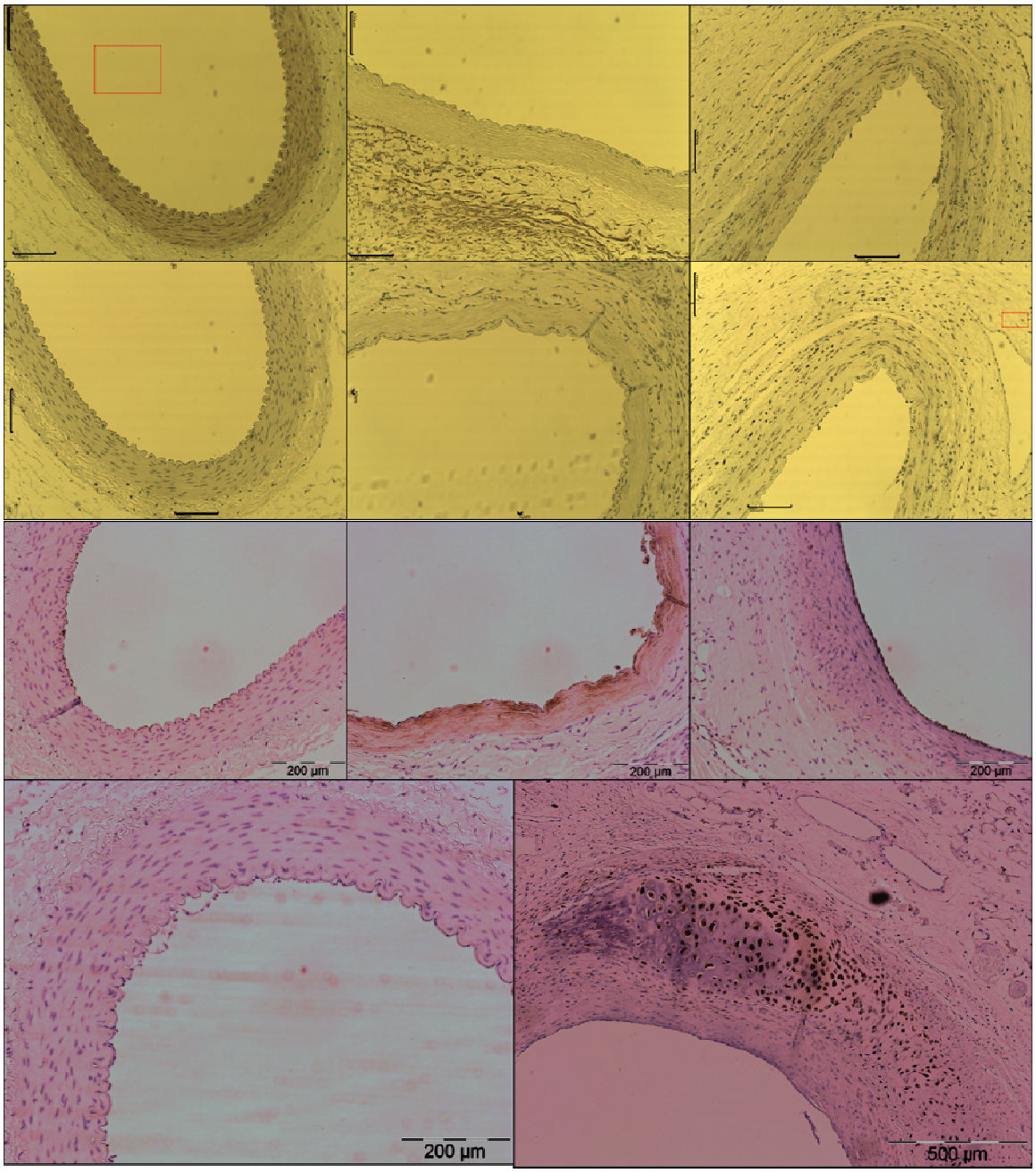

Figure VI-3 - Immunohistochemistry results at one and five weeks: SMA (top row) , PCNA (second row) and VWF (third row) stains of control arteries (left images) , IRE-treated arteries after one week (middle images) and after five weeks (right images). SMA stain demonstrates the absence of vascular smooth muscle cells in NTIRE-treated arteries compared with the control artery (top row). VWF shows that the endothelial layers at both one and five weeks post ablation are functional and produce the VWF molecule (third row). Bottom line shows immunohistochemisty of S-100, with control artery on the left and treated artery after 5 weeks on the right showing cartilaginous metaplasia with cells positive for S-100.

4. Discussion

❖ *Failure of prototype B*

The failure of prototype B was due to the detachment of the silver-coated ink electrodes from the angioplasty balloon. Detachment occurred in those area of the balloon that were folded in its deflated state.

The device worked properly in *ex-vivo* simulation. In these simulation, the device was inserted into a cube of an agar gel with electric conductivity similar to that of biological tissue. It failed in potential difference of 400 Volts (high enough for IRE according to finite-element simulations). In those ex-vivo experiment, the device was not deflated, folded and advanced through 4F introducer catheter. This is why it worked properly *ex-vivo* and failed *in-vivo*.

Following the failure two options were considered:

1. Use the same prototype but with a thicker silver-coated ink coating.
2. Work with a new, more robust electrode design, that will not be damaged when passed through an introducer.

Since the need to fold the balloon could not be avoided in the setting of a balloon coated with conductive electrodes, it was decided to work with Prototype C.

❖ *Successful endovascular IRE with prototype C*

The independent pathology report of Charles River concluded that ablation at 7 days included all layers of the T. Media , as well as all the circumference of the arterial segments that were treated. Similar results reported at 35 days. Although difficult to

describe quantitatively, ablation efficiency with prototype C was very high. In all slides evaluated it was noted that more than 75% of the VSMC population was destroyed. Moreover, additional analysis of the same slides at the lab showed that in most areas the VSMC population was destroyed almost entirely.

Thus, it can concluded that prototype C can deliver non-thermal IRE pulses in an endovascular minimally-invasive approach with very high efficiency. This is probably the first example in the literature of such a device.

However, it is important to mention here a manuscript entitled "*Intravascular Electroporation Markedly Attenuates Neointima Formation After Balloon Injury of the Carotid Artery in the Rat*" that was published by Dev et al. in 2000.[116] In that manuscript, the investigators tried to evaluate whether local delivery of heparin can attenuate neointimal formation. In order to achieve their goal, the assembled an endovascular device that consisted of a longitudinal unipolar electrode at the center of a inflatable balloon made of a porous membrane. They injected heparin into the balloon, and applied 4 pulses of 100 volts amplitude and 20 milliseconds pulse duration at 1 Hz. They evaluated the combined effect of heparin and electric field, but not the effect electric field per se. However, due to the small diameter of the rat carotid arteries, the long pulses, and the effective attenuation of neointima formation , it seems plausible that the reason for the success of their experiment was not the introduction of heparin molecules into the intracellular space, but rather the induction of IRE across the vessel walls. Unfortunately, the investigators did not evaluate the effect of the electric field without heparin, nor did they simulate the electric field distribution or the thermal

damage. Therefore, their work cannot be considered a biological proof for endovascular IRE attenuation of neointima formation.

❖ *Neointima and cartilaginous metaplasia*

The appearance of local cartilaginous metaplasia at 35 days is consistent with the plasticity of the adult vascular smooth muscle cell phenotype and its role in vascular calcifications.[124,125] Schulick et al. demonstrated that overexpression of transforming growth factor β1 (TGF-β1) in arterial endothelium causes hyperplasia, apoptosis, and cartilaginous metaplasia.[126] In their study, intimal proliferation and cartilaginous metaplasia peaked at 4 weeks following TGF-β1 expression. Four weeks later, both neointima and cartilaginous metaplasia regressed and disappeared, in parallel with the cessation of TGF-β1 expression. The authors concluded that the VSMC are capable of transdifferentiation into a chondrocytic phenotype, and that the phenomenon was transient and reversible. However, authors could not rule out the possibility of blood-born cells as being the source of the observed chondorcytes.

In another study, Taylor et al. examined the pathological effects of extensive radiofrequency (RF) energy applications in the pulmonary veins in dogs.[127] In their study, pulmonary veins were examined at 4 weeks, 6-8 weeks and 10-14 weeks following radiofrequency ablation of the vessel wall. As early as four weeks following the ablation , neointima was observed with small regions of chondroblasts, chondroclasts, and cartilage formation in the thickened intima. At 6-8 weeks, regions of cartilaginous metaplasia with chondroblasts and chondroclasts were noticed in the media and underlying tissue of several pulmonary veins. At 10-14 weeks, occasional small and highly organized regions of osseous metaplasia and bone marrow were noted in the thickened intima.

In the same lines, the results of IRE ablation at 35 days presented above (Page 109) demonstrated asymmetrical, fibrous neointima as well as local areas of cartilaginous metaplasia. This observation should be attributed to the extensive ablation of the VSMC population in the IRE-treated segments, and can be explained by multiple processes:

1. Paracrine release of TGF-β1 by inflammatory cells in the perivascular area. TGF-β1 is known to be released following arterial injury and , an as mentioned earlier, contributes to cartilaginous metaplasia.[128]
2. Change in the local environment of VSMC due to chronic inflammation. Sutra et al. demonstrated that superoxide production contributed to osteoblastic differentiation of vascular smooth muscle cells.[129] During chronic inflammation, enhanced production of reactive oxygen species (such as superoxide anion and H_2O_2) within arterial wall by inflammatory cells might change the local environment and thus promote VSMC transdifferentiation.
3. The a-cellular environment, with its intact extra-cellular scaffold might encourage transdifferentiation of local VSMC to matrix producing cells in order to mechanically support the extra-cellular scaffold.

VII. CHAPTER SEVEN: ENDOVASCULAR IRE ATTENUATES LUMINAL LOSS

1. Motivation and objectives

The results of the previous chapter demonstrated the feasibility and efficiency of endovascular IRE ablation. The objective of the present experiment was to determine whether endovascular IRE following balloon angioplasty could decrease post-angioplasty luminal loss and neointimal formation.

2. Methods

Computer simulations and device assembly were described above, with the only difference being the diameter of the device. In this experiment we used a larger diameter of 3 millimeter, in order to ensure good contact with the vessel wall (which was dilated during the angioplasty, and therefore was slightly larger).

Sixteen New-Zealand white rabbits weighing 3.6-4.6 Kg were used in this study. Animals received humane care from a properly trained professional in compliance with both the Principals of Laboratory Animal Care and the Guide for the Care and Use of Laboratory Animals, published by the National Institute of Health. Intramuscular injection of Ketamin (35mg/kg body weight) and Xylazine (5 mg/kg body weight) was used for anesthesia induction, followed by endotracheal intubation and isoflurane for anesthesia maintenance. A single intravenous Pancuronium dose (0.1mg/kg) was used to attenuate muscle contractions. Animals were monitored continuously (oxygen saturation, ECG monitor, blood pressure, respiratory rate, CO2 production and core body temperature), and were under full heparinization during the entire procedure (Heparin

loading dose of 75-100 mg/Kg followed by ACT monitoring). Under sterile technique, the areas over the right and left femoral arteries were exposed. Arteriotomy was performed, and a 4F introducer was placed in each of the femoral artery.

Under angiography guidance, a standard non-complaint angioplasty balloon catheters with balloon diameter of 3 mm and length of 2 cm were advanced to the first 2 cm of the iliac arteries, adjacent to the aortic bifurcation. Balloons were inflated for one minute three times (one minute between each inflation, inflation pressure of 5 atmospheres), and were then pulled back along the iliac arteries in order to induce endothelial denudation.

After both arteries were damaged, the endovascular IRE device was randomly inserted into one of the two iliac arteries. The device was advanced to the aortic bifurcation, and inflated along the first two centimeters of the right iliac artery and then along the next 2 cm of the same artery. IRE protocol included 90 direct current pulses of 100 microseconds at 4 Hz frequency. Potential difference was 600 volts. Pulses were applied using a high voltage pulse generator intended for clinical electroporation procedures (NanoKnife Generator, software version 2.0.6, Angiodynamics, Queensbury, NY). Current and voltage were recorded by the pulse generator during pulse application.

ECG was recorded and printed before, during and immediately after the procedure. After removal of the IRE device, control angiography was performed to confirm patency of the vessels and to rule out any local bleeding. Then, the iliac artery was ligated, and the surgical wound was closed. Animals recovered and were kept in the animal facility for 35 days follow up. At the end of the follow up period, animals were anesthetized as described above, and a follow-up angiogram was done through the abdominal aorta.

Angiography was used to measure the total patent area of the first 4 centimeters of both iliac arteries, as well as the point of minimal luminal diameter within these segments. The total patent areas were compared with baseline angiograms, as well as with the control arteries of the contra lateral artery. Animals were then euthanized with an overdose of Phenobarbital, and the arterial vasculature was perfused with formalin using a perfusing pressure of 150 mmHg . For all animals, both iliac arteries (4cm segments starting from the aortic bifurcation) were harvested and sent to histology for processing and evaluation.

❖ *Histology*

Formalin-fixed, 4 cm long intact segments of the left and right iliac arteries from all rabbits were submitted for evaluation by an independent pathology laboratory (Charles River Laboratories Pathology Associates). Six consecutive sections were prepared from each iliac segment. The tissues were processed through and embedded in paraffin. From each paraffin block, six 5 µm sections were prepared and stained with hematoxylin & eosin (H&E), Masson's trichrome (MT), and Verhoeff's elastin (VE) stains. The sections were qualitatively evaluated microscopically by an independent pathology expert (Charles River Laboratories Pathology Associates), who was blinded with respect to the slide's numbers. In addition, morphometric analysis of all sections was used to measure total area of the Tunica Media, neointima, arterial lumen, total arterial area defined by the external elastic lamina and the total area defined by the internal elastic lamina.

❖ *Statistical analysis*

Data derived from in vivo angiographic examination and morphometric histology were analyzed by a one-sided paired t test. Linear regression was performed to determine the

correlation between two continuous data (Pearson's correlation test for independent data). Additionally, the point of minimal angiographic luminal diameter was identified in each iliac artery at 35 days, and mean values of measurements (n=12) were compared with control arteries of the same animal (one-sided paired t test). Data are presented as mean±SD . A value of P<.01 was considered significant.

3. Results

Angioplasty damage and endothelial denudation was successful in all 32 iliac arteries. IRE endovascular device could not be deployed in one artery due to torturous iliac anatomy. In addition, three other IRE-treated arteries were excluded from the analysis due to malalignment of the device electrodes (confirmed by high currents during the procedure as well as evidence of electrode arching by post-treatment device inspection). Thus, total of 24 arteries of 12 animals were included in the final analysis. Electroporation pulses were well tolerated, with no acute bleeding, no hemodynamic compromise and no E.C.G changes during or following the procedure. Animal recovery was uneventful, with no evidence of would infection and no limb ischemia during the follow-up period.

❖ *Iliac angiography*

At the end of the procedure, total area of the first 4 cm of the iliac arteries was 0.94±0.14 cm2 for the control arteries and 1.05±0.12 cm2 for the IRE-treated arteries (P = 0.03, non significant). After 35 days, total area of control arteries was reduced to 0.58±0.22 cm2 for control vessels versus 0.85±0.18 cm2 for the IRE-treated vessels (48% increase, p = 0.001). Total vessel area at the angiogram was reduced in both groups compared with baseline angiogram: for the control group, total area was reduced by 38±24% and for

IRE-treated group by 18±19% (p = 0.009). Point of minimal lumen diameter along the first four centimeters of the iliac arteries was 0.11 ± 0.06 cm in the control group compared with 0.21±0.09 cm in the IRE-treated group (94% increase, p = 0.004).

	Control	**IRE-treated**	**Change**	**P value**
Total area (cm^2)	0.58±0.22	0.85±0.18	46% increase	0.001
Luminal Loss (= End/Baseline)	38%±24%	18%±19%	53% decrease	<0.001
Point of maximal stenosis (cm)	0.11±0.06	(0.21±0.09)	91% increase	0.004

❖ *Histology*

Average neointimal area was 33% smaller in the IRE-treated group compared with control (0.26 ± 0.23 vs. 0.39 ±0.14 mm2,p = 0.0006). Average Tunica Media area was 20% larger in the IRE-treated group compared with control (0.42 ± 0.18 vs. 0.36 ± 0.07 mm2, p = 0.0061). Average lumen area was non-significantly 4% larger in the IRE-treated group compared with control (1.35 ± 0.73 vs. 1.30 ±0.52 mm2 , p = 0.45). Lumen areas were strongly and linearly correlated with total artery size in both the control and the IRE-treated group (r=0.97 and r=0.91 respectively, both with p<0.001). Neointimal areas did not correlate linearly with total artery size in either the control or the IRE-treated group (r=0.49 and r=0.17 respectively).

Ten of the twelve IRE-treated arteries showed marked mural ablation of all six sections evaluated. The damage consisted of loss of medial smooth muscle cells or significant decrease in muscle cell sarcoplasm. Ten segments contained foci of cartilaginous

metaplasia, some with mineralization. Out of 72 arterial sections of 12 IRE-treated iliac segments, two sections showed patent dissection within the artery wall. Mural inflammation was rare, and mild. The inflammation was associated with metaplastic changes in the ablated artery.

Figure VII-1: Angiogram at 35 days showing control artery (left iliac artery, on the right side of the image) and IRE-ablated artery (right iliac artery). The ablated vessel is wider and regular compared with the control artery which is stenotic and irregular.

4. Discussion

The results presented in this chapter show, for the first time, that endovascular IRE immediately following balloon angioplasty can attenuate neointimal formation. In addition, it can decrease post-angioplasty luminal loss and increase the diameter at the point of minimal luminal diameter.

❖ *Neointimal area reduction*

The average area of neointimal formation in IRE-treated vessels was reduced by one third compared with control arteries. The reduction percentage is lower compared with other studies evaluating neointimal attenuation with new endovascular technologies. However, most studies used a double or triple-damage model, with average neointimal areas in control vessels reaching 0.7-1mm^2.[130-136] Our control group had a relatively low average neointimal area (0.39 mm^2), and therefore the IRE-ablation reduction was less prominent. Since the neointimal formation in the double and triple-damage models is also dependant on the VSMC population, it is plausible that with these models IRE-treated vessels will demonstrate high percentage of neointimal attenuation.

The reduction of neointimal area by one third might have also been influenced by the alignment of the device electrodes. Three devices out of sixteen failed due to electrodes malalignment resulting arching and high current failure. This problem might have compromised the efficiency of all devices, but not to the extent of device failure. Since the only real-time control over the process was current measurements, this problem remains partially speculative. However, if indeed some of the electrodes were not aligned properly, there might have been areas of the vessel wall that were not electroporation well enough to induce IRE. Therefore, a superior device design might result in better neointimal reduction.

❖ *Luminal loss reduction*

IRE-treated vessels experienced a 50% reduction in luminal loss and 91% increase in the width of the minimal luminal diameter. These results correlate with the reduction of neointimal formation seen in the morphometric analysis. Luminal loss is influenced by

both neointimal growth as well as by arterial remodeling and elastic recoil. The increase in the arterial lumen seen in the angiography is the results of a dramatic change in the healing process of the vessel wall following angioplasty. Cellular components play a pivotal role in both neointimal formation as well as in vascular remodeling, and the indistinctive ablation of all cellular components have probably resulted attenuation of both processes.

Another important observation is that all IRE-treated vessels were smaller in diameter compared with the baseline angiography. This observation supports the hypothesis that IRE does not damage the collagen fibrils and therefore does not compromise the tensile properties of the vessel wall. A reduction in the tensile strength of the vessel wall would have resulted in aneurysm formation , with enlarged vessel diameter at follow-up angiography.

❖ *Cartilaginous metaplasia and medial dissection*

Evidence of cartilaginous metaplasia was demonstrated and discussed in the previous chapter. In the results described here we encounter for the first time three IRE-treated and one control vessel with patent arterial medial dissection, of them two IRE-treated vessels are included in the final analysis. The observation that medial dissection was not demonstrated with native arteries in the previous chapter is supported by previous studies showing that dissection of the arterial wall is frequent concomitant of the balloon angioplasty process.[137] The small number of observation makes it impossible to draw conclusions on the effect of IRE treatment on post-angioplasty medial dissection, and therefore further research is needed in order to address this issue.

VIII. CHAPTER EIGHT: CONCLUSIONS AND FUTURE RESEARCH

1. Endovascular IRE and the problem of restenosis

As discussed in Chapter I , in the era of stents implantations, the major reason for in-stent restenosis is neointimal formation. The problems of elastic recoil and vascular remodeling are addressed with stent implantation, whereas the migration and proliferation of VSMC remain as the major challenge. Drug eluting stents offer an elegant solution for the problem, but with some concerns left unanswered (revascularizations, late stent thrombosis and heavy economic burden). Endovascular IRE offers a new, innovative, non-thermal approach for the local ablation of the VSMC population in the proximity of the stent.

The theoretical and experimental work presented here supports the feasibility and efficiency of endovascular IRE. Its advantages , from both the fundamental science and well as from the practical-clinical perspective, include: high efficiency, non-biological mechanism of action, sparing of extra-cellular components, short intervention time, and design simplicity. Two main disadvantages are muscle twitching and limited size of treated volume of tissue. Each advantage and disadvantage is discussed separately.

❖ *Advantage 1: Highly efficient ablation of the entire vessel wall*

As discussed in Chapter , ninety pulses of 1,750 V/cm successfully ablated 94% of the VSMC population. Moreover, cells were destroyed in all of the layers of the Tunica Media. Similar results were achieved with the endovascular approach presented in Chapter VI. Although difficult to compare with the efficiency of other technologies (such as radiofrequency ablation[138,139] or cryoablation[140]), IRE offers efficient method to

destroy cells in a defined volume of tissue. Due to the exponential decay of the electric field, ablation is limited to cells within the first few hundred micrometers near the electrodes, with minor damage to structures outside of the vessel wall.

With respect to the clinical problem of restenosis, ablation efficiency is highly important. Neointimal formation is the result of oligoclonal proliferation of VSMC originating in the *Tunica Intima* , as well as migration from the *Tunica Media* into the intima. The ability of endovascular IRE to destroy cells across all of the *Tunica Media* layers will prevent not only proliferation but also potential migration of VSMC.

❖ *Advantage 2: Non-biological phenomenon*

Adaptation is universal across all biological systems. When the insult to the VSMC population is chronic (few weeks or months) , some cells might be able to adapt and overcome the insult. This might be the reason for restenosis of drug-eluting stents, where anti-proliferative drugs are released for weeks following the implantation of the stent.

As for endovascular IRE - the insult is immediate. Since the phenomenon is based solely on the properties of the electric field, and since the pulses can be delivered in few seconds (90 pulses at 4 Hz will take 22.5 seconds), endovascular IRE leaves no room for biological adaptation and will efficiently destroy all VSMC population in the *Tunica Media* and *Tunica Intima*.

❖ *Advantage 3: Intact extra-cellular scaffold*

The non-thermal nature of endovascular IRE is its main advantages. While the electric field is bound to create heat according to Joule heating effect, the ultra-short pulses combined with relatively low frequency can induce IRE with no significant rise in the

temperature of the treated volume. The non-thermal nature of endovascular IRE was demonstrated in Chapter II, while calculations with other electrode assemblies demonstrated the non-thermal nature of IRE for other clinical applications.[15,91,141]

Due to its non-thermal nature, IRE does not damage extra-cellular matrix. This creates minimal damage within the tissue treated, with minor inflammatory response. It was shown in Chapter VI that at 7 days as well as at 35 days following endovascular IRE, inflammatory response was moderate and was mostly limited to the *Tunica Adventitia* (perivascular inflammation), with minimal inflammatory involvement of the *Tunica Media.*

With respect to the biomechanics of the arterial wall, the non-thermal nature of endovascular IRE has an important additional advantage: maintaining the tensile strength of the vessel wall. By not damaging extra-cellular components, IRE protects collagen which is the main load carrying element in blood vessels. Maintaining the tensile strength of the artery prevents aneurysm formation or complete failure of the vessel wall, and therefore improves the safety of endovascular IRE as a vessel wall ablation technique. [142]

The non-thermal nature of endovascular IRE has another important advantage with respect to the endothelial layer. IRE destroys endothelial cells together with the VSMC population, but these cell populations have distinct regeneration potential. As demonstrated in Chapter IV, VSMC did not repopulate the Tunica Media of the carotid artery after 28 days. In contrast, as early as seven days following IRE application, the endothelial layer showed remarkable regeneration. A plausible explanation for the

endothelium recovery is that the basal lamina of the endothelial layer was not damaged, and served as a scaffold for immediate repopulation of the endothelium with circulating progenitor endothelial cells. The potential of endothelial progenitor cells, their role in re-endothelialization and their cytokine-induced recruitment was discussed thoroughly elsewhere. [78,70,71]

❖ *Advantage 4: Short intervention time*

Balloon angioplasty and stent implantation can be performed in acute or elective settings. In the acute settings, the angioplasty is preformed in order to renew blood flow to infracted myocardium during acute myocardial infarction , and the time interval from the sudden occlusion to the reopening of the artery is critical. In the elective setting, patients with chest angina are referred to the cardiac catheterization lab in order to dilate a chronic non critical stenosis in one or more of their coronary arteries.

With all endovascular technologies, during the treatment the flow through the treated segment is compromised, and therefore there is a decrease in oxygen delivery to the myocardial muscle. Therefore, intervention time is critical in the settings of acute MI , but is also important in the settings of elective PCI.

Most available technologies require treatment duration of one minute to a few minutes. Some of them separate treatment to several intervals in order to restore coronary blood flow to the myocardium. Treatment duration of endovascular brachytherapy is between two to more than ten minutes.[50] Endovascular radiofrequency ablation requires few minutes of local treatment (Taylor et al. used three or four 120-seconds radiofrequency energy applications to ablate the pulmonary vein).[127] Supercooling to -10°C requires

two minutes in order to induce apoptosis of VSMC, with shorter treatment periods failing to efficiently destroy the cells in-vivo.[42] Treatment with photodynamic therapy required 10-12 intervals of 45 seconds in order to attenuate restenosis in porcine coronary arteries.[53] Local heating of the arterial wall to 50°C for 60 seconds was also demonstrated to attenuate restenosis. [143]

Compared with all of the above mentioned modalities, endovascular IRE efficiently destroyed the entire VSMC population of the *Tunica Media* in 22.5 seconds (!!) . This short intervention time will allow physicians to use endovascular IRE as a preventive strategy even in the settings of primary PCI during acute MI.

❖ *Advantage 5: Simplicity*

Although some aspects of the electroporation mechanism are complex and still not fully understood, the method is simple to implement: application of high electric field across biological tissue. The endovascular design that was theoretically examined in Chapter II and experimentally evaluated in Chapter VI is relatively simple. It consists of four longitudinal electrodes on top of a standard inflatable balloon. In contrast to cryoplasty or radiofrequency ablation, the device is compact, there is no need to monitor the temperature, blood flow does not interferes with temperature modeling, and treatment duration is short. Moreover, in contrast to photodynamic therapy or other DNA-based therapies, endovascular IRE does not require any adjuvant pharmacological agent, and is dependent only on the electric field applied.

The simplicity of electrode design is further supported by readily available electroporation generator machines that can be used with no additional customizations.

Therefore, endovascular IRE can be used by physicians in any catheterization lab with no need for expensive equipment or special training for the treating physician.

❖ *Disadvantage 1: Muscle contractions*

From the clinical perspective, muscle contraction during electroporation is a major disadvantage. The intensity of the contraction depends on the duration , height and frequency of the DC pulses. DC pulses induce muscle twitching in two mechanisms:

1. Indirect excitation (primary) - DC pulses depolarize myelinated nerves and induce a nerve action potential that travels along the nerves' membrane and reaches the neuromuscular junction. At the neuromuscular junction, the action potential triggers the release of the neurotransmitter acetylcholine, which ultimately causes the muscle to contract. This is the primary cause for muscle contractions due to DC pulses.

2. Direct excitation - DC pulses can depolarize the muscle membrane and induce local contraction. However, this is a minor mechanism, and it accounts for only 3%-7% of the contractions. Most of the contractions are due to indirect nerve stimulation.[144]

The phenomena of muscle twitching can be decreased significantly with the use of muscle relaxants (e.g. Pancuronium). However, muscle relaxants mandate endotracheal intubation and general anesthesia. The need for general anesthesia is only acceptable in situations where the alternative to IRE is surgery (for example, solid tumor ablation). However, PCI procedures are performed without general anesthesia, and therefore the muscle twitching of endovascular IRE is a major drawback.

Possible solution to the problem might include local anesthesia or nerve block. Another solution is a better electrodes design, with a much smaller distance between adjacent

electrodes. This will decrease the electric potential and the electric current used, and will therefore decrease the extent of muscle twitching.

❖ *Disadvantage 2: Diameter of ablated zone*

The electric field distributions follows the Laplace equation, with exponential decrease of electric field magnitude as the distance from the electrodes increases. This was not a problem in the experiments described above because the thickness of vessel wall of the rabbit iliac arteries was approximately 200 μm. However, when designing a device for clinical use, one needs to take into consideration atherosclerotic coronary arteries with a larger plaque and a thicker intima. In these arteries, the thickness of the area-to-treat can be 500 μm or even 1 mm. In order to achieve successful IRE ablation, the electric potential difference between the electrodes will have to be increased significantly. However, increasing the electric potential will be limited by both the maximal current density of the electrodes assembly as well as by the resistive heating of the treated tissue.

Solutions to this problem might include better electrode design, with superior electric field distribution. Another solution is increasing the number of pulses. As shown in Chapters III and IV, increasing the number of pulses can compensate for decreased electric field magnitude.

2. Endovascular IRE and other clinical problems

The results presented in Chapter VI demonstrated, for the first time, the feasibility of VSMC ablation using endovascular IRE. The prototype used in these experiments can also be used for other clinical problems. Application of a relatively uniform electric field

across blood vessel walls in an endovascular approach has some straightforward clinical applications that are presented here.

❖ *Cardiac arrhythmias*

In the field of cardiac electrophysiology, endovascular radiofrequency ablation is used to treat cardiac arrhythmias in a minimally invasive approach. It's most often used to treat supraventricular tachyarrhythmias (such as atrial fibirillation, atrial flutter, paroxysmal supra ventricular tachycardia etc.) in selected patients by ablation of aberrant conduction pathways and/or ectopic foci of tachyarrhythmias. A common RF ablation protocol includes circumferential ablation of the pulmonary veins, separating them from the rest of the left atrium. Ablation time with RF catheters is between 60 and 120 seconds with temperature usually reaching 60°C.[145]

Some of the complication of RF ablation are not specific, and can happen with any ablation technique that involves endovascular catheter and cell ablation (e.g. high grade AV block, valve trauma, infections, proarrythmias etc.) . However, some of the complications of RF ablation are the result of heat-induced necrosis in the treated area. Excessive heat in the cardiac atrium or pulmonary veins, with resulting necrosis and inflammation, can cause pulmonary vein stenosis [146], as well as vascular or atrial wall injury.

In-vivo experiments with pigs have already demonstrated the efficient ablation of atria walls with standard IRE.[147] Endovascular IRE can be used in an approach similar to RF ablation. The advantages of IRE over RF ablation include: better localization of the ablation damage (based only on electric field distribution without the problem of blood

convection), shorter ablation time, and minimal non-thermal damage to the extra-cellular matrix with only minor inflammatory response (reduced chance of wall perforation), as well as probable reduced cost due to the simplicity of IRE application.

The only disadvantage would be muscle contractions, but synchronization of the electroporation pulses with the R waves of the ECG can minimize the effect of muscle contractions by inducing contractions that overlap with the heart's beat.

❖ *Arteriovenous Fistulas failure*

Chronic hemodialysis and renal transplant are the only two options for patients with end stage renal disease, with most patients treated with chronic hemodialysis. One of the main challenges in hemodialysis is vascular access, surgically created by a fistulae between a vein and an artery. Failure of arteriovenous communications (arteriovenous fistula, AVF) used for chronic hemodialysis is a major clinical problem, with most AVF lasting few hundred days. VSMC proliferation is the major process contributing to the failure of AVF.[148] Based on the results presented above , endovascular IRE might be able to prolong the survival of AVF by destroying the VSMC population. Endovascular IRE might be used as either preventive strategy (immediately after the surgical procedure) or as a therapeutic strategy (only in those patients with significant occlusion of the AVF).

❖ *Septal ablation for hypertrophic obstructive cardiomyopathy*

Hypertrophic cardiomyopathy is characterized by a thickened nondilated left ventricle. In some cases, the hypertrophic inter-ventricular septum causes an obstruction to the

outflow of blood from the left ventricle to the system circulation. Treatment options includes medical management, surgery or alcohol septal ablation.[149]

Septal ablation was introduced in 1994, and includes percutaneous injection of 1-3ml of 96-98% alcohol into a septal coronary artery to create necrosis and permanent myocardial infarction in the septum.

Endovascular IRE can be an innovative alternative to alcohol septal ablation. An endovascular catheter can be advanced to the left ventricle, and with a direct contact of endovascular electrodes ECG-synchronized electroporation pulses can ablate large volume of the myocardial muscle. The main advantage of endovascular IRE over alcohol septal ablation would be better anatomic localization of the ablated area without the limited factor of varying coronary anatomy.

- ***Local drugs or DNA-molecules delivery to blood vessels' wall.***

Currently, intensive basic science research as well as human clinical trials are evaluating electroporation as a preferred non-viral method for gene-therapy and/or local drug delivery. [14] Using electroporation pulses, membranes of cells in a well defined volume can be temporarily opened allowing DNA-molecules or therapeutic agents to passively penetrate cells' cytoplasm.

Although the work presented in Chapter VI focused on IRE, the same endovascular device can deliver electroporation pulses that will induce reversible electroporation of the VSMC in the blood vessel walls.

Atherosclerotic plaque formation is influenced by systemic conditions (genetics, hypertension, cholesterol, inflammatory processes etc.) , but it is also influenced by local

conditions (such as vessel wall shear stress, flow separation etc.). From the clinical perspective it can be viewed as a local vascular pathology. Therefore, gene-therapy or local drug-delivery interventions might prove to be efficient in preventing or attenuating atherosclerotic/restenosis plaque formation in areas of critical importance (coronary, renal and carotid arteries).

❖ *Barrett's Esophagus*

Barrett's esophagus is the term used to describe metaplasia (abnormal change) of the epithelium at the lower segment of the esophagus. It is marked by columnar epithelia in the lower esophagus, replacing the normal squamous cell epithelium. It is associated with 30- to 52-fold increase in the occurrence of esophageal cancer compared with the normal population. First line of treatment is prevention (life-style change, antacids therapy). However, for high grade metaplasia treatment options include surgery (esophagectomy - surgical removal of a portion of the esophagus), endoscopic mucosal resection , and nonsurgical endovascular destruction of the metaplastic cells (laser thermal ablation, photodynamic therapy).[150]

There is a clinical need for a minimally-invasive, endoscopic method for destroying epithelium of the lower esophagus. A prototype endoscopic IRE device similar to the one presented here, will be able to efficiently destroy the endothelial lining. The exponential behavior of the electric field can serve as an advantage, enabling ablation of the mucosal layer with minimal damage to deeper structures. IRE might prove to be a simple-to-use, minimally invasive endoscopic treatment for patients with metaplasia who did not develop malignant cancer, but would like to remove the metaplastic tissue without surgery.

IX. REFERENCES

[1] J.C. Weaver and Y. Chizmadzhev, "Electroporation," *Handbook of biological effects of electromagnetic fields*, CRC Press, 2007, pp. 293-332.

[2] J. Weaver, "Electroporation of cells and tissues," *IEEE Transactions on Plasma Science*, vol. 28, Feb. 2000, pp. 24 - 33.

[3] R. Davalos, L. Mir, and B. Rubinsky, "Tissue Ablation with Irreversible Electroporation," *Annals of Biomedical Engineering*, vol. 33, 2005, pp. 223-231.

[4] W. Krassowska and P. Filev, "Modeling Electroporation in a Single Cell," *Biophys. J.*, vol. 92, Jan. 2007, pp. 404-417.

[5] P. Vernier and M. Ziegler, "Nanosecond Field Alignment of Head Group and Water Dipoles in Electroporating Phospholipid Bilayers," *J. Phys. Chem. B*, vol. 111, 2007, pp. 12993-12996.

[6] T. Gowrishankar and J. Weaver, "Electrical behavior and pore accumulation in a multicellular model for conventional and supra-electroporation," *Biochemical and Biophysical Research Communications*, vol. 349, 2006, pp. 643-653.

[7] W.S. Meaking, J. Edgerton, C.W. Wharton, and R.A. Meldrum, "Electroporation-induced damage in mammalian cell DNA," *Biochimica Et Biophysica Acta*, vol. 1264, Dec. 1995, pp. 357-62.

[8] F. Hofmann, H. Ohnimus, C. Scheller, W. Strupp, U. Zimmermann, and C. Jassoy, "Electric Field Pulses Can Induce Apoptosis," *Journal of Membrane Biology*, vol. 169, May. 1999, pp. 103-109.

[9] J. Piñero, M. López-Baena, T. Ortiz, and F. Cortés, "Apoptotic and necrotic cell death are both induced by electroporation in HL60 human promyeloid leukaemia cells," *Apoptosis*, vol. 2, May. 1997, pp. 330-336.

[10] N. Matsuki, T. Ishikawa, Y. Imai, and T. Yamaguchi, "Low voltage pulses can induce apoptosis," *Cancer Letters*, vol. 269, Sep. 2008, pp. 93-100.

[11] E. Neumann, M. Schaefer-Ridder, Y. Wang, and P.H. Hofschneider, "Gene transfer into mouse lyoma cells by electroporation in high electric fields.," *The EMBO Journal*, vol. 1, 1982, pp. 841–845.

[12] H. Aihara and J. Miyazaki, "Gene transfer into muscle by electroporation in vivo," *Nat Biotech*, vol. 16, 1998, pp. 867-870.

[13] M.R. Prausnitz, V.G. Bose, R. Langer, and J.C. Weaver, "Electroporation of mammalian skin: a mechanism to enhance transdermal drug delivery," *Proceedings of the National Academy of Sciences of the United States of America*, vol. 90, 1993, pp. 10504-10508.

[14] A.M. Bodles-Brakhop, R. Heller, and R. Draghia-Akli, "Electroporation for the Delivery of DNA-based Vaccines and Immunotherapeutics: Current Clinical Developments," *Mol Ther*, Feb. 2009.

[15] R. Davalos, B. Rubinsky, and L. Mir, "Theoretical analysis of the thermal effects during in vivo tissue electroporation," *Bioelectrochemistry*, vol. 61, 2003, pp. 99-107.

[16] Y. Fung, "Chapter 8: Mechanical Properties and Active Remodeling of Blood Vessels," *Biomechanics: Mechanical Properties of Living Tissues*, Springer-Verlag New-York, Inc., 1997, pp. 321-391.

[17] S.M. Schwartz, D. deBlois, and E.R.M. O'Brien, "The Intima : Soil for Atherosclerosis and Restenosis," *Circ Res*, vol. 77, 1995, pp. 445-465.

[18] A. Zampetaki, J.P. Kirton, and Q. Xu, "Vascular repair by endothelial progenitor cells," *Cardiovasc Res*, vol. 78, Jun. 2008, pp. 413-421.

[19] A. Grøntzig, "TRANSLUMINAL DILATATION OF CORONARY-ARTERY STENOSIS," *The Lancet*, vol. 311, Feb. 1978, p. 263.

[20] D.L. Fischman, M.B. Leon, D.S. Baim, R.A. Schatz, M.P. Savage, I. Penn, K. Detre, L. Veltri, D. Ricci, M. Nobuyoshi, M. Cleman, R. Heuser, D. Almond, P.S. Teirstein, R.D. Fish, A. Colombo, J. Brinker, J. Moses, A. Shaknovich, J. Hirshfeld, S. Bailey, S. Ellis, R. Rake, S. Goldberg, and The Stent Restenosis Study Investigators, "A Randomized Comparison of Coronary-Stent Placement and Balloon Angioplasty in the Treatment of Coronary Artery Disease," *N Engl J Med*, vol. 331, 1994, pp. 496-501.

[21] W.S. Weintraub, "The Pathophysiology and Burden of Restenosis," *The American Journal of Cardiology*, vol. 100, Sep. 2007, pp. S3-S9.

[22] E. Topol, R. Califf, H. Weisman, S. Ellis, J. Tcheng, S. Worley, R. Ivanhoe, B. George, D. Fintel, M. Weston, K. Sigmon, K. Anderson, K. Lee, and J. Willerson, "Randomised trial of coronary intervention with antibody against platelet IIb/IIIa iritegrin for reduction of clinical restenosis: results at six months," *The Lancet*, vol. 343, Apr. 1994, pp. 881-886.

[23] C.E. Hjemdahl-Monsen, J.A. Ambrose, S. Borrico, M. Cohen, W. Sherman, D. Alexopoulos, R. Gorlin, and V. Fuster, "Angiographic patterns of balloon inflation during percutaneous transluminal coronary angioplasty: role of pressure-diameter curves in studying distensibility and elasticity of the stenotic lesion and the mechanism of dilation," *Journal of the American College of Cardiology*, vol. 16, Sep. 1990, pp. 569-75.

[24] D. Ardissino, S. Di Somma, J. Kubica, P. Barberis, P.A. Merlini, E. Eleuteri, S. De Servimd, E. Bramucci, G. Specchia, and C. Montemartini, "Influence of elastic recoil on restenosis after successful coronary angioplasty in unstable angina pectoris," *The American Journal of Cardiology*, vol. 71, Mar. 1993, pp. 659-663.

[25] M. Haude, R. Erbel, H. Issa, and J. Meyer, "Quantitative analysis of elastic recoil after balloon angioplasty and after intracoronary implantation of balloon-expandable Palmaz-Schatz stents," *J Am Coll Cardiol*, vol. 21, 1993, pp. 26-34.

[26] A. Lafont, L.A. Guzman, P.L. Whitlow, M. Goormastic, J.F. Cornhill, and G.M. Chisolm, "Restenosis After Experimental Angioplasty : Intimal, Medial, and Adventitial Changes Associated With Constrictive Remodeling," *Circ Res*, vol. 76, 1995, pp. 996-1002.

[27] T. Kakuta, J. Currier, C. Haudenschild, T. Ryan, and D. Faxon, "Differences in compensatory vessel enlargement, not intimal formation, account for restenosis after angioplasty in the hypercholesterolemic rabbit model," *Circulation*, vol. 89, Jun. 1994, pp. 2809-2815.

[28] Y. Shi, M. Pieniek, A. Fard, J. O'Brien, J.D. Mannion, and A. Zalewski, "Adventitial Remodeling After Coronary Arterial Injury," *Circulation*, vol. 93, 1996, pp. 340-348.

[29] H. Rud Andersen, M. M  ng, M. Thorwest, and E. Falk, "Remodeling Rather Than Neointimal Formation Explains Luminal Narrowing After Deep Vessel Wall Injury : Insights From a Porcine Coronary (Re)stenosis Model," *Circulation*, vol. 93, 1996, pp. 1716-1724.

[30] H. Luo, T. Nishioka, N.L. Eigler, J.S. Forrester, M.C. Fishbein, H. Berglund, and R.J. Siegel, "Coronary Artery Restenosis After Balloon Angioplasty in Humans Is Associated With Circumferential Coronary Constriction," *Arterioscler Thromb Vasc Biol*, vol. 16, 1996, pp. 1393-1398.

[31] V. Lindner and M.A. Reidy, "Proliferation of smooth muscle cells after vascular injury is inhibited by an antibody against basic fibroblast growth factor," *Proceedings of the National Academy of Sciences of the United States of America*, vol. 88, 1991, pp. 3739-3743.

[32] A.W. Clowes, M.A. Reidy, and M.M. Clowes, "Kinetics of cellular proliferation after arterial injury. I. Smooth muscle growth in the absence of endothelium," *Laboratory Investigation; a Journal of Technical Methods and Pathology*, vol. 49, Sep. 1983, pp. 327-33.

[33] A.W. Clowes, M.M. Clowes, and M.A. Reidy, "Kinetics of cellular proliferation after arterial injury. III. Endothelial and smooth muscle growth in chronically denuded vessels," *Laboratory Investigation; a Journal of Technical Methods and Pathology*, vol. 54, Mar. 1986, pp. 295-303.

[34] D.J. Grainger, H.L. Kirschenlohr, J.C. Metcalfe, P.L. Weissberg, D.P. Wade, and R.M. Lawn, "Proliferation of human smooth muscle cells promoted by lipoprotein(a)," *Science*, vol. 260, 1993, pp. 1655-1658.

[35] A. Jamal, M. Bendeck, and B. Langille, "Structural changes and recovery of function after arterial injury," *Arterioscler Thromb Vasc Biol*, Mar. 1992.

[36] M.A. Costa, M. Sabate, W.J. van der Giessen, I.P. Kay, P. Cervinka, J.M.R. Ligthart, P. Serrano, V.L.M.A. Coen, P.C. Levendag, and P.W. Serruys, "Late Coronary Occlusion After Intracoronary Brachytherapy," *Circulation*, vol. 100, Aug. 1999, pp. 789-792.

[37] M. Salame, S. Verheye, S. Mulkey, N. Chronos, S. King, I. Crocker, and K. Robinson, "The Effect of Endovascular Irradiation on Platelet Recruitment at Sites of Balloon Angioplasty in Pig Coronary Arteries," *Circulation*, vol. 101, Mar. 2000, pp. 1087-1090.

[38] E. Cheneau, M. John, J. Fournadjiev, R. Chan, H. Kim, L. Leborgne, R. Pakala, H. Yazdi, A. Ajani, R. Virmani, and R. Waksman, "Time Course of Stent Endothelialization After Intravascular Radiation Therapy in Rabbit Iliac Arteries," *Circulation*, vol. 107, Apr. 2003, pp. 2153-2158.

[39] M.R. Bennett, "IN-STENT STENOSIS: PATHOLOGY AND IMPLICATIONS FOR THE DEVELOPMENT OF DRUG ELUTING STENTS," *Heart*, vol. 89, 2003, pp. 218-224.

[40] R. Hoffmann, G.S. Mintz, G.R. Dussaillant, J.J. Popma, A.D. Pichard, L.F. Satler, K.M. Kent, J. Griffin, and M.B. Leon, "Patterns and Mechanisms of In-Stent Restenosis: A Serial Intravascular Ultrasound Study," *Circulation*, vol. 94, 1996, pp. 1247-1254.

[41] J.A. Painter, G.S. Mintz, S.C. Wong, J.J. Popma, A.D. Pichard, K.M. Kent, L.F. Satler, and M.B. Leon, "Serial intravascular ultrasound studies fail to show evidence of chronic Palmaz-Schatz stent recoil," *The American Journal of Cardiology*, vol. 75, Feb. 1995, pp. 398-400.

[42] W. Yiu, S. Cheng, and B. Sumpio, "Vascular Smooth Muscle Cell Apoptosis Induced by "Supercooling" and Rewarming," *J Vasc Interv Radiol*, vol. 17, Dec. 2006, pp. 1971-1977.

[43] M. Fava, S. Loyola, A. Polydorou, P. Papapavlou, A. Polydorou, O. Mendiz, and J. Joye, "Cryoplasty for Femoropopliteal Arterial Disease: Late Angiographic Results of Initial Human Experience," *J Vasc Interv Radiol*, vol. 15, Nov. 2004, pp. 1239-1243.

[44] J. Laird, M. Jaff, G. Biamino, T. McNamara, D. Scheinert, P. Zetterlund, E. Moen, and J. Joye, "Cryoplasty for the Treatment of Femoropopliteal Arterial Disease: Results of a Prospective, Multicenter Registry," *J Vasc Interv Radiol*, vol. 16, Aug. 2005, pp. 1067-1073.

[45] R. Samson, D. Showalter, M. Lepore, and S. Ames, "CryoPlasty Therapy of the Superficial Femoral and Popliteal Arteries: A Single Center Experience," *Vascular and Endovascular Surgery*, vol. 40, Dec. 2007, pp. 446-450.

[46] J. Tanguay, P. Geoffroy, J. Dorval, and M. Sirois, "Percutaneous endoluminal arterial cryoenergy improves vascular remodelling after angioplasty," *Thrombosis and Haemostasis*, vol. 92, 2004, pp. 1114-1121.

[47] R. Waksman, A. Ajani, R. White, E. Pinnow, R. Mehran, A. Bui, R. Deible, L. Gruberg, G. Mintz, L. Satler, A. Pichard, K. Kent, and J. Lindsay, "Two-year follow-up after beta and gamma intracoronary radiation therapy for patients with diffuse in-stent restenosis," *The American Journal of Cardiology*, vol. 88, 2001, pp. 425-428.

[48] M. Leon, P. Teirstein, J. Moses, P. Tripuraneni, A. Lansky, S. Jani, S. Wong, D. Fish, S. Ellis, D. Holmes, D. Kerieakes, and R. Kuntz, "Localized Intracoronary Gamma-Radiation Therapy to Inhibit the Recurrence of Restenosis after Stenting," *N Engl J Med*, vol. 344, Jan. 2001, pp. 250-256.

[49] P. Teirstein and R. Kuntz, "New Frontiers in Interventional Cardiology: Intravascular Radiation to Prevent Restenosis," *Circulation*, vol. 104, Nov. 2001, pp. 2620-2626.

[50] E. Minar, B. Pokrajac, T. Maca, R. Ahmadi, C. Fellner, M. Mittlbock, W. Seitz, R. Wolfram, and R. Potter, "Endovascular Brachytherapy for Prophylaxis of Restenosis After Femoropopliteal Angioplasty : Results of a Prospective Randomized Study," *Circulation*, vol. 102, 2000, pp. 2694-2699.

[51] J.R. Laird, A.J. Carter, W.M. Kufs, T.G. Hoopes, A. Farb, S.H. Nott, R.E. Fischell, D.R. Fischell, R. Virmani, and T.A. Fischell, "Inhibition of Neointimal Proliferation With Low-Dose Irradiation From a β-Particle-Emitting Stent," *Circulation*, vol. 93, Feb. 1996, pp. 529-536.

[52] R. Seabra-Gomes, "Intracoronary brachytherapy for restenosis: an efficient technique in the struggle for survival?," *Eur Heart J*, vol. 23, 2002, pp. 1319-1321.

[53] R. Waksman, I. Leitch, J. Roessler, H. Yazdi, R. Seabron, F. Tio, R. Scott, R. Grove, S. Rychnovsky, B. Robinson, R. Pakala, and E. Cheneau, "Intracoronary photodynamic therapy reduces neointimal growth without suppressing re-endothelialisation in a porcine model," *Heart*, vol. 92, Aug. 2006, pp. 1138-1144.

[54] R. Mansfield, S. Bown, and J. McEwan, "Photodynamic therapy: shedding light on restenosis," *Heart*, vol. 86, Dec. 2001, pp. 612-618.

[55] G. Stone, S. Ellis, D. Cox, J. Hermiller, C. O'Shaughnessy, J. Mann, M. Turco, R. Caputo, P. Bergin, J. Greenberg, J. Popma, M. Russell, and T. the, "A Polymer-Based, Paclitaxel-Eluting Stent in Patients with Coronary Artery Disease," *N Engl J Med*, vol. 350, Jan. 2004, pp. 221-231.

[56] J. Moses, M. Leon, J. Popma, P. Fitzgerald, D. Holmes, C. O'Shaughnessy, R. Caputo, D. Kereiakes, D. Williams, P. Teirstein, J. Jaeger, R. Kuntz, and S. the,

"Sirolimus-Eluting Stents versus Standard Stents in Patients with Stenosis in a Native Coronary Artery," *N Engl J Med*, vol. 349, Oct. 2003, pp. 1315-1323.

[57] J.J. Popma, D.S. Baim, and F.S. Resnic, "Chapter 55 -Percutaneous Coronary and Valvular Intervention," *Braunwald's Heart Diseases*, pp. 1429-1436.

[58] P.A. Calvert and M.R. Bennett, "Restenosis Revisited," *Circ Res*, vol. 104, Apr. 2009, pp. 823-825.

[59] S. Ligthart, F. Vlemmix, N. Dendukuri, and J.M. Brophy, "The cost-effectiveness of drug-eluting stents: a systematic review," *CMAJ*, vol. 176, 2007, pp. 199-205.

[60] B. Lagerqvist, S. James, U. Stenestrand, J. Lindback, T. Nilsson, L. Wallentin, and S. the, "Long-Term Outcomes with Drug-Eluting Stents versus Bare-Metal Stents in Sweden," *N Engl J Med*, vol. 356, Mar. 2007, pp. 1009-1019.

[61] A.T. Ong, E.P. McFadden, E. Regar, P.P. de Jaegere, R.T. van Domburg, and P.W. Serruys, "Late Angiographic Stent Thrombosis (LAST) Events With Drug-Eluting Stents," *Journal of the American College of Cardiology*, vol. 45, Jun. 2005, pp. 2088-2092.

[62] C. Stettler, S. Wandel, S. Allemann, A. Kastrati, M.C. Morice, A. Sch$\blacklozenge$mig, M.E. Pfisterer, G.W. Stone, M.B. Leon, J.S. de Lezo, J. Goy, S. Park, M. Sabat$\blacklozenge$, M.J. Suttorp, H. Kelbaek, C. Spaulding, M. Menichelli, P. Vermeersch, M.T. Dirksen, P. Cervinka, A.S. Petronio, A.J. Nordmann, P. Diem, B. Meier, M. Zwahlen, S. Reichenbach, S. Trelle, S. Windecker, and P. J$\blacklozenge$ni, "Outcomes associated with drug-eluting and bare-metal stents: a collaborative network meta-analysis," *The Lancet*, vol. 370, pp. 937-948.

[63] P.W. Serruys, M. Morice, A.P. Kappetein, A. Colombo, D.R. Holmes, M.J. Mack, E. Stahle, T.E. Feldman, M. van den Brand, E.J. Bass, N. Van Dyck, K. Leadley, K.D. Dawkins, F.W. Mohr, and the SYNTAX Investigators, "Percutaneous Coronary Intervention versus Coronary-Artery Bypass Grafting for Severe Coronary Artery Disease," *N Engl J Med*, 2009, p. NEJMoa0804626.

[64] K. Makinen, H. Manninen, M. Hedman, P. Matsi, H. Mussalo, E. Alhava, and S. Yla-Herttuala, "Increased Vascularity Detected by Digital Subtraction Angiography after VEGF Gene Transfer to Human Lower Limb Artery: A Randomized, Placebo-Controlled, Double-Blinded Phase II Study," *Mol Ther*, vol. 6, 2002, pp. 127-133.

[65] M. Shibata, H. Suzuki, M. Nakatani, S. Koba, E. Geshi, T. Katagiri, and Y. Takeyama, "The involvement of vascular endothelial growth factor and flt-1 in the process of neointimal proliferation in pig coronary arteries following stent implantation," *Histochemistry and Cell Biology*, vol. 116, Dec. 2001, pp. 471-481.

[66] M. Hedman, J. Hartikainen, M. Syvanne, J. Stjernvall, A. Hedman, A. Kivela, E. Vanninen, H. Mussalo, E. Kauppila, S. Simula, O. Narvanen, A. Rantala, K.

Peuhkurinen, M. Nieminen, M. Laakso, and S. Yla-Herttuala, "Safety and Feasibility of Catheter-Based Local Intracoronary Vascular Endothelial Growth Factor Gene Transfer in the Prevention of Postangioplasty and In-Stent Restenosis and in the Treatment of Chronic Myocardial Ischemia. Phase II Results of the Kuopio Angiogenesis Trial (KAT)," *Circulation*, May. 2003, p. 01.CIR.0000070540.80780.92.

[67] S. Janssens, D. Flaherty, Z. Nong, O. Varenne, N. van Pelt, C. Haustermans, P. Zoldhelyi, R. Gerard, and D. Collen, "Human Endothelial Nitric Oxide Synthase Gene Transfer Inhibits Vascular Smooth Muscle Cell Proliferation and Neointima Formation After Balloon Injury in Rats," *Circulation*, vol. 97, 1998, pp. 1274-1281.

[68] F.C. Aubart, Y. Sassi, A. Coulombe, N. Mougenot, C. Vrignaud, P. Leprince, P. Lechat, A. Lompre, and J. Hulot, "RNA Interference Targeting STIM1 Suppresses Vascular Smooth Muscle Cell Proliferation and Neointima Formation in the Rat," *Mol Ther*, Dec. 2008.

[69] Tobias Walker, Hans Peter Wendel, Claudia Raabe, Patricya Wyechnik, Liane Spranger, Olaf Heidenreich, Albertus M. Scheule, Alfred Nordheim, and Gerhard Ziemer, "Graft Protection in Bypass Surgery: siRNA-Mediated Silencing of Adhesion Molecules," Jan. 2009.

[70] T. He, L.A. Smith, S. Harrington, K.A. Nath, N.M. Caplice, and Z.S. Katusic, "Transplantation of Circulating Endothelial Progenitor Cells Restores Endothelial Function of Denuded Rabbit Carotid Arteries," *Stroke*, vol. 35, 2004, pp. 2378-2384.

[71] D. Kong, L.G. Melo, M. Gnecchi, L. Zhang, G. Mostoslavsky, C.C. Liew, R.E. Pratt, and V.J. Dzau, "Cytokine-Induced Mobilization of Circulating Endothelial Progenitor Cells Enhances Repair of Injured Arteries," *Circulation*, vol. 110, 2004, pp. 2039-2046.

[72] T. Meurice, C. Bauters, X. Hermant, V. Codron, E. VanBelle, E.P.M. Fadden, J. Lablanche, M.E. Bertrand, and P. Amouyel, "Effect of ACE inhibitors on angiographic restenosis after coronary stenting (PARIS): a randomised, double-blind, placebo-controlled trial," *The Lancet*, vol. 357, Apr. 2001, pp. 1321-1324.

[73] D.P. Faxon, "Effect of high dose angiotensin-converting enzyme inhibition on restenosis: Final results of the MARCATOR study, a multicenter, double-blind, placebo-controlled trial of cilazapril," *Journal of the American College of Cardiology*, vol. 25, Feb. 1995, pp. 362-369.

[74] R. von Essen, R. Ostermaier, E. Grube, W. Maurer, U. Tebbe, R. Erbel, M. Roth, W. Oel, J. Brom, and G. Weidinger, "Effects of Octreotide Treatment on Restenosis After Coronary Angioplasty : Results of the VERAS Study," *Circulation*, vol. 96, 1997, pp. 1482-1487.

[75] S.G. Ellis, G.S. Roubin, J. Wilentz, J.S. Douglas, and S.B. King, "Effect of 18- to 24-hour heparin administration for prevention of restenosis after uncomplicated coronary angioplasty," *American Heart Journal*, vol. 117, Apr. 1989, pp. 777-782.

[76] M. Wu and M. Thiagarajan, "ROLE OF ENDOTHELIUM IN THROMBOSIS AND HEMOSTASIS," *Annual Review of Medicine*, vol. 47, 1996, p. 315.

[77] W. van der Giessen, P. Serruys, H. van Beusekom, L. van Woerkens, H. van Loon, L. Soei, B. Strauss, K. Beatt, and P. Verdouw, "Coronary stenting with a new, radiopaque, balloon-expandable endoprosthesis in pigs," *Circulation*, vol. 83, May. 1991, pp. 1788-1798.

[78] T. Asahara, T. Murohara, A. Sullivan, M. Silver, R. van der Zee, T. Li, B. Witzenbichler, G. Schatteman, and J.M. Isner, "Isolation of Putative Progenitor Endothelial Cells for Angiogenesis," *Science*, vol. 275, Feb. 1997, pp. 964-966.

[79] S. Gabriel, R.W. Lau, and C. Gabriel, "The dielectric properties of biological tissues: II. Measurements in the frequency range 10 Hz to 20 GHz," *Physics in Medicine and Biology*, vol. 41, 1996, pp. 2251-2269.

[80] Jing Liu and L. Xu, "Estimation of blood perfusion using phase shift in temperature response to sinusoidal heating at the skin surface," *Biomedical Engineering, IEEE Transactions on*, vol. 46, 1999, pp. 1037-1043.

[81] E.H. Wissler, "Pennes' 1948 paper revisited," *J Appl Physiol*, vol. 85, Jul. 1998, pp. 35-41.

[82] E. Maor, A. Ivorra, J. Leor, and B. Rubinsky, "The Effect of Irreversible Electroporation on Blood Vessels," *Technology in Cancer Research and Treatment*, vol. 6, Aug. 2007, pp. 255-360.

[83] N.T. Wright, "On a Relationship Between the Arrhenius Parameters from Thermal Damage Studies," *Journal of Biomechanical Engineering*, vol. 125, Apr. 2003, pp. 300-304.

[84] R.V. Davalos and B. Rubinsky, "Temperature considerations during irreversible electroporation," *International Journal of Heat and Mass Transfer*, vol. 51, Nov. 2008, pp. 5617-5622.

[85] K.R. Diller and J.A. Pearce, "Issues in Modeling Thermal Alterations in Tissues," *Annals of the New York Academy of Sciences*, vol. 888, 1999, pp. 153-164.

[86] L. Clerc, "Directional differences of impulse spread in trabecular muscle from mammalian heart.," *J Physiol*, vol. 255, 1976, pp. 335-346.

[87] A. Ivorra, L. Miller, and B. Rubinsky, "Electrical impedance measurements during electroporation of rat liver and muscle," *13th International Conference on Electrical Bioimpedance and the 8th Conference on Electrical Impedance Tomography*, 2007, pp. 130-133.

[88] J.A.P. Ramtin Agah, "Rate process model for arterial tissue thermal damage: Implications on vessel photocoagulation," *Lasers in Surgery and Medicine*, vol. 15, 1994, pp. 176-184.

[89] L. Miller, J. Leor, and B. Rubinsky, "Cancer Cells Ablation with Irreversible Electroporation," *Technol Cancer Res Treat*, vol. 4, Dec. 2005, pp. 699-705.

[90] B. Rubinsky, "Irreversible electroporation in medicine," *Technology in Cancer Research & Treatment*, vol. 6, Aug. 2007, pp. 255-60.

[91] B. Rubinsky, G. Onik, and P. Mikus, "Irreversible electroporation: a new ablation modality--clinical implications," *Technology in Cancer Research & Treatment*, vol. 6, Feb. 2007, pp. 37-48.

[92] A.T. Esser, K.C. Smith, T.R. Gowrishankar, and J.C. Weaver, "Towards solid tumor treatment by irreversible electroporation: intrinsic redistribution of fields and currents in tissue," *Technology in Cancer Research & Treatment*, vol. 6, Aug. 2007, pp. 261-74.

[93] B. Al-Sakere, F. André, C. Bernat, E. Connault, P. Opolon, R. Davalos, B. Rubinsky, and L. Mir, "Tumor Ablation with Irreversible Electroporation," *PLoS ONE*, vol. 2, 2007, p. e1135.

[94] T. Matsumura, R. Konishi, and Y. Nagai, "Culture substrate dependence of mouse fibroblasts survival at 4 degrees C," *In Vitro*, vol. 18, Jun. 1982, pp. 510-4.

[95] L. Raptis and K.L. Firth, "Electrode Assemblies Used for In Vivo DNA Delivery by Electroporation," *Electroporation Protocols: Preclinical and Clinical Gene Medicine*, Humana Press, 2008, pp. 61-89.

[96] S. Kwee, H.V. Nielsen, and J.E. Celis, "Electropermeabilization of human cultured cells grown in monolayers : Incorporation of monoclonal antibodies," *Bioelectrochemistry and Bioenergetics*, vol. 23, Feb. 1990, pp. 65-80.

[97] Q. Zheng and D.C. Chang, "High-efficiency gene transfection by in situ electroporation of cultured cells," *Biochimica et Biophysica Acta (BBA) - Gene Structure and Expression*, vol. 1088, Jan. 1991, pp. 104-110.

[98] B. Valič, M. Golzio, M. Pavlin, A. Schatz, C. Faurie, B. Gabriel, J. Teissié, M. Rols, and D. Miklavčič, "Effect of electric field induced transmembrane potential on spheroidal cells: theory and experiment," *European Biophysics Journal*, vol. 32, Oct. 2003, pp. 519-528.

[99] S. Boitano, E. Dirksen, and M. Sanderson, "Intercellular propagation of calcium waves mediated by inositol trisphosphate," *Science*, vol. 258, Oct. 1992, pp. 292-295.

[100] T. Yang, W.C. Heiser, and J.M. Sedivy, "Efficient in situ electroporation of mammalian cells grown on microporous membranes," *Nucl. Acids Res.*, vol. 23, Aug. 1995, pp. 2803-2810.

[101] Chun-Ping Jen, Wei-Ming Wu, Min Li, and Yu-Cheng Lin, "Site-specific enhancement of gene transfection utilizing an attracting electric field for DNA plasmids on the electroporation microchip," *Microelectromechanical Systems, Journal of*, vol. 13, 2004, pp. 947-955.

[102] N. Pavselj, Z. Bregar, D. Cukjati, D. Batiuskaite, L. Mir, and D. Miklavcic, "The course of tissue permeabilization studied on a mathematical model of a subcutaneous tumor in small animals," *Biomedical Engineering, IEEE Transactions on*, vol. 52, 2005, pp. 1373-1381.

[103] V.M. Jackson, S.J. Trout, and T.C. Cunnane, "Regional variation in electrically-evoked contractions of rabbit isolated pulmonary artery," *Br J Pharmacol*, vol. 137, Oct. 2002, pp. 488-496.

[104] T.J. Liao and H. Nishikawa, "The variation of action potential and impedance in human skeletal muscle during voluntary contraction," *The Tohoku Journal of Experimental Medicine*, vol. 173, Jul. 1994, pp. 303-9.

[105] C.A. Shiffman, R. Aaron, and S.B. Rutkove, "Electrical impedance of muscle during isometric contraction," *Physiological Measurement*, vol. 24, Feb. 2003, pp. 213-34.

[106] M. Ward, G. Pasterkamp, A. Yeung, and C. Borst, "Arterial Remodeling : Mechanisms and Clinical Implications," *Circulation*, vol. 102, Sep. 2000, pp. 1186-1191.

[107] M. Davies and P. Hagen, "Pathobiology of intimal hyperplasia," *Br J Surg.*, vol. 81, Sep. 1994, pp. 1254-69.

[108] A. Touchard and R. Schwartz, "Preclinical Restenosis Models: Challenges and Successes," *Toxicol Pathol*, vol. 34, Jan. 2006, pp. 11-18.

[109] E. Maor, A. Ivorra, J. Leor, and B. Rubinsky, "Irreversible Electroporation Attenuates Neointimal Formation After Angioplasty," *Biomedical Engineering, IEEE Transactions on*, vol. 55, 2008, pp. 2268-2274.

[110] M. Clarke, N. Figg, J. Maguire, A. Davenport, M. Goddard, T. Littlewood, and M. Bennett, "Apoptosis of vascular smooth muscle cells induces features of plaque vulnerability in atherosclerosis," *Nat Med*, vol. 12, 2006, pp. 1075-1080.

[111] C. Chen, S. Smye, M. Robinson, and J. Evans, "Membrane electroporation theories: a review," *Medical and Biological Engineering and Computing*, vol. 44, Mar. 2006, pp. 5-14.

[112] Y. Huang and B. Rubinsky, "Micro-electroporation: improving the efficiency and understanding of electrical permeabilization of cells," *Biomed. Microdevices*, vol. 3, 1999, pp. 145-150.

[113] M. Pavlin, M. Kanduser, M. Rebersek, G. Pucihar, F. Hart, R. Magjarevic, and D. Miklavcic, "Effect of Cell Electroporation on the Conductivity of a Cell Suspension," *Biophys. J.*, vol. 88, 2005, pp. 4378-4390.

[114] R. Davalos, B. Rubinsky, and D. Otten, "A Feasibility Study for Electrical Impedance Tomography as a Means to Monitor Tissue Electroporation for Molecular Medicine," *IEEE Trans. Biomed. Eng.*, vol. 49, 2002, pp. 400-403.

[115] D. Cukjati, D. Batiuskaite, F. Andre, D. Miklavcic, and L. Mir, "Real time electroporation control for accurate and safe in vivo non-viral gene therapy," *Bioelectrochemistry*, vol. 70, 2007, pp. 501-507.

[116] B. Dev, A. Hofmann, B. Dev, and P. Rabussay, "Intravascular Electroporation Markedly Attenuates Neointima Formation After Balloon Injury of the Carotid Artery in the Rat," *J Interven Cardiol*, vol. 13, 2000, pp. 331-338.

[117] R. Davalos and B. Rubinsky, "Tissue ablation with irreversible electroporation - Patent Application 20070043345," Feb. 2007.

[118] J. Edd, L. Horowitz, R. Davalos, L. Mir, and B. Rubinsky, "In vivo results of a new focal tissue ablation technique: irreversible electroporation.," *IEEE Trans Biomed Eng*, vol. 53, Jul. 2006, pp. 1409-15.

[119] M. Narayanaswamy, K. Wright, and K. Kandarpa, "Animal Models for Atherosclerosis, Restenosis, and Endovascular Graft Research," *J Vasc Interv Radiol*, vol. 11, Jan. 2000, pp. 5-17.

[120] D. Faxon, V. Weber, C. Haudenschild, S. Gottsman, W. McGovern, and T. Ryan, "Acute effects of transluminal angioplasty in three experimental models of atherosclerosis," *Arterioscler Thromb Vasc Biol*, vol. 2, Mar. 1982, pp. 125-133.

[121] V. Verin, Y. Popowski, P. Urban, J. Belenger, M. Redard, M. Costa, M. Widmer, M. Rouzaud, P. Nouet, E. Grob, M. Schwager, J.M. Kurtz, and W. Rutishauser, "Intra-arterial Beta Irradiation Prevents Neointimal Hyperplasia in a Hypercholesterolemic Rabbit Restenosis Model," *Circulation*, vol. 92, Oct. 1995, pp. 2284-2290.

[122] R.L. Wilensky, K.L. March, I. Gradus-Pizlo, G. Sandusky, N. Fineberg, and D.R. Hathaway, "Vascular Injury, Repair, and Restenosis After Percutaneous Transluminal Angioplasty in the Atherosclerotic Rabbit," *Circulation*, vol. 92, Nov. 1995, pp. 2995-3005.

[123] H.R. Baumgartner, "The role of blood flow in platelet adhesion, fibrin deposition, and formation of mural thrombi," *Microvascular Research*, vol. 5, Mar. 1973, pp. 167-179.

[124] K.A. Hruska, "Vascular Smooth Muscle Cells in the Pathogenesis of Vascular Calcification," *Circ Res*, vol. 104, Mar. 2009, pp. 710-711.

[125] M.Y. Speer, H. Yang, T. Brabb, E. Leaf, A. Look, W. Lin, A. Frutkin, D. Dichek, and C.M. Giachelli, "Smooth Muscle Cells Give Rise to Osteochondrogenic Precursors and Chondrocytes in Calcifying Arteries," *Circ Res*, vol. 104, Mar. 2009, pp. 733-741.

[126] A.H. Schulick, A.J. Taylor, W. Zuo, C. Qiu, G. Dong, R.N. Woodward, R. Agah, A.B. Roberts, R. Virmani, and D.A. Dichek, "Overexpression of transforming growth factor β1 in arterial endothelium causes hyperplasia, apoptosis, and cartilaginous metaplasia," *Proceedings of the National Academy of Sciences of the United States of America*, vol. 95, Jun. 1998, pp. 6983-6988.

[127] G.W. Taylor, G.N. Kay, X. Zheng, S. Bishop, and R.E. Ideker, "Pathological Effects of Extensive Radiofrequency Energy Applications in the Pulmonary Veins in Dogs," *Circulation*, vol. 101, Apr. 2000, pp. 1736-1742.

[128] M.W. Majesky, V. Lindner, D.R. Twardzik, S.M. Schwartz, and M.A. Reidy, "Production of transforming growth factor beta 1 during repair of arterial injury," *The Journal of Clinical Investigation*, vol. 88, Sep. 1991, pp. 904-10.

[129] T. Sutra, M. Morena, A. Bargnoux, B. Caporiccio, B. Canaud, and J. Cristol, "Superoxide production: A procalcifying cell signalling event in osteoblastic differentiation of vascular smooth muscle cells exposed to calcification media," *Free Radical Research*, vol. 42, 2008, pp. 789 - 797.

[130] M. Kollum, S. Kaiser, R. Kinscherf, J. Metz, W. Kubler, and C. Hehrlein, "Apoptosis After Stent Implantation Compared With Balloon Angioplasty in Rabbits : Role of Macrophages," *Arterioscler Thromb Vasc Biol*, vol. 17, 1997, pp. 2383-2388.

[131] C. Hehrlein, M. Stintz, R. Kinscherf, K. Schlosser, E. Huttel, L. Friedrich, P. Fehsenfeld, and W. Kubler, "Pure ⍰-ParticleEmitting Stents Inhibit Neointima Formation in Rabbits," *Circulation*, vol. 93, 1996, pp. 641-645.

[132] C. Hehrlein, C. Gollan, K. Donges, J. Metz, R. Riessen, P. Fehsenfeld, E. von Hodenberg, and W. Kubler, "Low-Dose Radioactive Endovascular Stents Prevent Smooth Muscle Cell Proliferation and Neointimal Hyperplasia in Rabbits," *Circulation*, vol. 92, 1995, pp. 1570-1575.

[133] C. Rogers, E.R. Edelman, and D.I. Simon, "A mAb to the β2-leukocyte integrin Mac-1 (CD11b/CD18) reduces intimal thickening after angioplasty or stent implantation in rabbits," *Proceedings of the National Academy of Sciences of the United States of America*, vol. 95, Aug. 1998, pp. 10134–10139.

[134] D.E. Drachman, E.R. Edelman, P. Seifert, A.R. Groothuis, D.A. Bornstein, K.R. Kamath, M. Palasis, D. Yang, S.H. Nott, and C. Rogers, "Neointimal thickening after stent delivery of paclitaxel: change in composition and arrest of growth over six months," *Journal of the American College of Cardiology*, vol. 36, Dec. 2000, pp. 2325-2332.

[135] A. Farb, P.F. Heller, S. Shroff, L. Cheng, F.D. Kolodgie, A.J. Carter, D.S. Scott, J. Froehlich, and R. Virmani, "Pathological Analysis of Local Delivery of Paclitaxel Via a Polymer-Coated Stent," *Circulation*, vol. 104, 2001, pp. 473-479.

[136] A. Farb, M. John, E. Acampado, F.D. Kolodgie, M.F. Prescott, and R. Virmani, "Oral Everolimus Inhibits In-Stent Neointimal Growth," *Circulation*, vol. 106, 2002, pp. 2379-2384.

[137] P.J. Fitzgerald, T.A. Ports, and P.G. Yock, "Contribution of localized calcium deposits to dissection after angioplasty. An observational study using intravascular ultrasound," *Circulation*, vol. 86, 1992, pp. 64-70.

[138] S.A. Curley, F. Izzo, P. Delrio, L.M. Ellis, J. Granchi, P. Vallone, F. Fiore, S. Pignata, B. Daniele, and F. Cremona, "Radiofrequency ablation of unresectable primary and metastatic hepatic malignancies: results in 123 patients," *Annals of Surgery*, vol. 230, Jul. 1999, pp. 1-8.

[139] A.S. Manolis, P.J. Wang, and N.A.M. Estes, "Radiofrequency Catheter Ablation for Cardiac Tachyarrhythmias," *Ann Intern Med*, vol. 121, 1994, pp. 452-461.

[140] I.S. Gill, A.C. Novick, A.M. Meraney, R.N. Chen, M.G. Hobart, G.T. Sung, J. Hale, D.K. Schweizer, and E.M. Remer, "Laparoscopic renal cryoablation in 32 patients," *Urology*, vol. 56, Nov. 2000, pp. 748-753.

[141] B. Al-Sakere, F. André, C. Bernat, E. Connault, P. Opolon, R.V. Davalos, B. Rubinsky, and L.M. Mir, "Tumor Ablation with Irreversible Electroporation," *PLoS ONE*, vol. 2, Nov. 2007, p. e1135.

[142] Y. Fung, "Chapter 7: Bioviscoelastic Solids," *Biomechanics: Mechanical Properties of Living Tissues*, Springer-Verlag New-York, Inc., 1997, pp. 242-320.

[143] C. Brasselet, E. Durand, F. Addad, F. Vitry, G. Chatellier, C. Demerens, M. Lemitre, R. Garnotel, D. Urbain, P. Bruneval, and A. Lafont, "Effect of local heating on restenosis and in-stent neointimal hyperplasia in the atherosclerotic rabbit model: a dose-ranging study," *Eur Heart J*, vol. 29, 2008, pp. 402-412.

[144] P. Crago, P. Peckham, J. Mortimer, and J. Van Der Meulen, "The choice of pulse duration for chronic electrical stimulation via surface, nerve, and intramuscular electrodes," *Annals of Biomedical Engineering*, vol. 2, 1974, pp. 252-264.

[145] C. Pappone, S. Rosanio, G. Oreto, M. Tocchi, F. Gugliotta, G. Vicedomini, A. Salvati, C. Dicandia, P. Mazzone, V. Santinelli, S. Gulletta, and S. Chierchia, "Circumferential Radiofrequency Ablation of Pulmonary Vein Ostia : A New Anatomic Approach for Curing Atrial Fibrillation," *Circulation*, vol. 102, 2000, pp. 2619-2628.

[146] I.M. Robbins, E.V. Colvin, T.P. Doyle, W.E. Kemp, J.E. Loyd, W.S. McMahon, and G.N. Kay, "Pulmonary Vein Stenosis After Catheter Ablation of Atrial Fibrillation," *Circulation*, vol. 98, 1998, pp. 1769-1775.

[147] J. Lavee, G. Onik, P. Mikus, and B. Rubinsky, “A Novel Nonthermal Energy Source for Surgical Epicardial Atrial Ablation: Irreversible Electroporation,” *The Heart Surgery Forum*, vol. 10, Apr. 2007, pp. E162 - E167.

[148] S.H. Swedberg, B.G. Brown, R. Sigley, T.N. Wight, D. Gordon, and S.C. Nicholls, “Intimal fibromuscular hyperplasia at the venous anastomosis of PTFE grafts in hemodialysis patients. Clinical, immunocytochemical, light and electron microscopic assessment,” *Circulation*, vol. 80, 1989, pp. 1726-1736.

[149] M. Barry J., “Chapter 65 - Hypertrophic Cardiomyopathy,” *Braunwald's Heart Diseases*, Saunders, Elsevier, 2008, pp. 1763-1773.

[150] B.F. Overholt, M. Panjehpour, and J.M. Haydek, “Photodynamic therapy for Barrett's esophagus: follow-up in 100 patients, „” *Gastrointestinal Endoscopy*, vol. 49, Jan. 1999, pp. 1-7.

X. APPENDIX 1

```
function [averageDamage,maximalDamage] = heatSimulation(fem,V0,pauseLength,pulseNumber)

format long;

A = 5.6E+63;

E=4.3E+5;

R=8.13;

RingArea = 1.07951E-05;

 % Initializing Mesh

fem.const(2)={V0};

fem.xmesh=meshextend(fem);

fem=multiphysics(fem);

 % Solving the electric field problem

fem.sol=femstatic(fem,   'solcomp',{'V'},  'outcomp',{'V'});

fem0=fem;

fem1 = fem0;

 %Solving for the temperature during the first 100 microseconds electroporation pulse

fem.sol=femtime(fem, 'u',fem1.sol, 'solcomp',{'T'},  'outcomp',{'T'},  'tlist',0:0.1E-4:1E-4,  'tout','tlist');

fem0=fem;

%Solving for the temperature during the interval following the first electroporation pulse

fem.sol=femtime(fem,  'init',fem0.sol, 'u',0, 'solcomp',{'T'}, 'outcomp',{'T'}, 'tlist', 0:(pauseLength/10):pauseLength,
'tout','tlist');

fem0=fem;

  % Initialing arrays for the maximal and average temperature values. Values are stored for 180 seconds after the last
electroporation pulse

maxT =
[0:pauseLength:pauseLength*pulseNumber,pauseLength*pulseNumber+1:1:pauseLength*pulseNumber+180;0:1:pulse
Number+180];

averageT =
[0:pauseLength:pauseLength*pulseNumber,pauseLength*pulseNumber+1:1:pauseLength*pulseNumber+180;0:1:pulse
Number+180];

maxT(2,1) = 310.15;

averageT(2,1) = 310.15;

%Updating  the value of the temperature after the first pulse

maxT(2,2) = postmax(fem,'T','solnum',11);
```

```
averageT(2,2) = postint(fem,'if((x^2+y^2)<(0.00225^2),T,0)','dl',2,'solnum',11);

%Iterative solution for the transient temperature during the entire electroporation pulses sequence

for i=2:pulseNumber


fem.sol=femtime(fem, 'init',fem0.sol, 'u',fem1.sol, 'solcomp',{'T'}, 'outcomp',{'T'}, 'tlist',[0:0.1E-4:1E-4], 'tout','tlist');

fem0=fem;

 fem.sol=femtime(fem, 'init',fem0.sol, 'u',0, 'solcomp',{'T'}, 'outcomp',{'T'}, 'tlist',0:(pauseLength/10):pauseLength,
'tout','tlist');

fem0=fem;

 maxT(2,i+1) = postmax(fem,'T','solnum',11);

 averageT(2,i+1) = postint(fem,'if((x^2+y^2)<(0.00225^2),T,0)','dl',2,'solnum',11);

 end

%Solving for the transient temperature during 3 minutes following the last electroporation pulse

fem.sol=femtime(fem, 'init',fem0.sol, 'u',0, 'solcomp',{'T'}, 'outcomp',{'T'}, 'tlist',0:1:180,                'tout','tlist');

% Updating the temperature values during the three minutes following the last electroporation pulse

for j=1:180

    maxT(2,pulseNumber+j+1) = postmax(fem,'T','solnum',j);

    averageT(2,pulseNumber+j+1) = postint(fem,'if((x^2+y^2)<(0.00225^2),T,0)','dl',2,'solnum',j);

end

% Calculating the average and maximal values of the Ω-integral expression in the domain based on the transient
temperature solutions

averageT(2,2:pulseNumber+181) = averageT(2,2:pulseNumber+181)/RingArea;

averageT(2,1:pulseNumber+181) = A*exp(-E./(averageT(2,1:pulseNumber+181)*R));

maxT(2,1:pulseNumber+181) = A*exp(-E./(maxT(2,1:pulseNumber+181)*R));

 %Calculating Ω using numerical integration

averageDamage =trapz(averageT(1,1:pulseNumber+181),averageT(2,1:pulseNumber+181));

maximalDamage =trapz(maxT(1,1:pulseNumber+181),maxT(2,1:pulseNumber+181));
```

XI. APPENDIX 2 - CHAPTER VI FIGURES

Figure XI-1 - Animal No. 2391 Left, Section #1/ VE/ 5X

Figure XI-2 - Animal No. 2391 Left, Section #2/ VE/ 5X

Figure XI-3 - Animal No. 2391 Left, Section #3/ VE/ 5X

Figure XI-4 - Animal No. 2391 Right, Section #1/ MT/ 5X

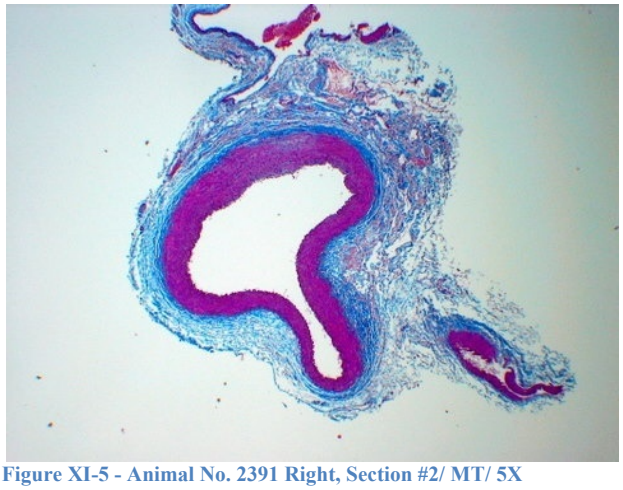

Figure XI-5 - Animal No. 2391 Right, Section #2/ MT/ 5X

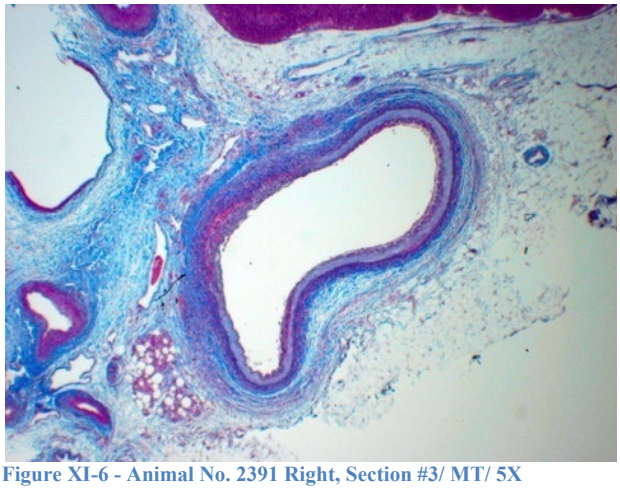

Figure XI-6 - Animal No. 2391 Right, Section #3/ MT/ 5X

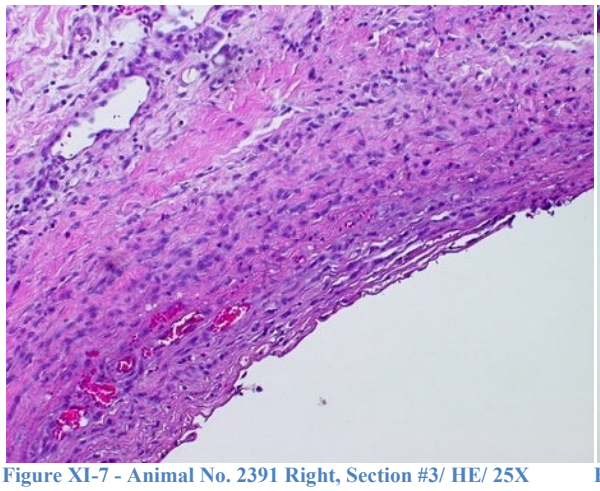

Figure XI-7 - Animal No. 2391 Right, Section #3/ HE/ 25X

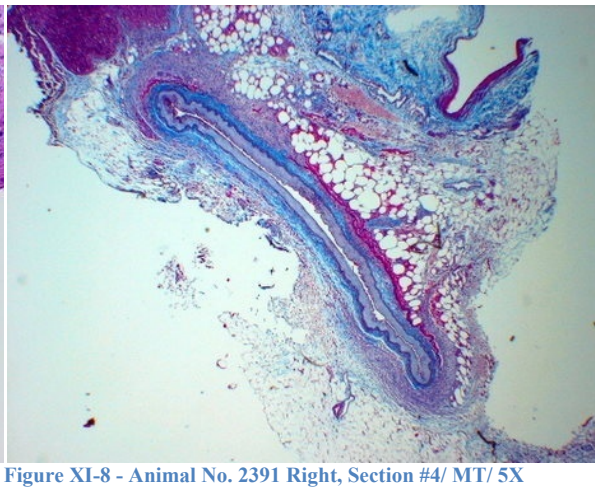

Figure XI-8 - Animal No. 2391 Right, Section #4/ MT/ 5X

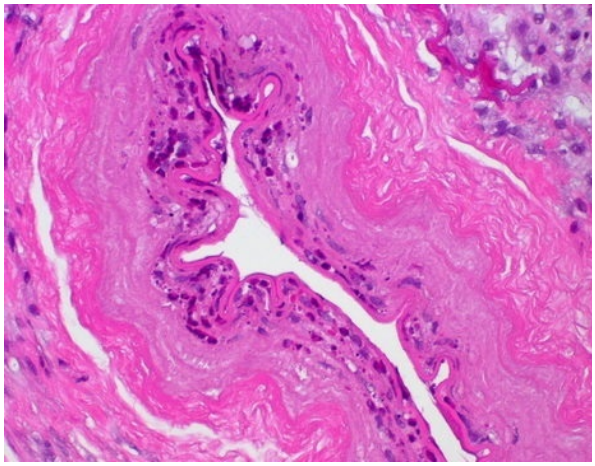

Figure XI-9 - Animal No. 2391 Right, Section #4/ HE/ 50X

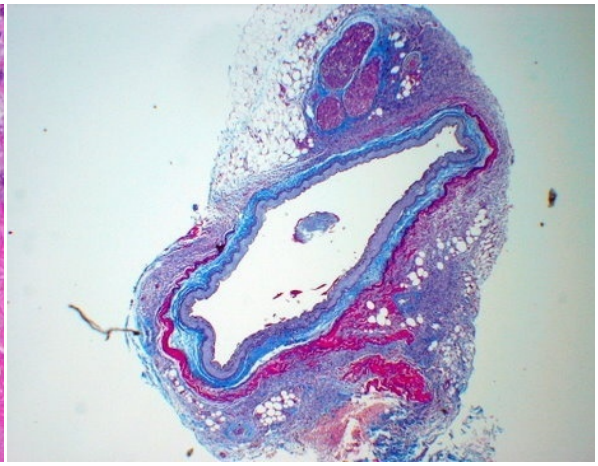

Figure XI-10 - Animal No. 2391 Right, Section #5/ MT/ 5X

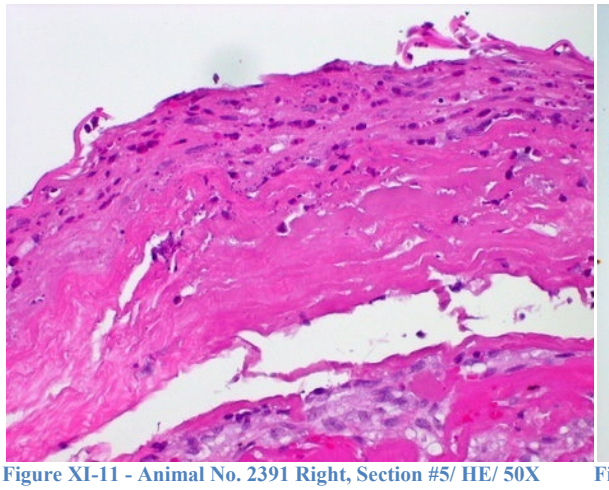

Figure XI-11 - Animal No. 2391 Right, Section #5/ HE/ 50X

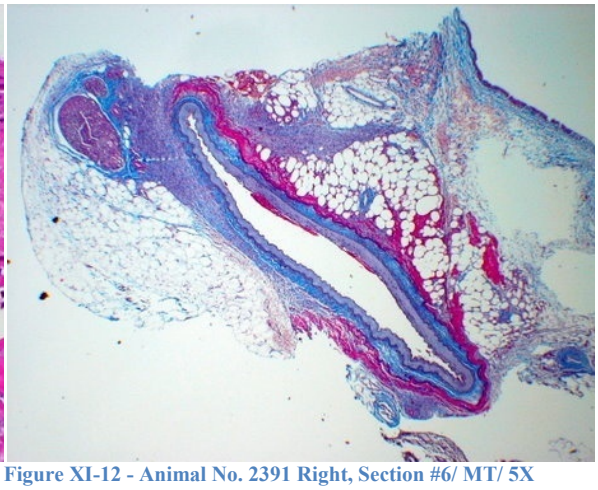

Figure XI-12 - Animal No. 2391 Right, Section #6/ MT/ 5X

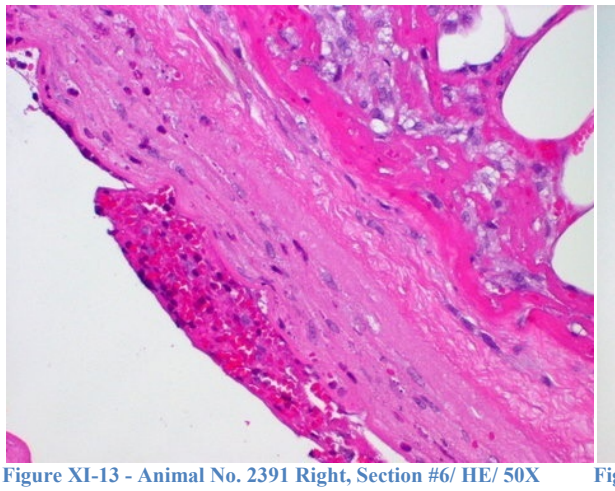

Figure XI-13 - Animal No. 2391 Right, Section #6/ HE/ 50X

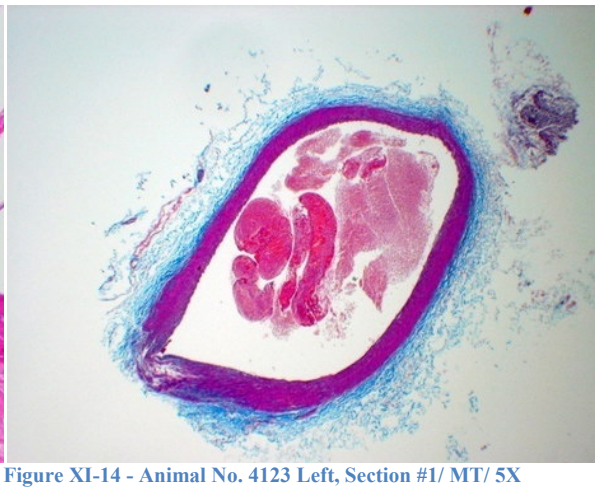

Figure XI-14 - Animal No. 4123 Left, Section #1/ MT/ 5X

Figure XI-15 - Animal No. 4123 Left, Section #2/ MT/ 5X

Figure XI-16 - Animal No. 4123 Left, Section #3/ MT/ 5X

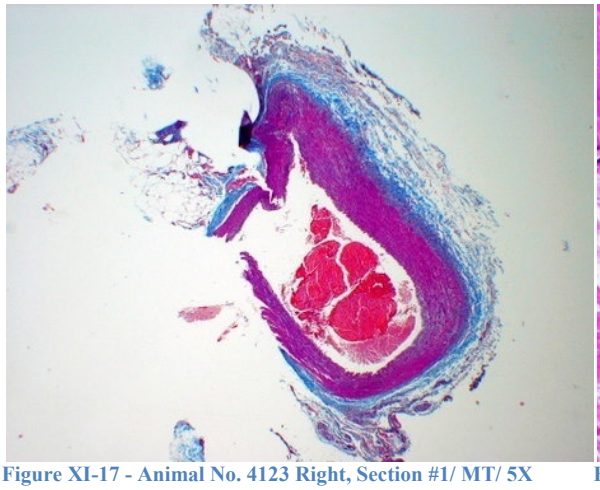

Figure XI-17 - Animal No. 4123 Right, Section #1/ MT/ 5X

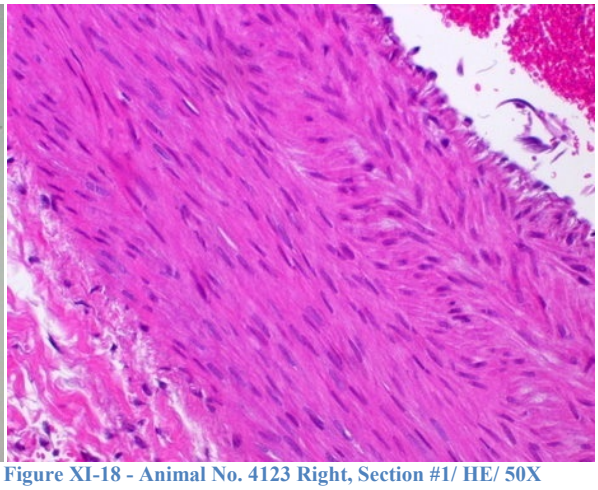

Figure XI-18 - Animal No. 4123 Right, Section #1/ HE/ 50X

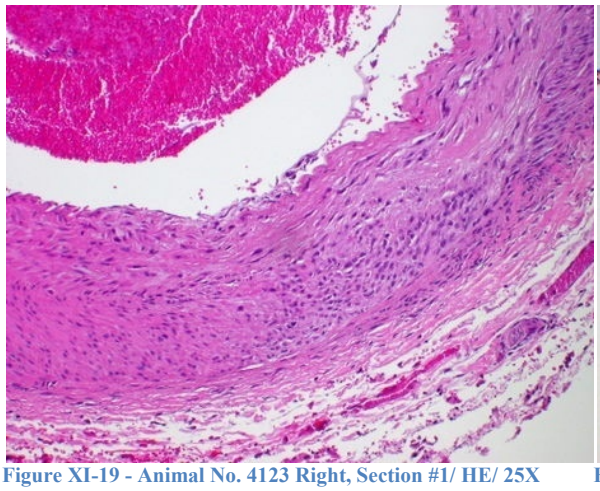

Figure XI-19 - Animal No. 4123 Right, Section #1/ HE/ 25X

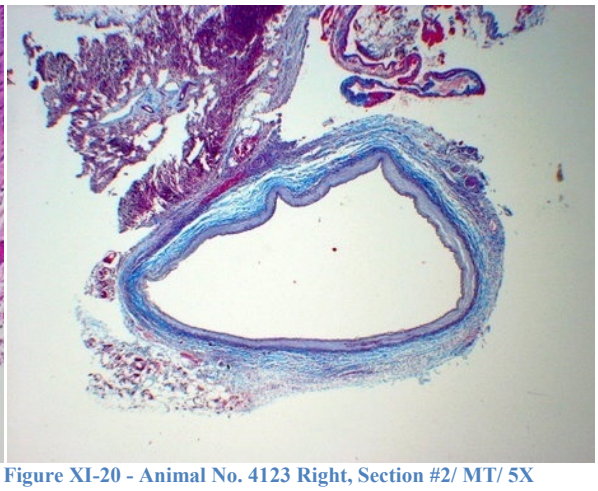

Figure XI-20 - Animal No. 4123 Right, Section #2/ MT/ 5X

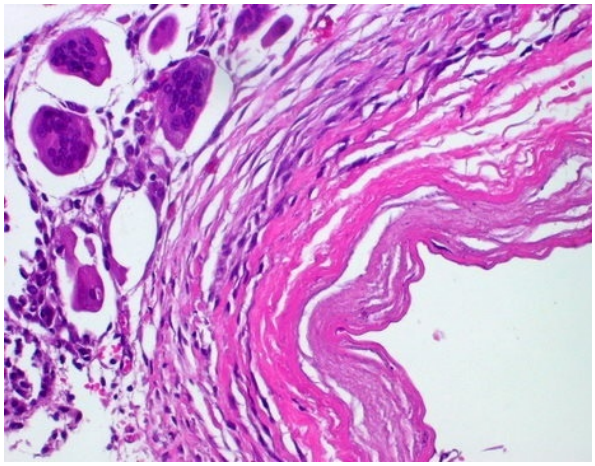

Figure XI-21 - Animal No. 4123 Right, Section #2/ HE/ 50X

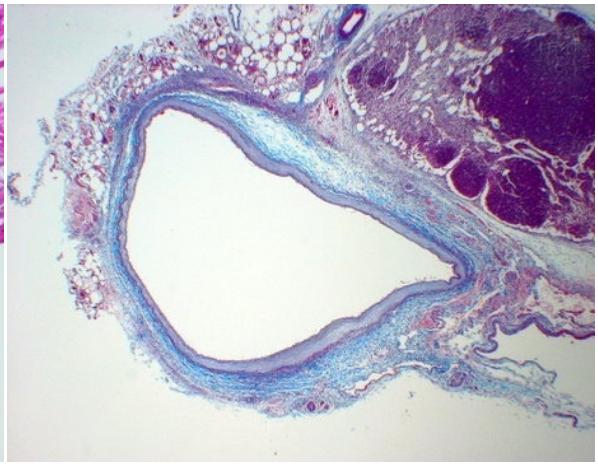

Figure XI-22 - Animal No. 4123 Right, Section #3/ MT/ 5X

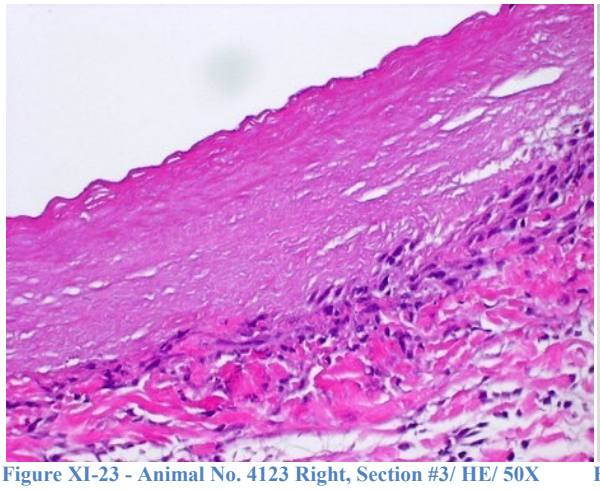

Figure XI-23 - Animal No. 4123 Right, Section #3/ HE/ 50X

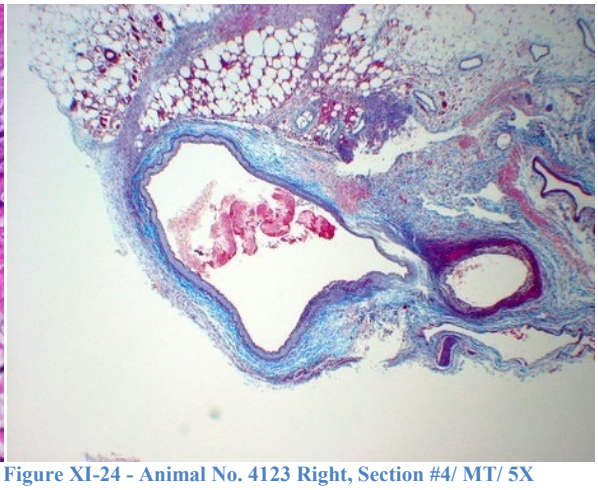

Figure XI-24 - Animal No. 4123 Right, Section #4/ MT/ 5X

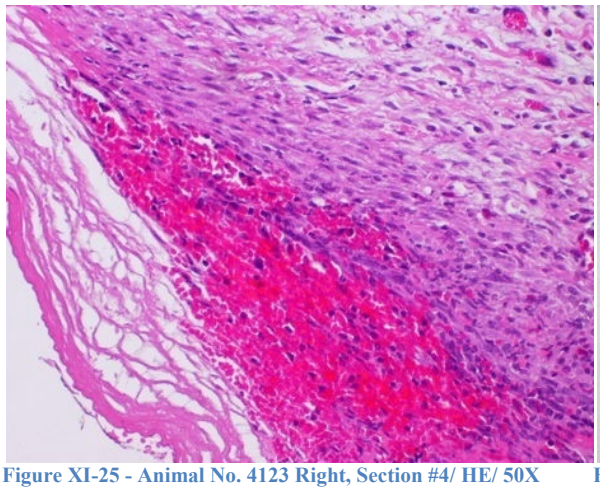

Figure XI-25 - Animal No. 4123 Right, Section #4/ HE/ 50X

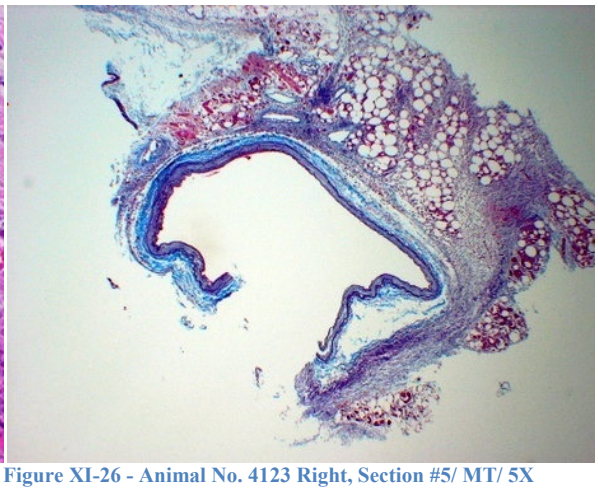

Figure XI-26 - Animal No. 4123 Right, Section #5/ MT/ 5X

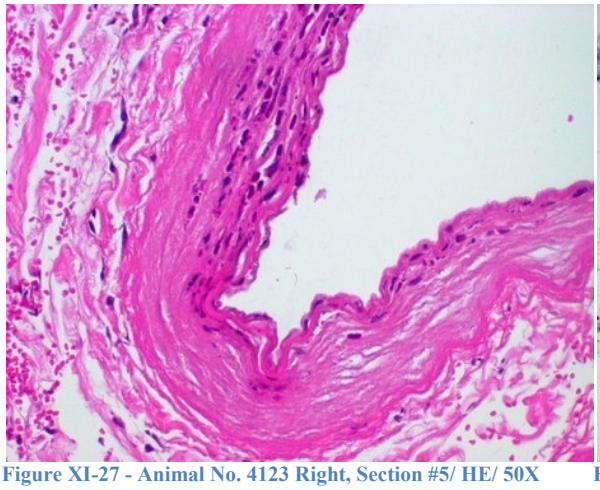

Figure XI-27 - Animal No. 4123 Right, Section #5/ HE/ 50X

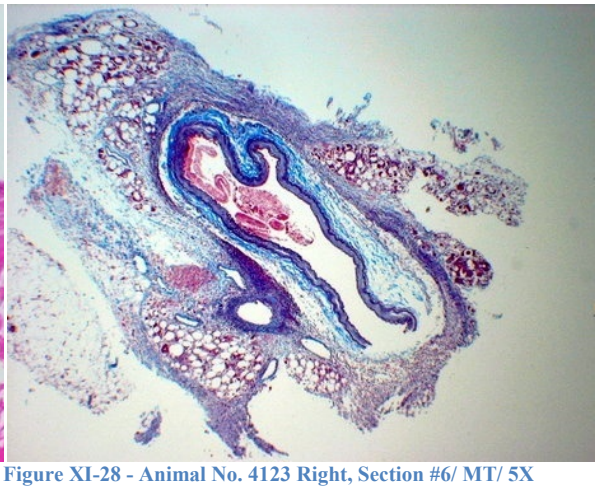

Figure XI-28 - Animal No. 4123 Right, Section #6/ MT/ 5X

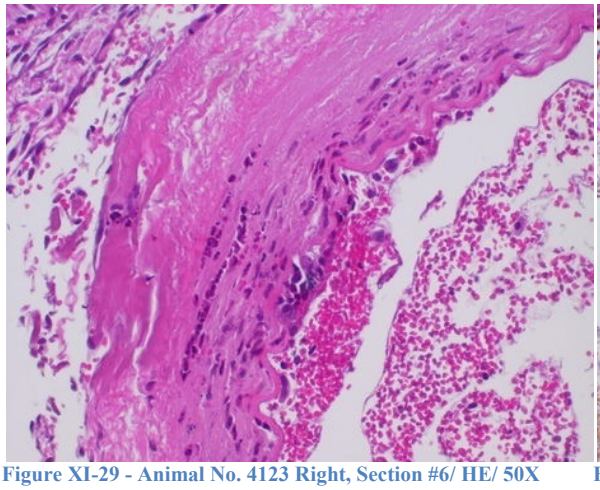

Figure XI-29 - Animal No. 4123 Right, Section #6/ HE/ 50X

Figure XI-30 - Animal No. 4124 Left, Section #1/ VE/ 10X

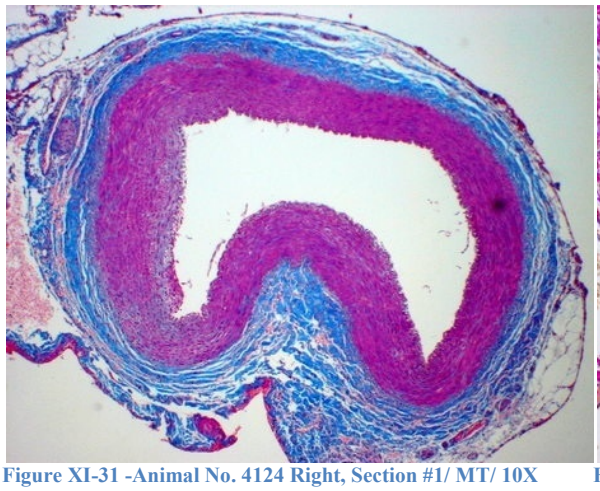

Figure XI-31 -Animal No. 4124 Right, Section #1/ MT/ 10X

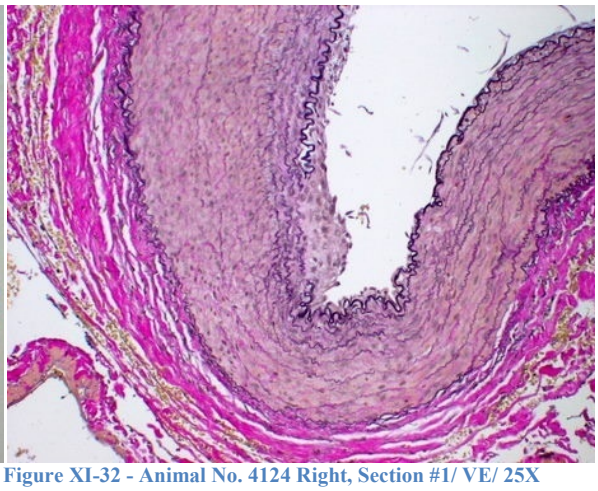

Figure XI-32 - Animal No. 4124 Right, Section #1/ VE/ 25X

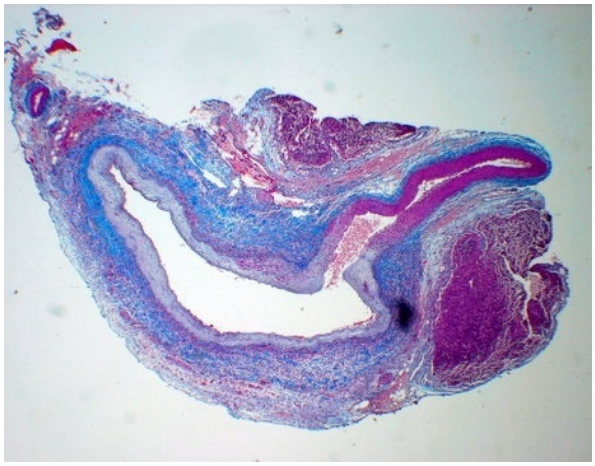

Figure XI-33 - Animal No. 4124 Right, Section #2/ MT/ 5X

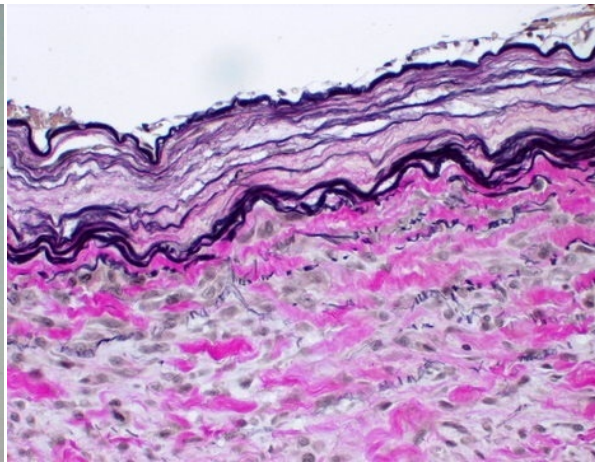

Figure XI-34 - Animal No. 4124 Right, Section #2/ VE/ 50X

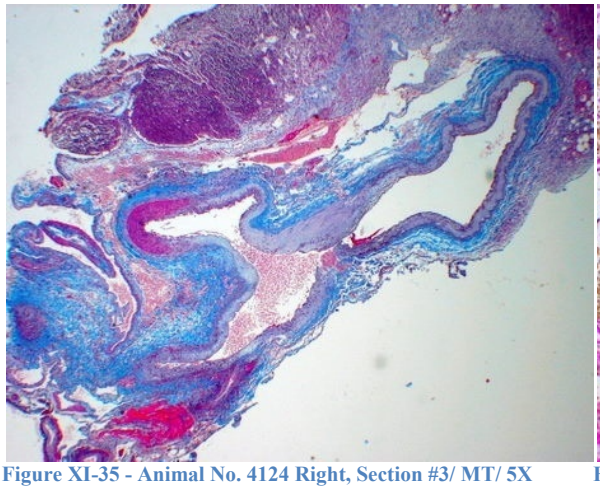

Figure XI-35 - Animal No. 4124 Right, Section #3/ MT/ 5X

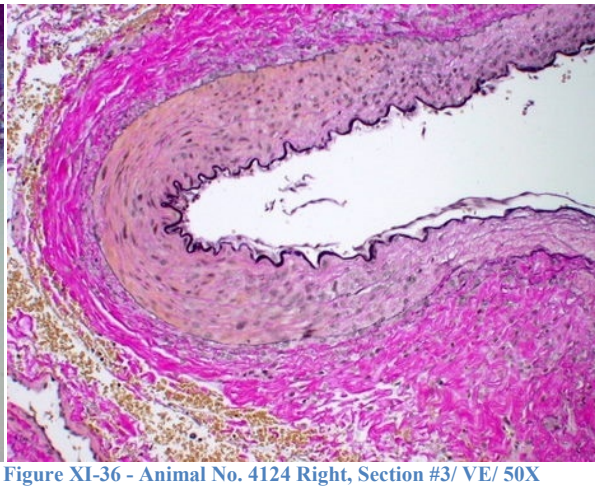

Figure XI-36 - Animal No. 4124 Right, Section #3/ VE/ 50X

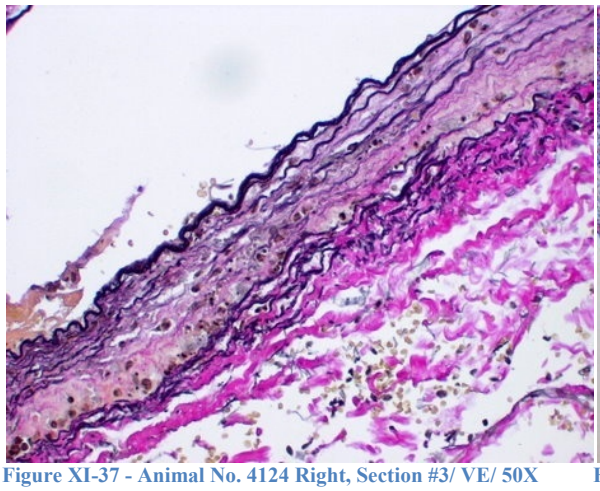

Figure XI-37 - Animal No. 4124 Right, Section #3/ VE/ 50X

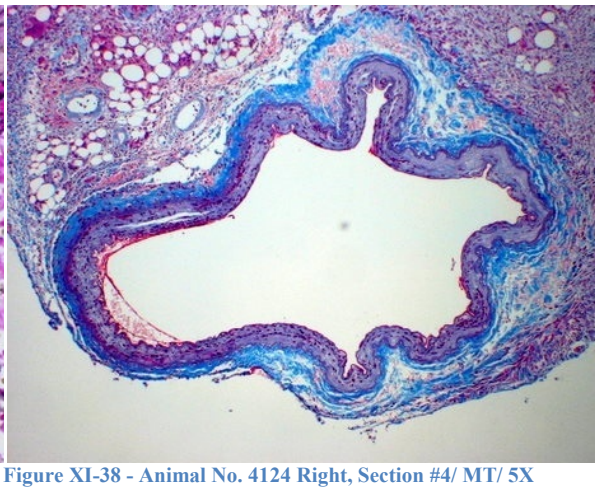

Figure XI-38 - Animal No. 4124 Right, Section #4/ MT/ 5X

Figure XI-39 - Animal No. 4124 Right, Section #4/ VE/ 50X

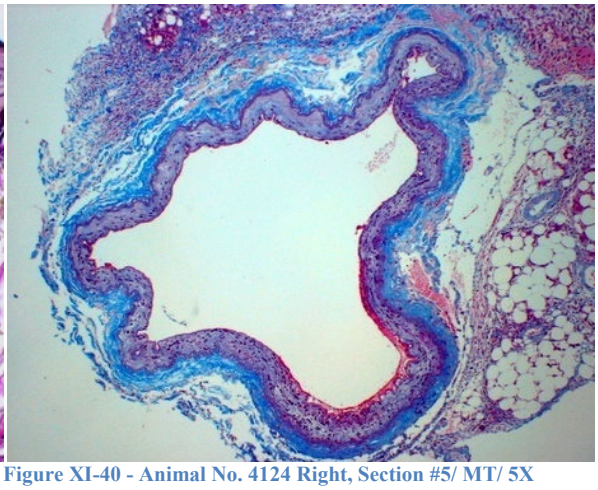

Figure XI-40 - Animal No. 4124 Right, Section #5/ MT/ 5X

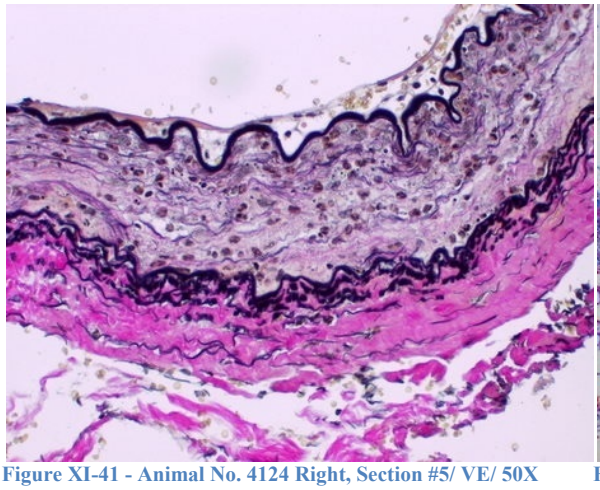

Figure XI-41 - Animal No. 4124 Right, Section #5/ VE/ 50X

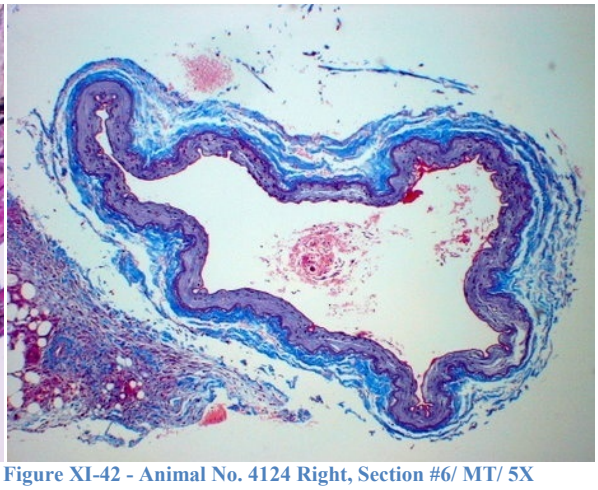

Figure XI-42 - Animal No. 4124 Right, Section #6/ MT/ 5X

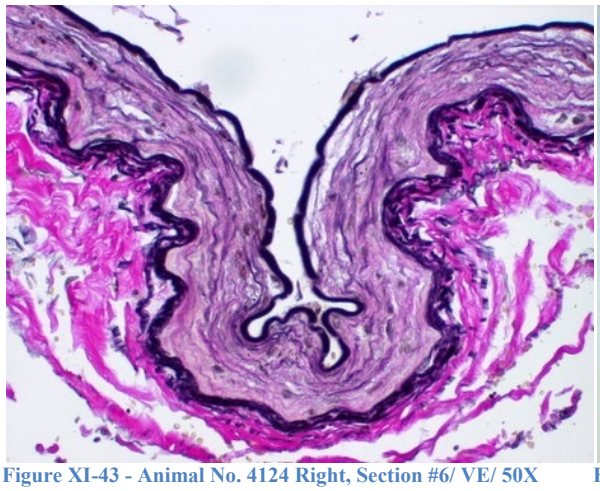

Figure XI-43 - Animal No. 4124 Right, Section #6/ VE/ 50X

Figure XI-44 - Animal No. 4131 Left, Section #1/ MT/ 5X

Figure XI-45 - Animal No. 4131 Left, Section #2/ MT/ 5X

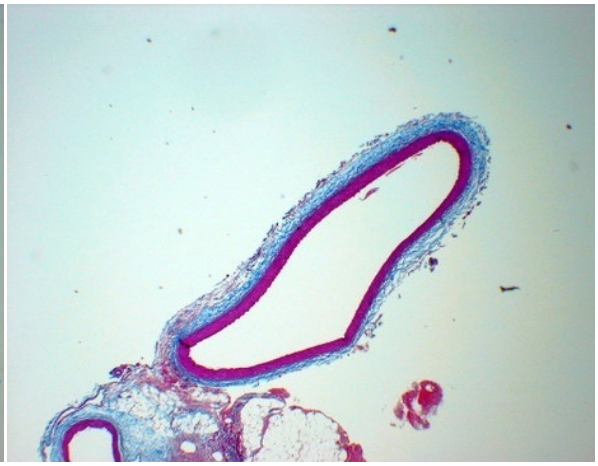

Figure XI-46 - Animal No. 4131 Left, Section #3/ MT/ 5X

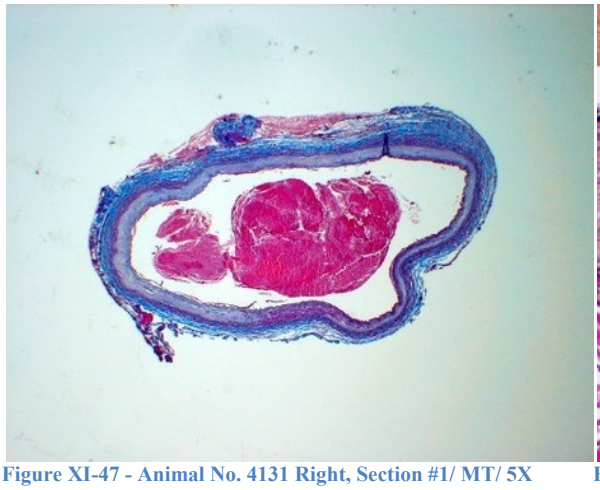

Figure XI-47 - Animal No. 4131 Right, Section #1/ MT/ 5X

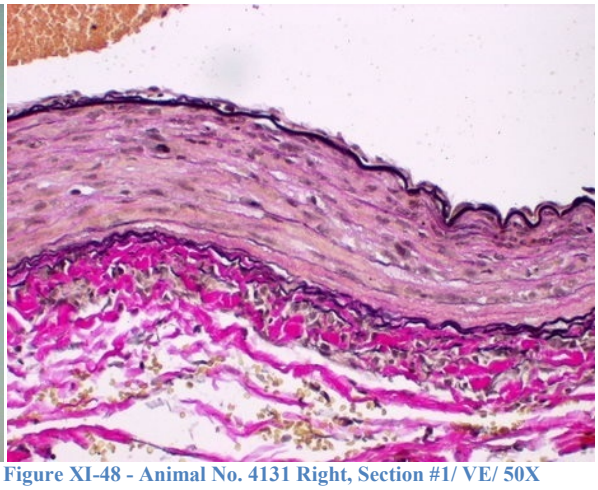

Figure XI-48 - Animal No. 4131 Right, Section #1/ VE/ 50X

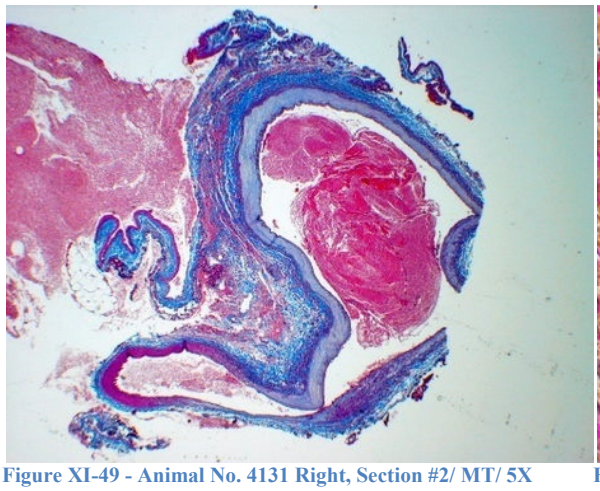

Figure XI-49 - Animal No. 4131 Right, Section #2/ MT/ 5X

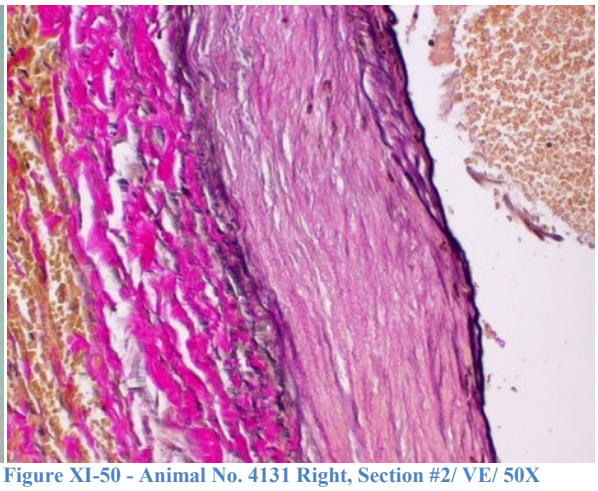

Figure XI-50 - Animal No. 4131 Right, Section #2/ VE/ 50X

Figure XI-51 - Animal No. 4131 Right, Section #3/ MT/ 5X

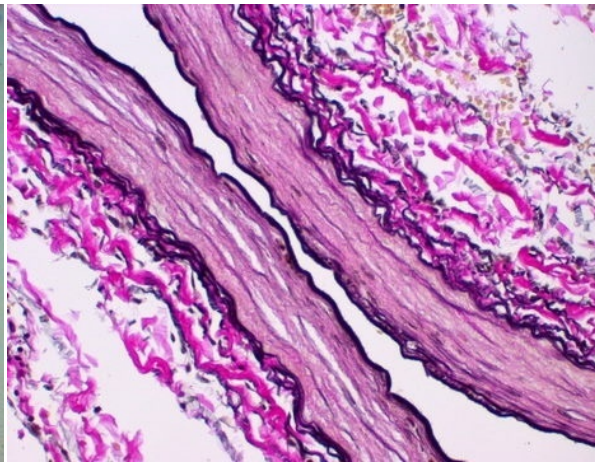

Figure XI-52 - Animal No. 4131 Right, Section #3/ VE/ 50X

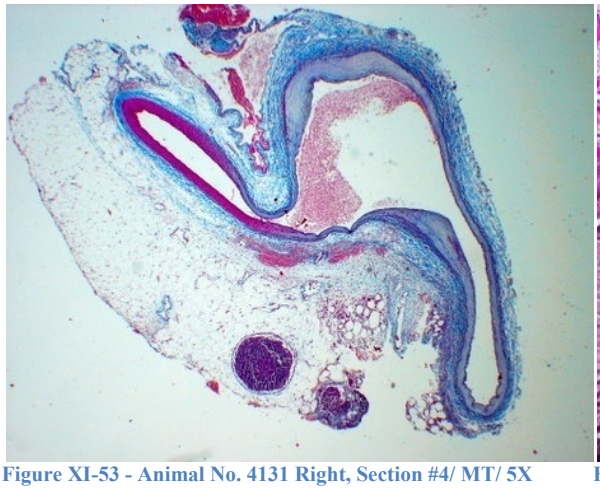

Figure XI-53 - Animal No. 4131 Right, Section #4/ MT/ 5X

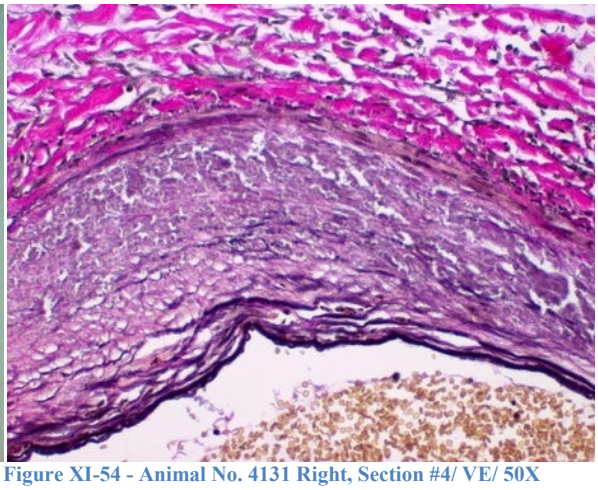

Figure XI-54 - Animal No. 4131 Right, Section #4/ VE/ 50X

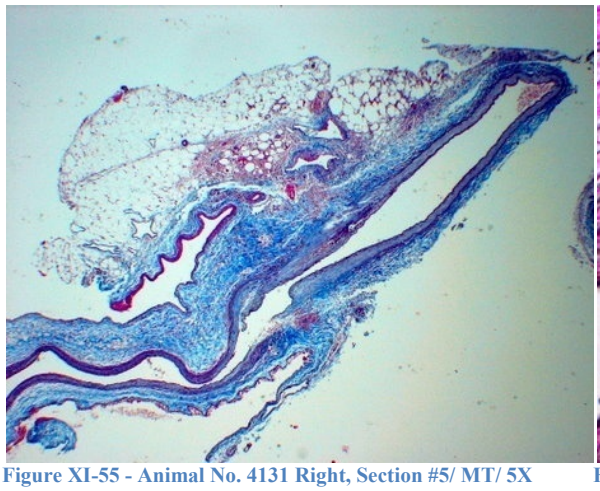

Figure XI-55 - Animal No. 4131 Right, Section #5/ MT/ 5X

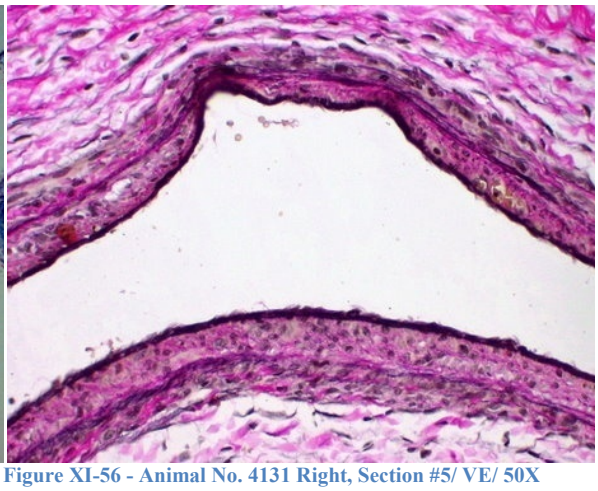

Figure XI-56 - Animal No. 4131 Right, Section #5/ VE/ 50X

Figure XI-57 - Animal No. 4131 Right, Section #6/ MT/ 5X

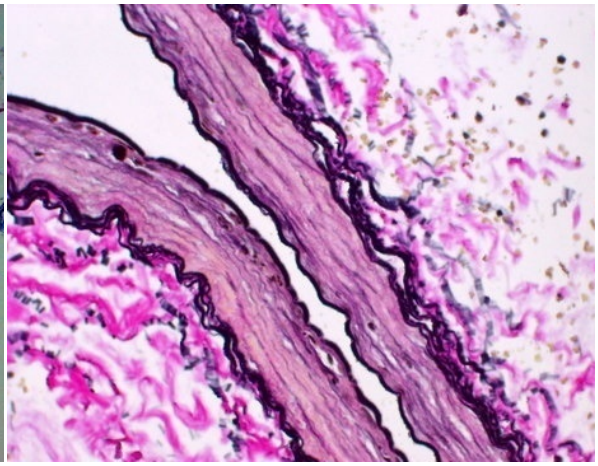

Figure XI-58 - Animal No. 4131 Right, Section #6/ VE/ 50X

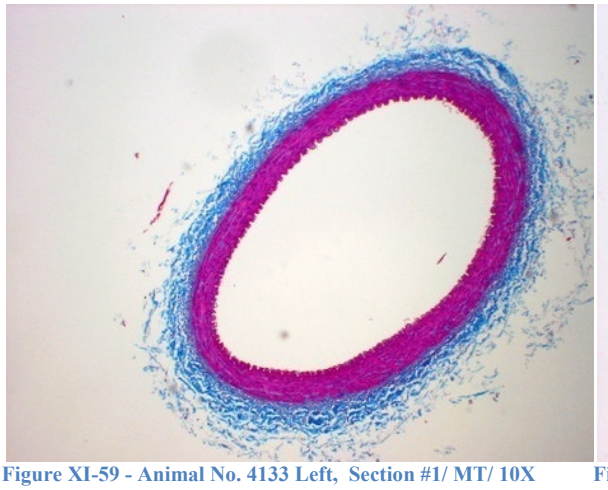

Figure XI-59 - Animal No. 4133 Left, Section #1/ MT/ 10X

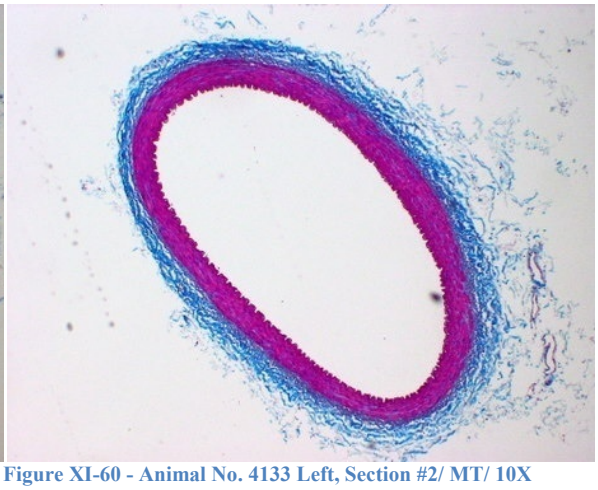

Figure XI-60 - Animal No. 4133 Left, Section #2/ MT/ 10X

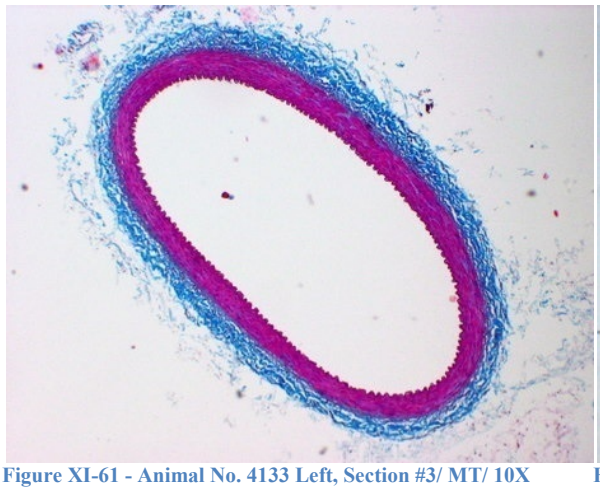

Figure XI-61 - Animal No. 4133 Left, Section #3/ MT/ 10X

Figure XI-62 - Animal No. 4133 Right, Section #1/ VE/ 5X

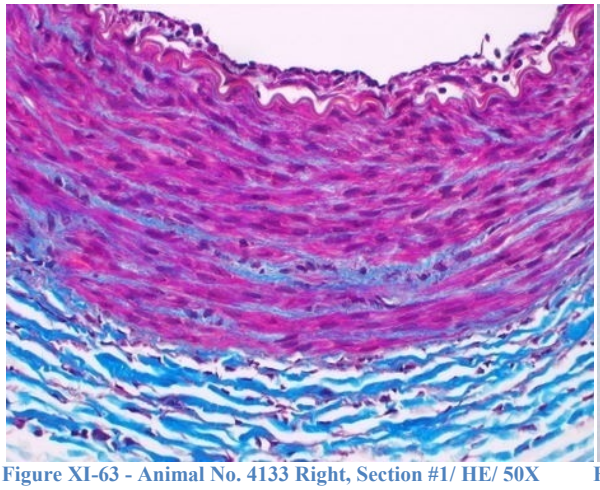

Figure XI-63 - Animal No. 4133 Right, Section #1/ HE/ 50X

Figure XI-64 - Animal No. 4133 Right, Section #2/ VE/ 5X

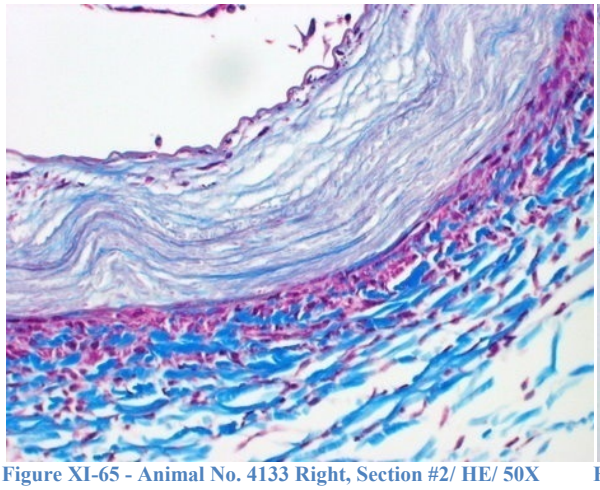

Figure XI-65 - Animal No. 4133 Right, Section #2/ HE/ 50X

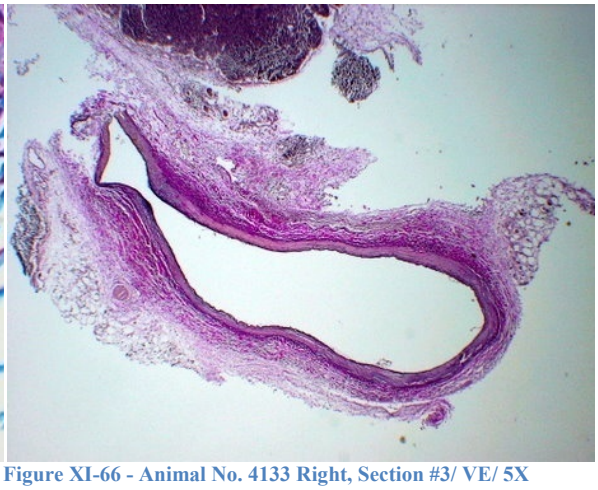

Figure XI-66 - Animal No. 4133 Right, Section #3/ VE/ 5X

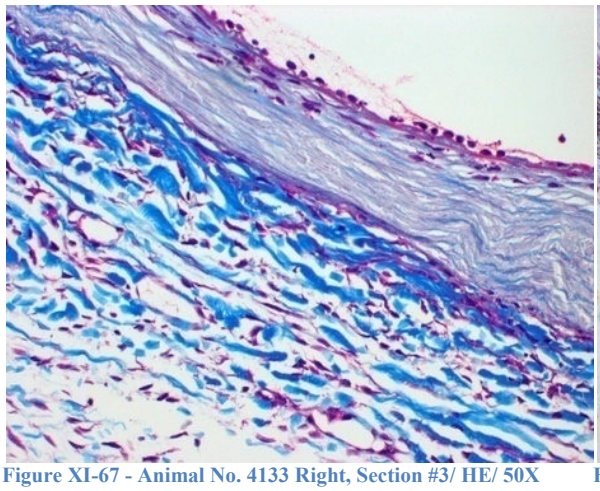

Figure XI-67 - Animal No. 4133 Right, Section #3/ HE/ 50X

Figure XI-68 - Animal No. 4133 Right, Section #4/ VE/ 5X

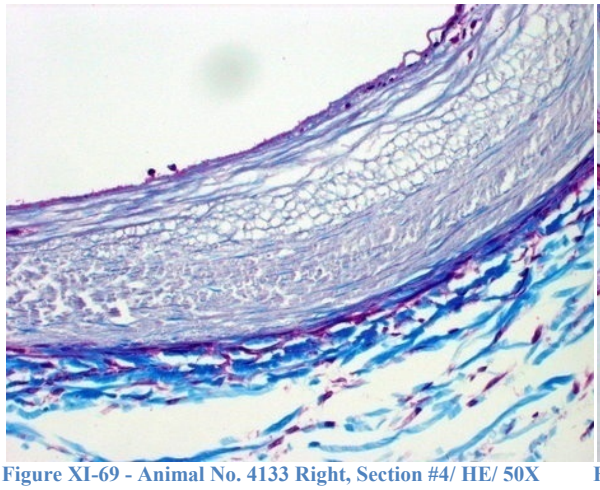

Figure XI-69 - Animal No. 4133 Right, Section #4/ HE/ 50X

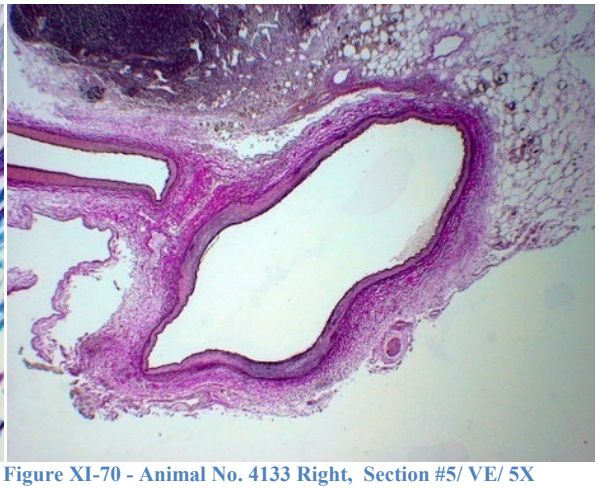

Figure XI-70 - Animal No. 4133 Right, Section #5/ VE/ 5X

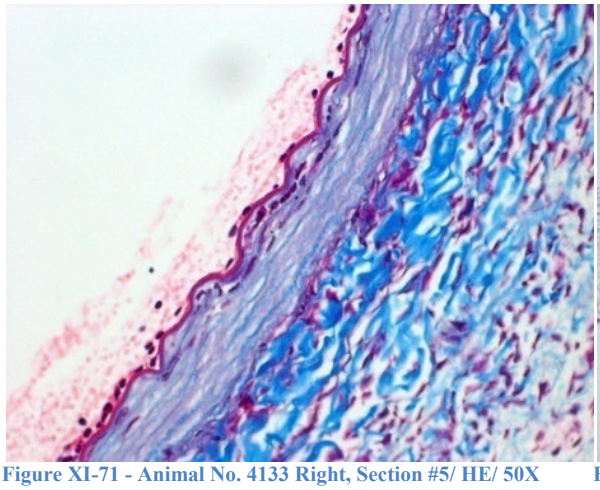

Figure XI-71 - Animal No. 4133 Right, Section #5/ HE/ 50X

Figure XI-72 - Animal No. 4133 Right, Section #6/ VE/ 5X

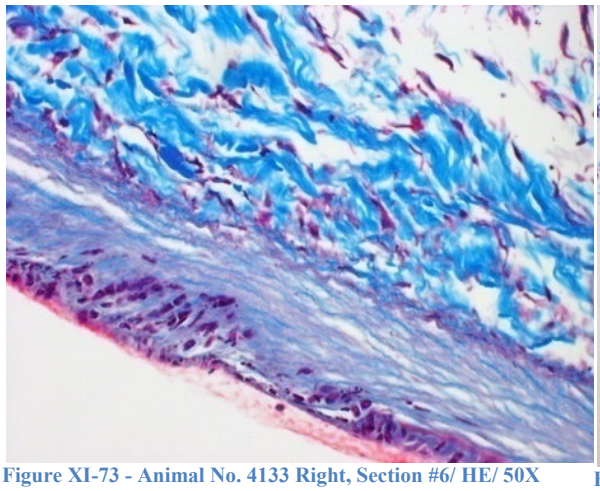

Figure XI-73 - Animal No. 4133 Right, Section #6/ HE/ 50X

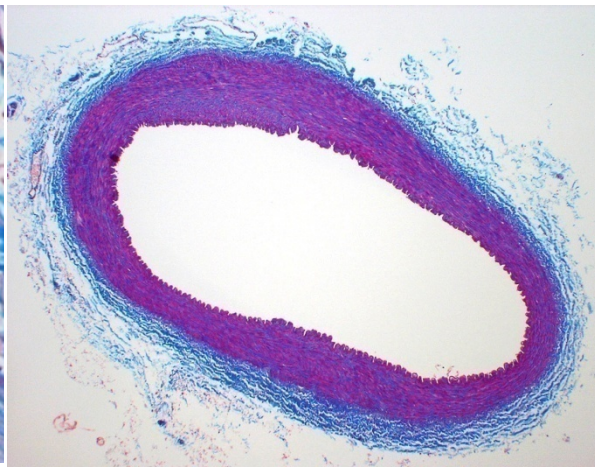

Figure XI-74 - Animal No. 304 Left, Section #1/ MT/ 10X

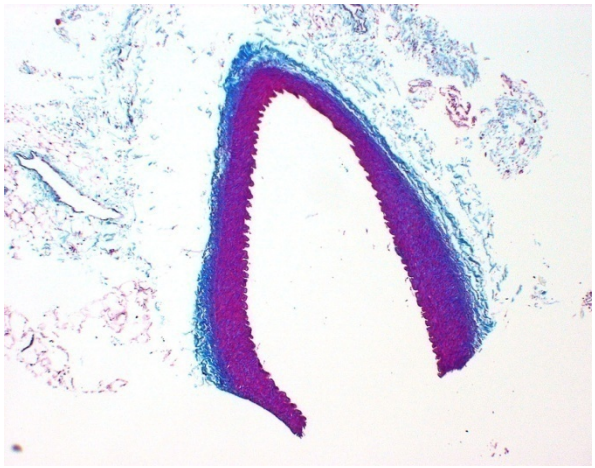

Figure XI-75 - Animal No. 304 Left, Section #2/ MT/ 10X

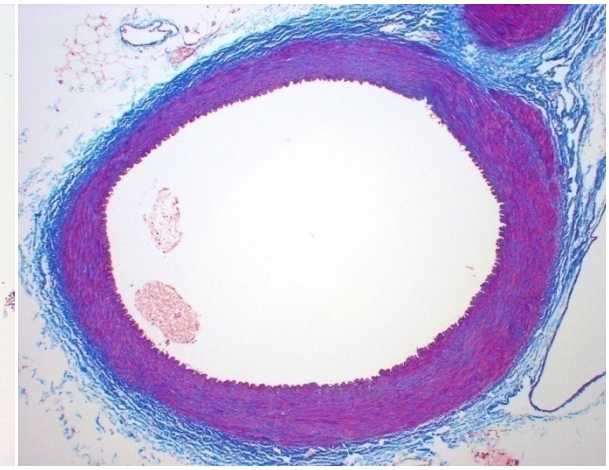

Figure XI-76 - Animal No. 304 Left, Section #3/ MT/ 10X

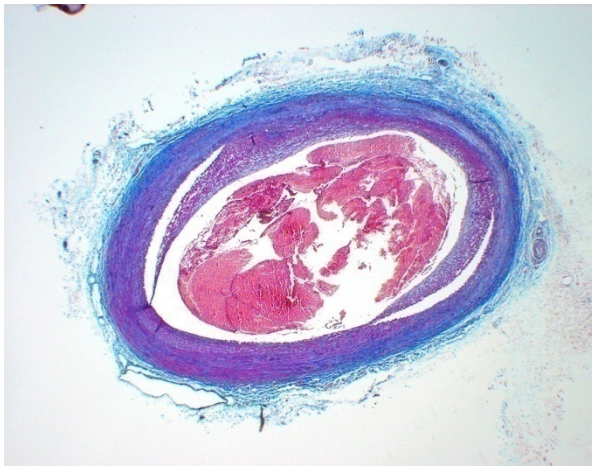

Figure XI-77 - Animal No. 304 Right, Section #1/ MT/ 5X

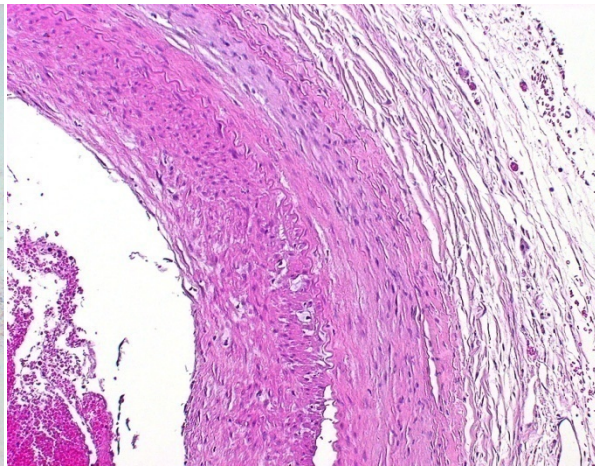

Figure XI-78 - Animal No. 304 Right, Section #1/ HE/ 25X

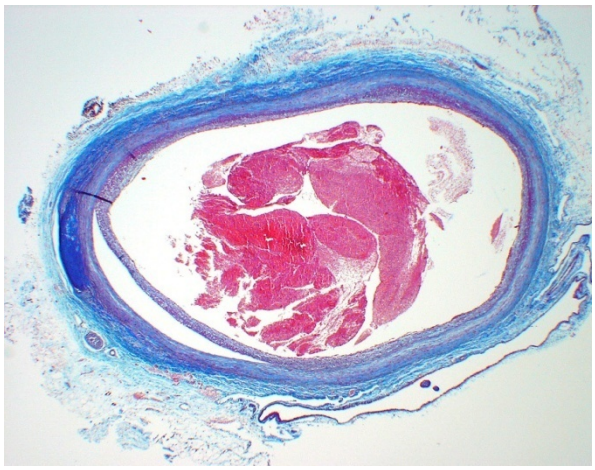

Figure XI-79 - Animal No. 304 Right, Section #2/ MT/ 5X

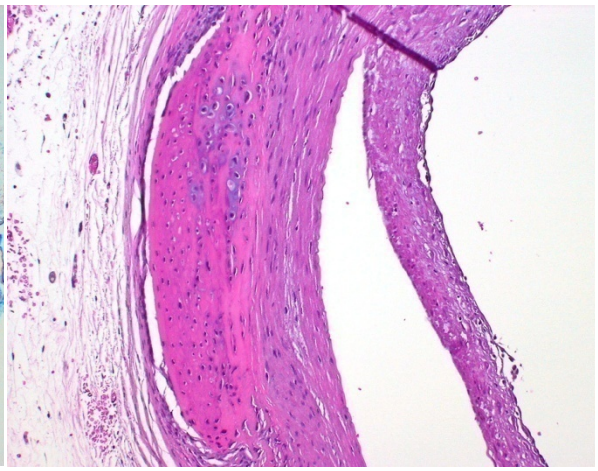

Figure XI-80 - Animal No. 304 Right, Section #2/ HE/ 25X

Figure XI-81 - Animal No. 304 Right, Section #3/ MT/ 5X

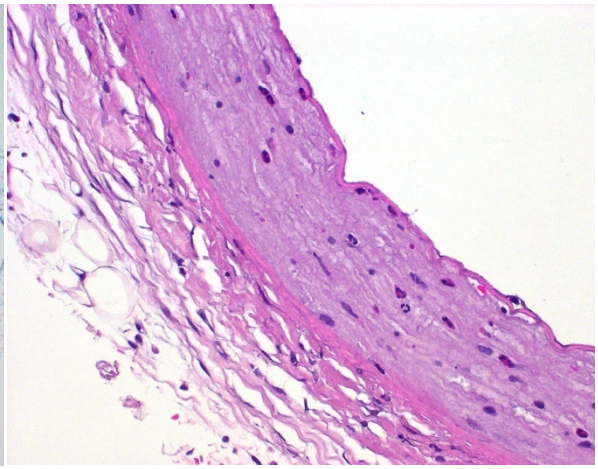

Figure XI-82 - Animal No. 304 Right, Section #3/ HE/ 50X

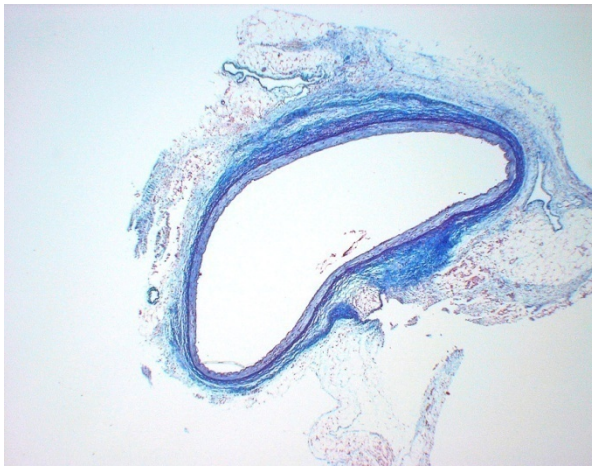

Figure XI-83 - Animal No. 304 Right, Section #4/ MT/ 5X

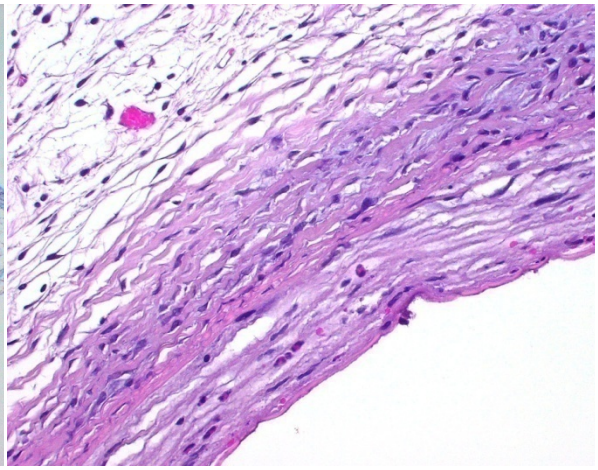

Figure XI-84 - Animal No. 304 Right, Section #4/ HE/ 50X

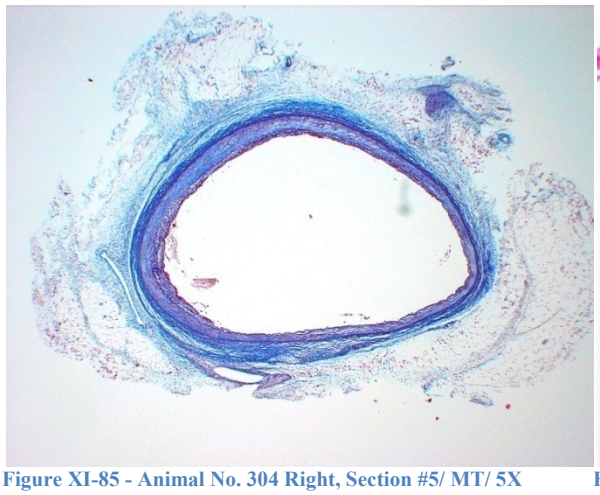

Figure XI-85 - Animal No. 304 Right, Section #5/ MT/ 5X

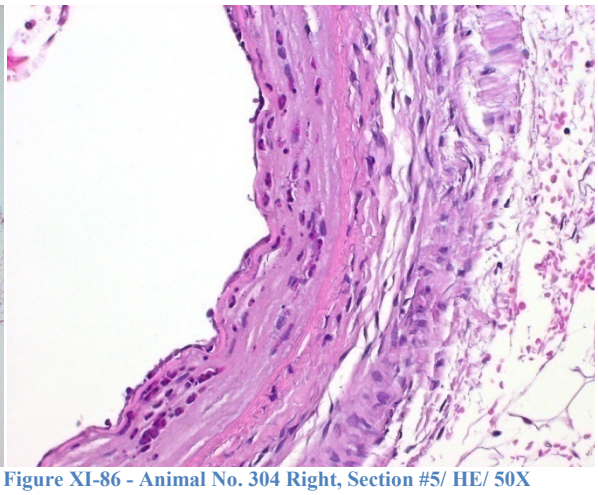

Figure XI-86 - Animal No. 304 Right, Section #5/ HE/ 50X

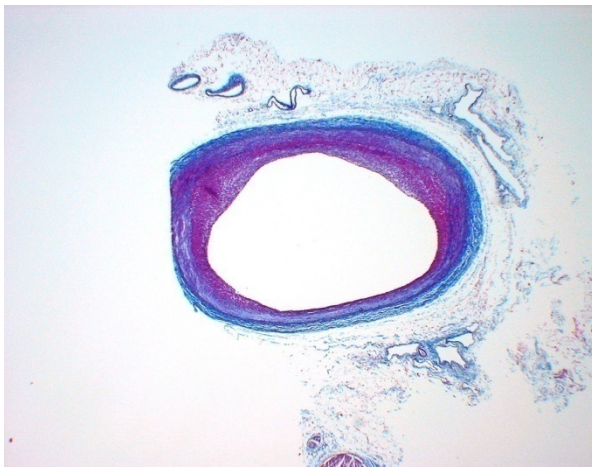

Figure XI-87 - Animal No. 304 Right, Section #6/ MT/ 5X

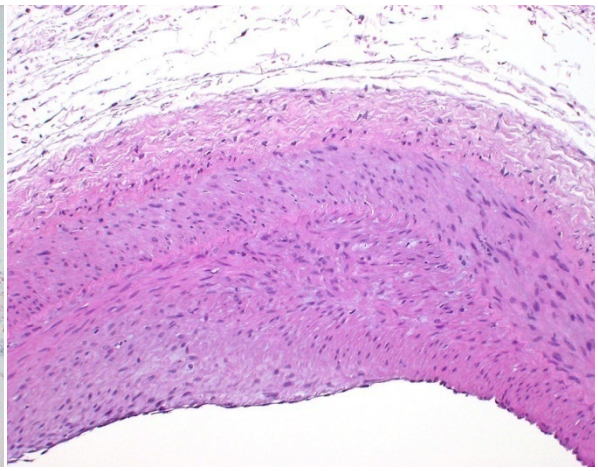

Figure XI-88 - Animal No. 304 Right, Section #6/ HE/ 25X

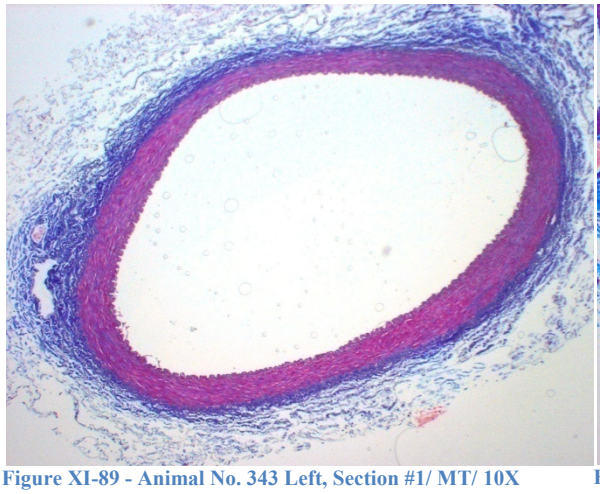

Figure XI-89 - Animal No. 343 Left, Section #1/ MT/ 10X

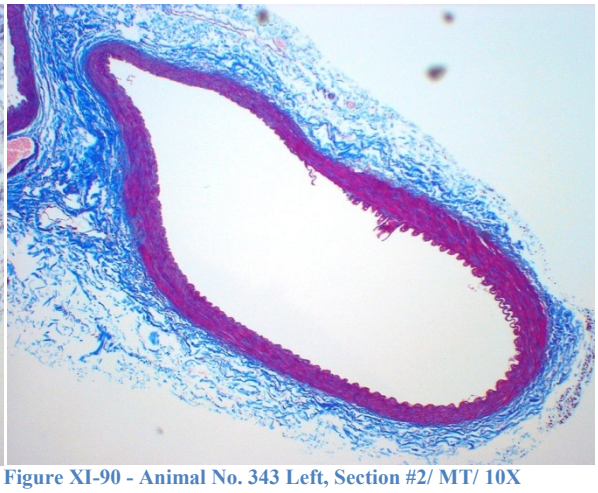

Figure XI-90 - Animal No. 343 Left, Section #2/ MT/ 10X

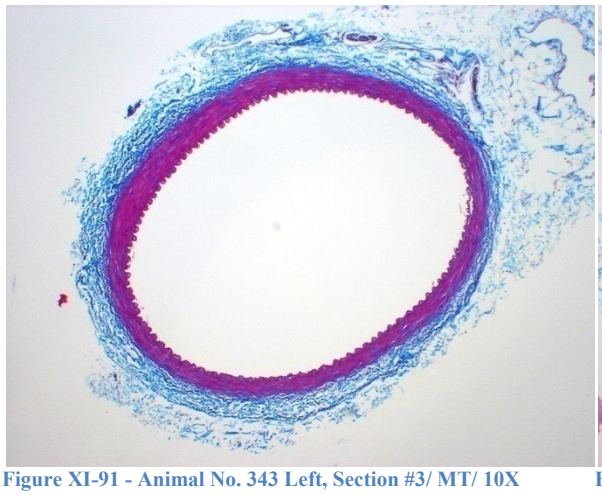

Figure XI-91 - Animal No. 343 Left, Section #3/ MT/ 10X

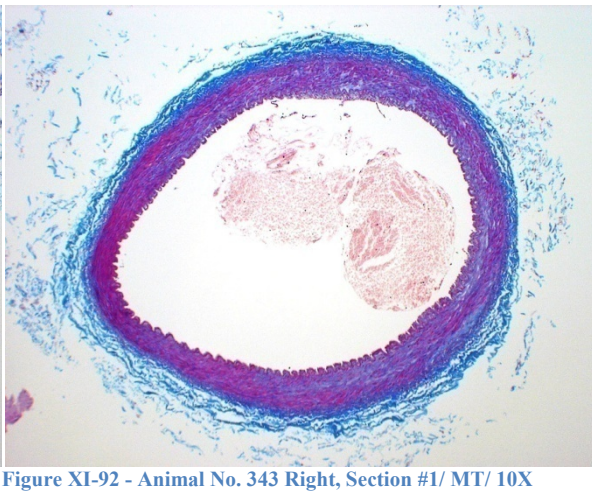

Figure XI-92 - Animal No. 343 Right, Section #1/ MT/ 10X

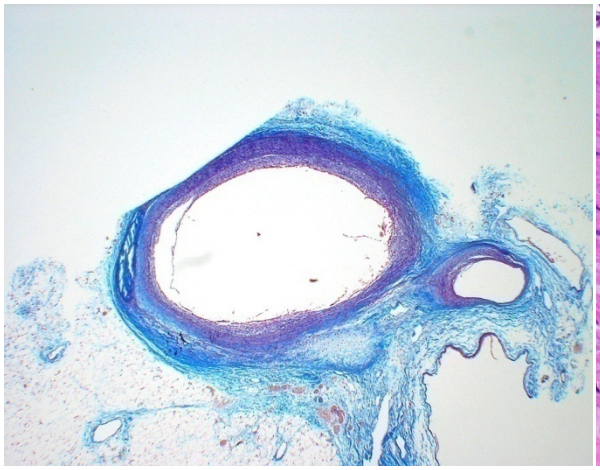

Figure XI-93 - Animal No. 343 Right, Section #2/ MT/ 5X

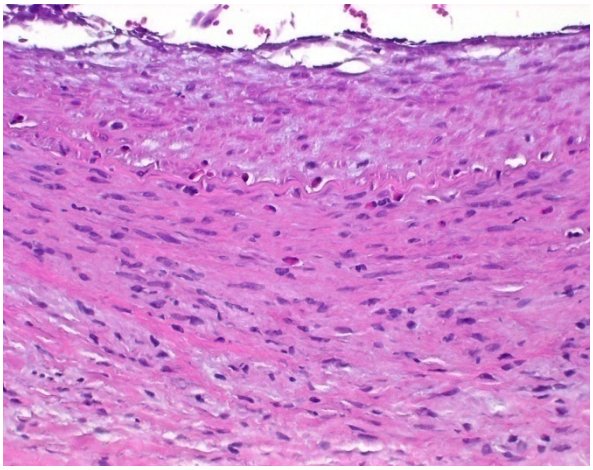

Figure XI-94 - Animal No. 343 Right, Section #2/ HE/ 50X

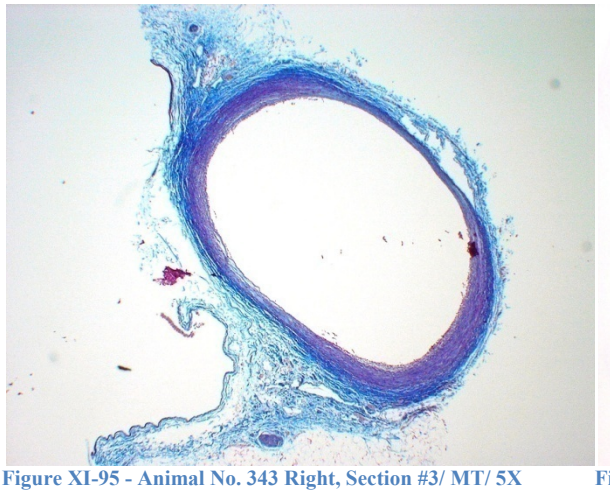

Figure XI-95 - Animal No. 343 Right, Section #3/ MT/ 5X

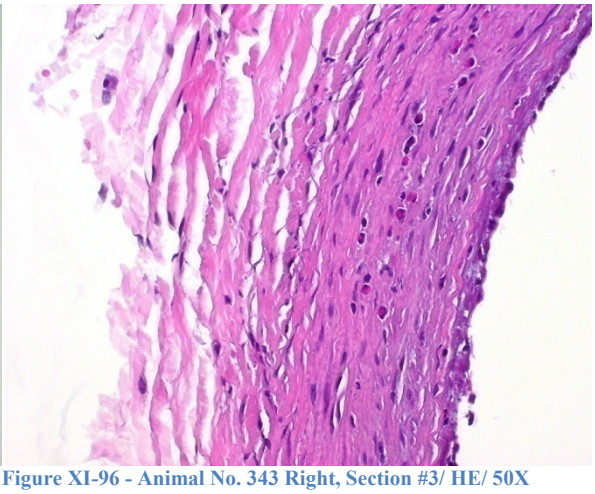

Figure XI-96 - Animal No. 343 Right, Section #3/ HE/ 50X

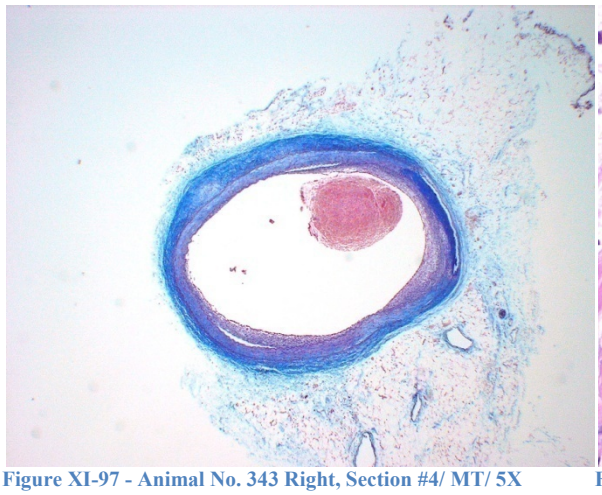

Figure XI-97 - Animal No. 343 Right, Section #4/ MT/ 5X

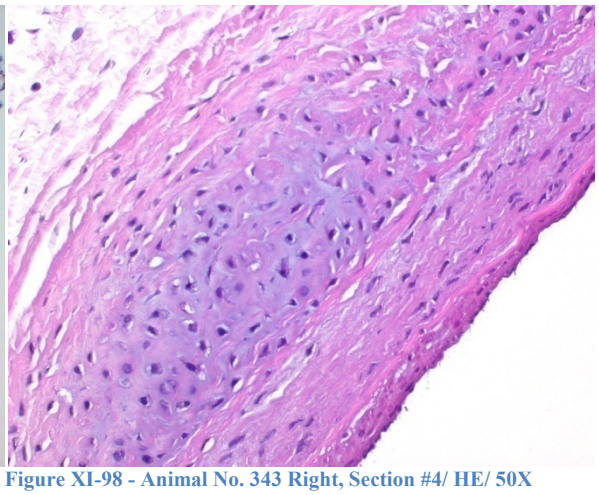

Figure XI-98 - Animal No. 343 Right, Section #4/ HE/ 50X

Figure XI-99 - Animal No. 343 Right, Section #5/ MT/ 5X

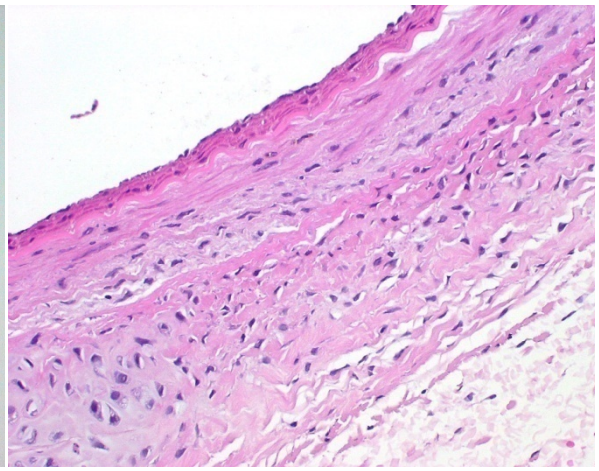

Figure XI-100 - Animal No. 343 Right, Section #5/ HE/ 50X

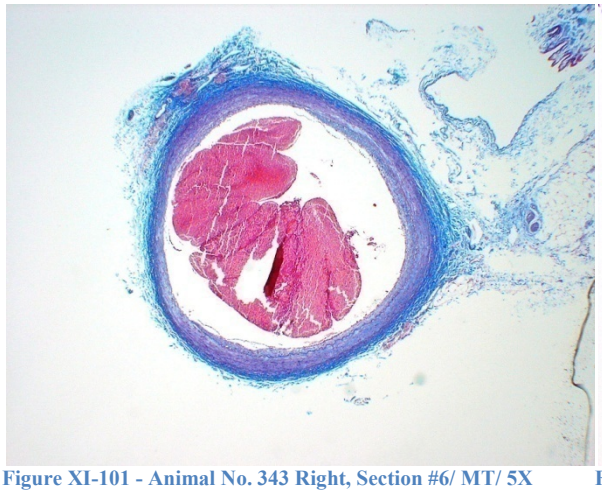

Figure XI-101 - Animal No. 343 Right, Section #6/ MT/ 5X

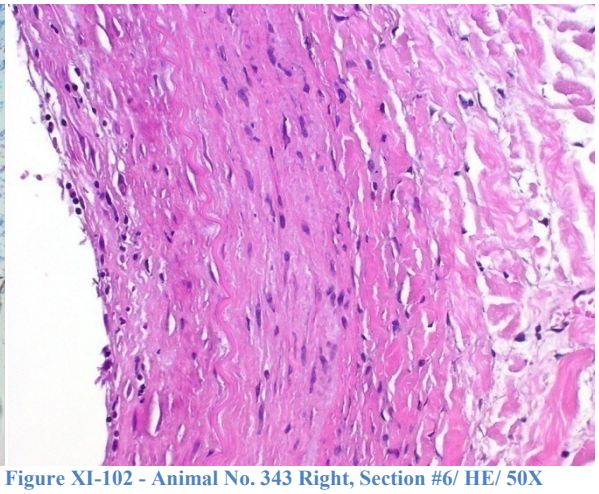

Figure XI-102 - Animal No. 343 Right, Section #6/ HE/ 50X

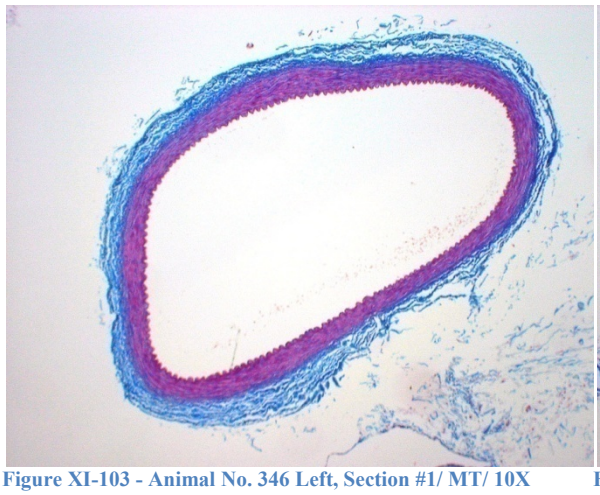

Figure XI-103 - Animal No. 346 Left, Section #1/ MT/ 10X

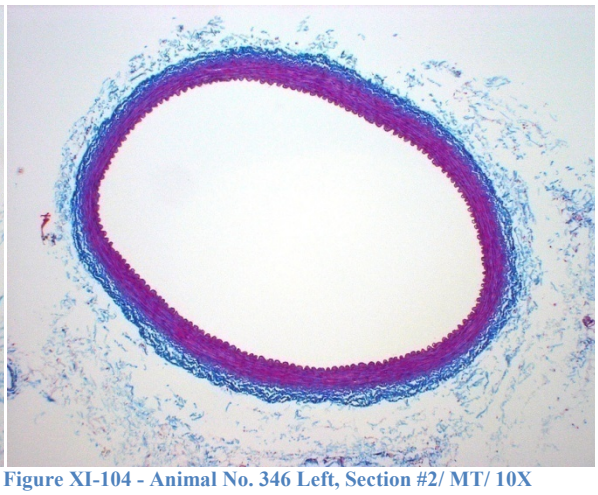

Figure XI-104 - Animal No. 346 Left, Section #2/ MT/ 10X

Figure XI-105 - Animal No. 346 Left, Section #3/ MT/ 5X

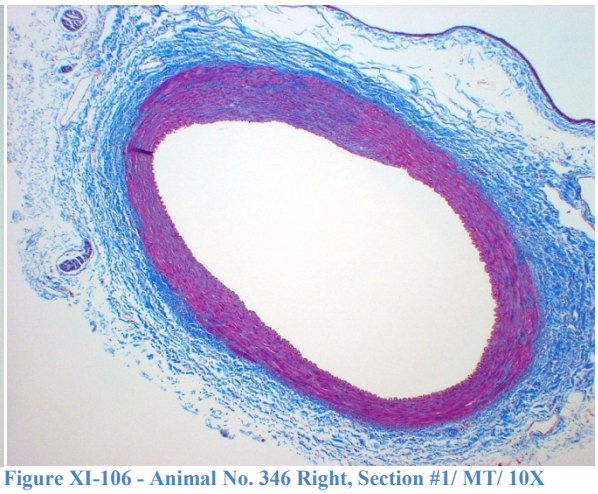

Figure XI-106 - Animal No. 346 Right, Section #1/ MT/ 10X

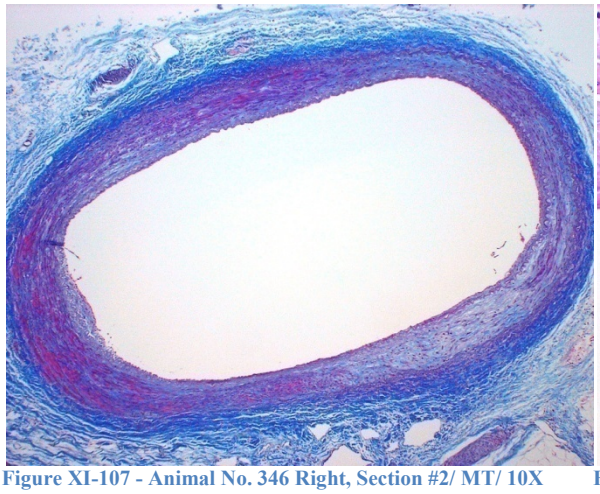

Figure XI-107 - Animal No. 346 Right, Section #2/ MT/ 10X

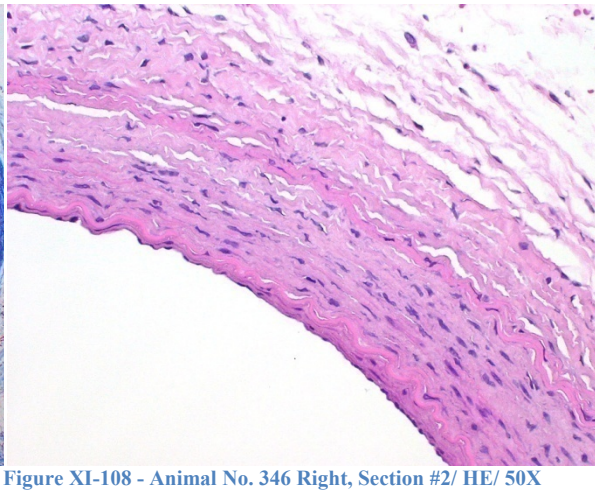

Figure XI-108 - Animal No. 346 Right, Section #2/ HE/ 50X

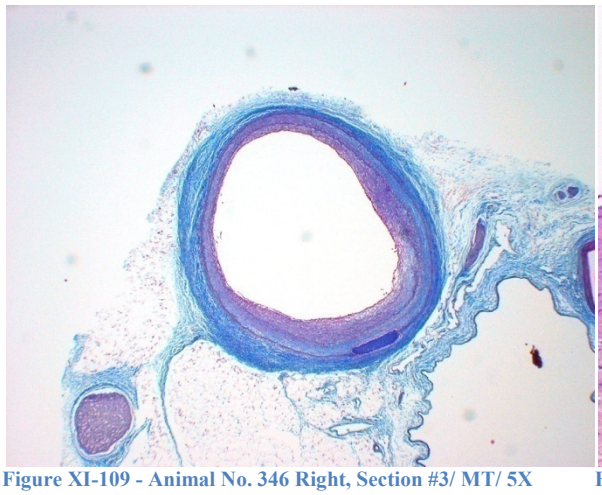

Figure XI-109 - Animal No. 346 Right, Section #3/ MT/ 5X

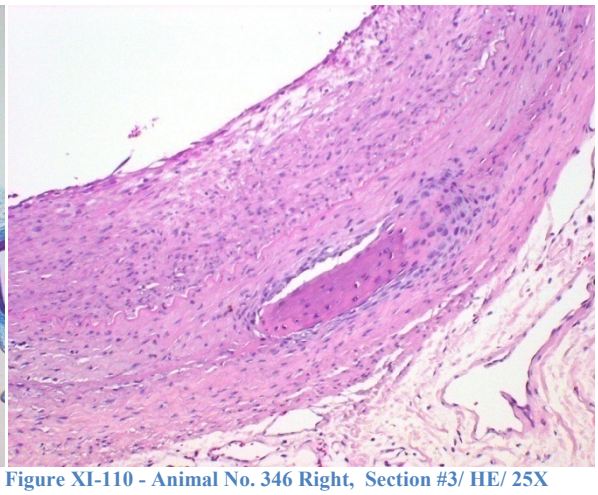

Figure XI-110 - Animal No. 346 Right, Section #3/ HE/ 25X

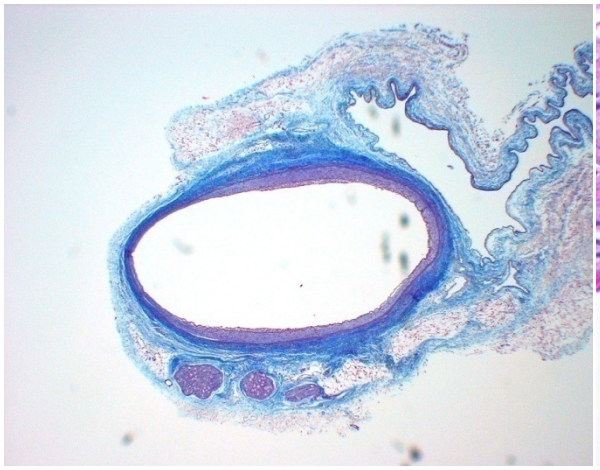

Figure XI-111 - Animal No. 346 Right , Section #4/ MT/ 5X

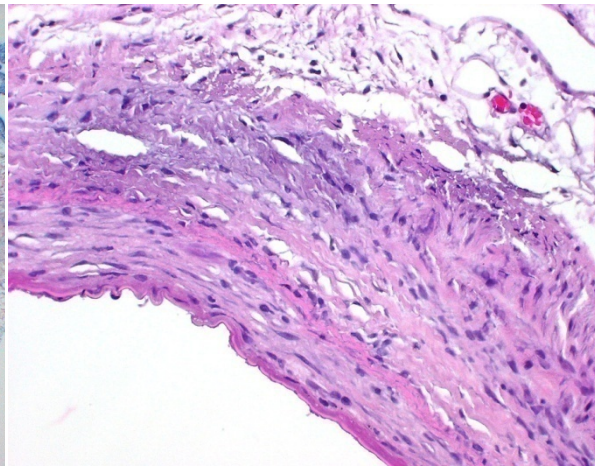

Figure XI-112 - Animal No. 346 Right, Section #4/ HE/ 50X

Figure XI-113 - Animal No. 346 Right, Section #5/ MT/ 5X

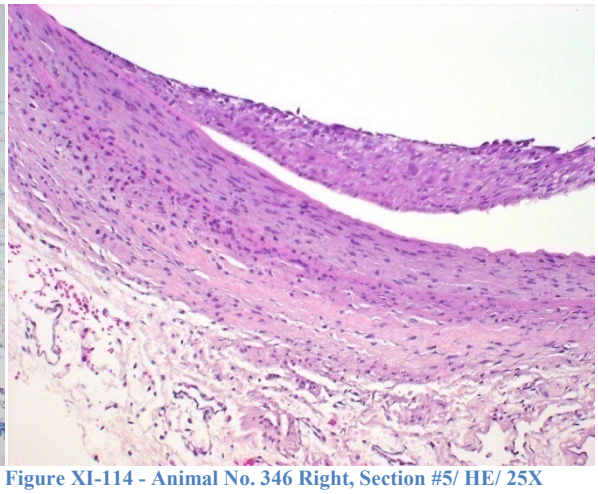

Figure XI-114 - Animal No. 346 Right, Section #5/ HE/ 25X

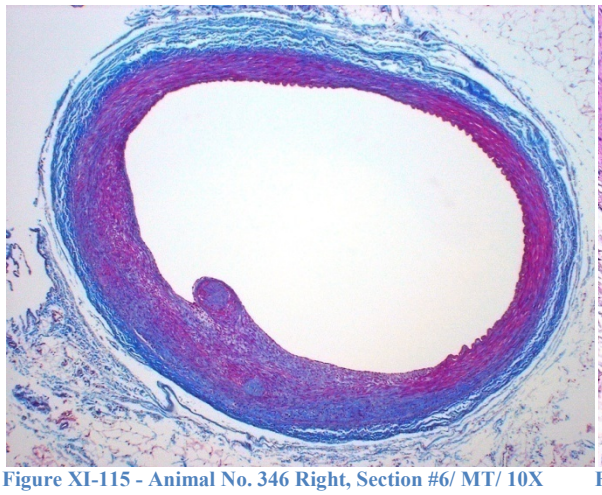

Figure XI-115 - Animal No. 346 Right, Section #6/ MT/ 10X

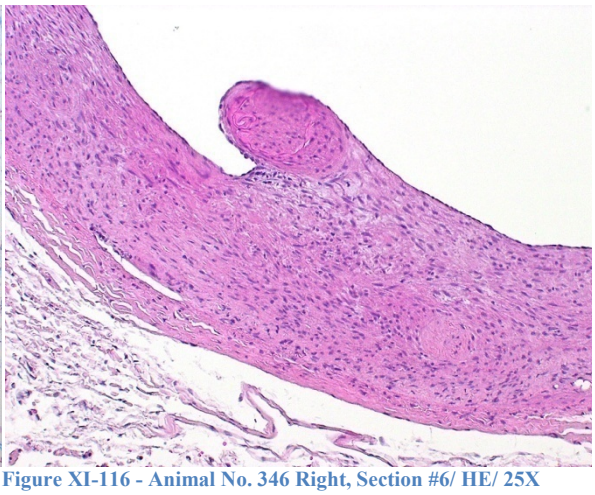

Figure XI-116 - Animal No. 346 Right, Section #6/ HE/ 25X

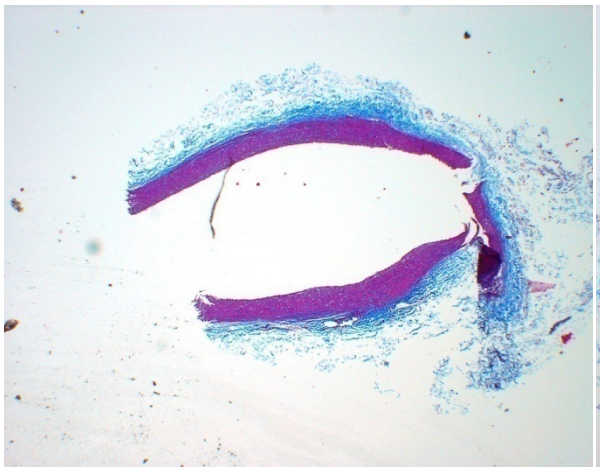

Figure XI-117 - Animal No. 4126 Left, Section #1/ MT/ 5X

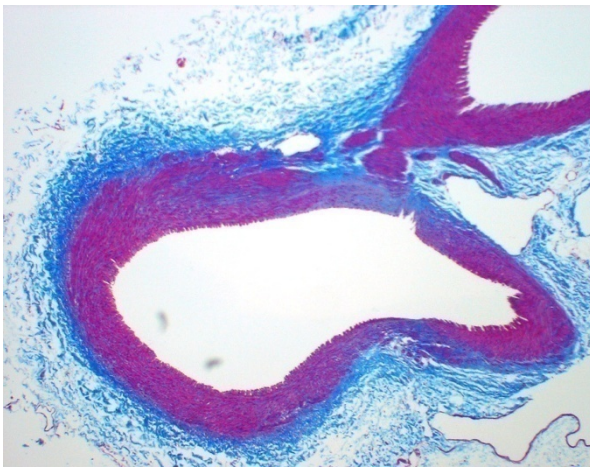

Figure XI-118 - Animal No. 4126 Left, Section #2/ MT/ 5X

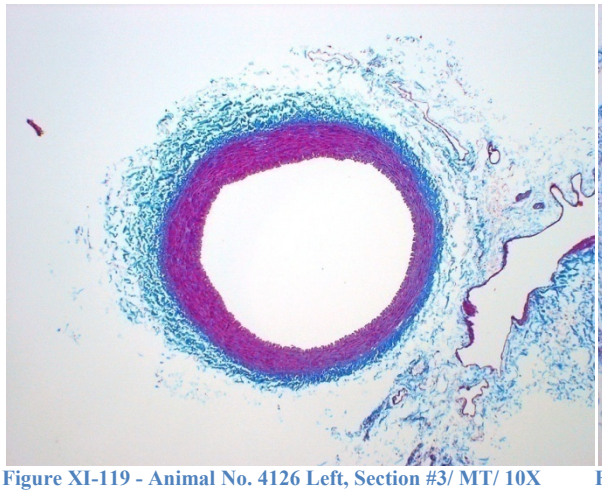

Figure XI-119 - Animal No. 4126 Left, Section #3/ MT/ 10X

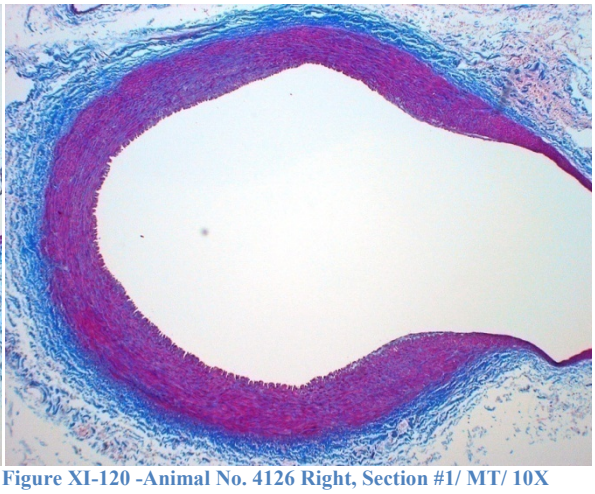

Figure XI-120 -Animal No. 4126 Right, Section #1/ MT/ 10X

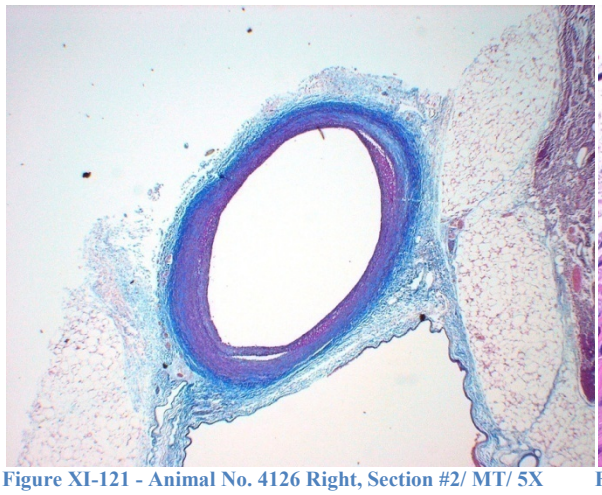

Figure XI-121 - Animal No. 4126 Right, Section #2/ MT/ 5X

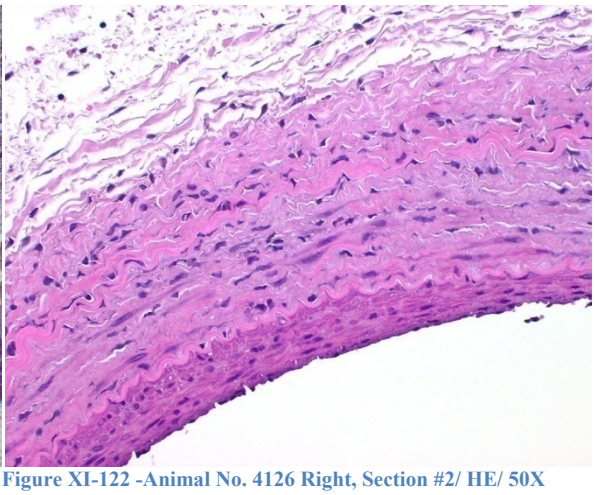

Figure XI-122 -Animal No. 4126 Right, Section #2/ HE/ 50X

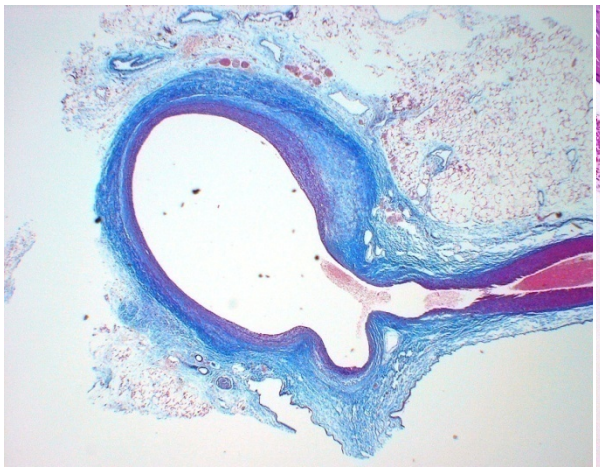

Figure XI-123 - Animal No. 4126 Right, Section #3/ MT/ 5X

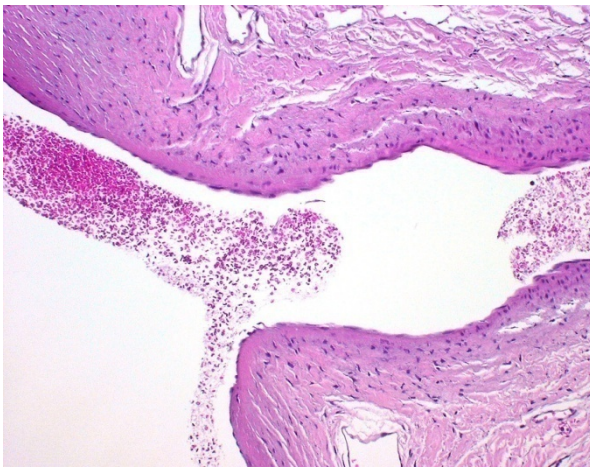

Figure XI-124 -Animal No. 4126 Right, Section #3/ HE/ 25X

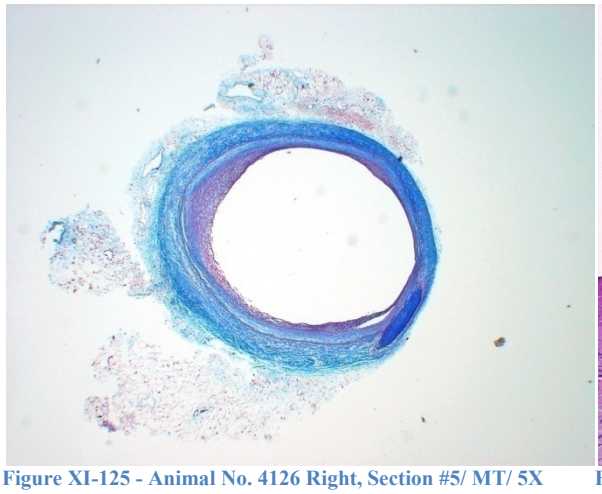

Figure XI-125 - Animal No. 4126 Right, Section #5/ MT/ 5X

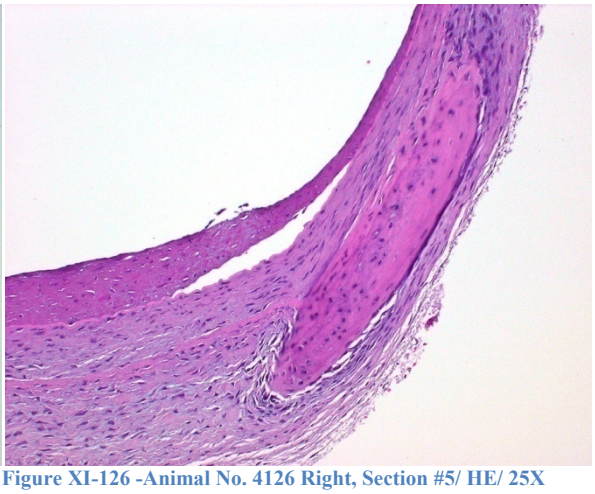

Figure XI-126 -Animal No. 4126 Right, Section #5/ HE/ 25X

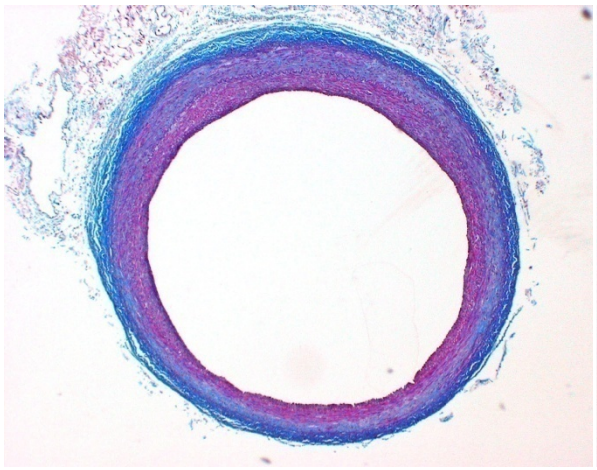

Figure XI-127 - Animal No. 4126 Right, Section #6/ MT/ 5X

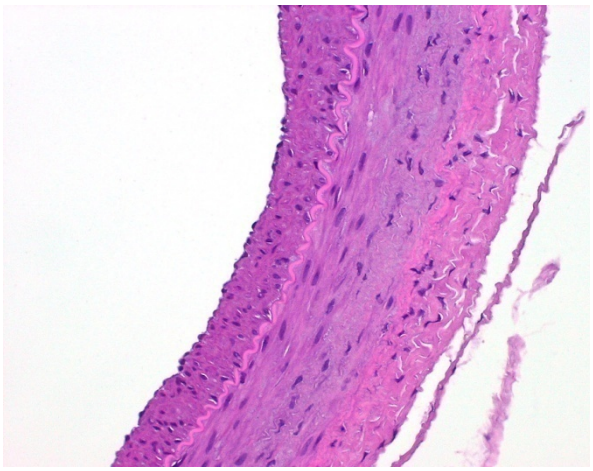

Figure XI-128 -Animal No. 4126 Right, Section #6/ HE/ 50X